The functional and molecular role of transglutaminase 2 in hematopoietic stem and progenitor cells

Die funktionelle und molekulare Rolle von Transglutaminase 2 in hämatopoetischen Stamm- und Progenitorzellen

Dissertation
zur Erlangung des Doktorgrades
der Naturwissenschaften

vorgelegt beim Fachbereich Biowissenschaften (FB15)
der Johann Wolfang Goethe-Universität
in Frankfurt am Main

von
Weijia Yu (Ika)
aus Guangdong, China

Frankfurt am Main 2023
(D 30)

Vom Fachbereich Biowissenschaften (FB 15) der

Johann Wolfgang Goethe - Universität als Dissertation angenommen.

Dekan:	Prof. Dr. Sven Klimpel
Gutachter:	Prof. Dr. Jörg Soppa
	Prof. Dr. Michael A. Rieger

Datum der Disputation:

Declaration

I herewith declare that I have not previously participated in any doctoral examination procedure in a mathematics or natural science discipline.

Frankfurt am Main, _____(Date) _____(Signature)

Weijia Yu

Author's Declaration

I herewith declare that I have produced my doctoral dissertation on the topic of "The functional and molecular role of transglutaminase 2 in hematopoietic stem and progenitor cells" independently and using only the tools indicated therein. In particular, all references borrowed from external sources are clearly acknowledged and identified. I confirm that I have respected the principles of good scientific practice and have not made use of the services of any commercial agency in respect of my doctorate.

Frankfurt am Main, _____(Date) _____(Signature)

Weijia Yu

Table of contents

Abbreviations

AGM	aorta-gonad-mesonephros
aHSC	active HSC
APL	acute promyelocytic leukemia
αTub	α-Tubulin
ATP	adenosine triphosphate
ATRA	all-trans retinoic acid
BM	bone marrow
BMMNC	bone marrow mononuclear cell
CDP	common dendritic progenitor
CLP	common-lymphoid progenitor
CMP	common-myeloid progenitor
CMV	cytomegalovirus
CO_2	carbon dioxide
DEG	differential expression gene
DBEC	distribution-based error correction
dHSC	dormant HSC
E	embryonic day
E. coli	*Escherichia coli*
ECM	extracellular matrix
ECS	epidermal cancer stem cell
EHT	endothelial-to-hematopoietic transition
ELP	early lymphoid progenitor
EPCR/CD201	endothelial protein C receptor
FACS	fluorescence-activated cell sorting
FC	fold change
FDR	false discovery rate
Flt3/CD135	FMS-like receptor tyrosine kinase-3
GDP	guanosine diphosphate
GMP	granulocyte-monocyte progenitor
GPCR	G protein-coupled receptor
GTP	guanosine triphosphate
HPT	hematopoietic tissue
HSC	hematopoietic stem cell
HSPC	hematopoietic stem and progenitor cell
HUVEC	human ubilical vein endothelial cells
i.p	intraperitoneally
i.v	intravenously
IGFBP	insulin-like growth factor binding protein
IL-	interleukin
IRES	Internal ribosome entry side
KO	knockout
LMPP	lymphoid-primed MPP

LRC	label-retaining cell
LSC	leukemic stem cell
LT-HSC	long-term repopulating HSC
MCS	multiple cloning site
MDP	monocyte–dendritic cell progenitor
MEP	megakaryocyte-erythroid progenitor
MOI	multiplicity of infection
MPP	multipotent progenitor
MSC	mesenchyme stem cell
NFkB	nuclear factor-kB
NK	natural killer cell
O_2	oxygen
ORF	open reading frame
PB	peripheral blood
PBMC	peripheral blood mononuclear cell
PC	principal component
PCA	principal component analysis
PDI	protein disulfide isomerase
polyIC	polyinosinic:polycytidylic acid
PPT	polypurine tract
PRE	post-transcriptional regulatory element
qPCR	quantitative polymerase chain reaction
RA	retinoic acid
Rb	retinoblastoma
RBC	red blood cell
RSEC	recursive substitution error correction
RSV	Rous Sarcoma Virus
Sca1	stem cell antigien 1
SFFV	spleen focus-forming virus
ST-HSC	short-term repopulating HSC
TGF-β	transforming growth factor β
Tgm2	transglutaminase 2
TNF	tumor necrosis factor
VSV	vesicular stomatitis virus
VSV-G	vesicularstomatitis virus G protein
WBC	white blood cell
WT	wild type
WTA	whole transcriptome analysis

List of Figures and Tables

Summary

Long-term repopulating hematopoietic stem cells (LT-HSCs) that reside in the bone marrow (BM) give rise to all blood cell types including erythrocytes, leukocytes and platelets. LT-HSCs are mainly quiescent during steady state hematopoiesis. LT-HSCs can process self-renewal to expand and maintain stemness, or commit to differentiation into short-term (ST) repopulating HSC and multipotent progenitors (MPPs). MPPs differentiate into oligopotent lineage-restricted progenitors which eventually produce all mature blood cell lineages, and thereby regenerate hematopoietic system.

Previous studies have shown in transcription profiles and quantitative PCR (qPCR) analysis that transglutaminase 2 (Tgm2) is one of the most upregulated genes in quiescent LT-HSCs in comparison to active HSCs, mobilized HSCs, ST-HSCs, MPPs, as well as leukemic stem cells (LSC). However, the reason why Tgm2 is strongly upregulated in dormant mouse LT-HSCs and what the role of Tgm2 is in LT-HSCs has not been investigated yet.

Tgm2, encoded by the *Tgm2* gene, is a multi-functional protein within the transglutaminase family. It has been found to be widely expressed inside and outside the cells. It consists of four domains and two functionally exclusive forms that are regulated by the Ca^{2+} and GTP concentration. Besides the most well-known transglutaminase enzymatic activity for transamidation, deamidation and crosslinking, Tgm2 acts also as a GTPase/ATPase, kinase, adhesion/scaffold protein, as well as disulfide isomerase. The role of Tgm2 in hematopoiesis remains elusive. Accordingly, the aim of this dissertation is to investigate the role of Tgm2 in murine hematopoiesis, especially in murine LT-HSCs.

Firstly, the expression of Tgm2 was analyzed in highly purified murine hematopoietic stem and progenitor cell (HSPC) populations. Low input label-free mass spectrometric proteomics and WES protein analysis confirmed the highly specific expression of Tgm2 in LT-HSCs at protein level. Already at the state of MPPs, Tgm2 protein was almost absent with further decline towards oligopotent progenitors. These results indicated Tgm2 as a specific protein marker for LT-HSCs, justifying the future generation of a fluorescent reporter mouse line based on endogenous Tgm2 tagging.

To delineate the functional and molecular role of Tgm2 in LT-HSCs, a conditional Tgm2 knockout mouse model was generated using the Mx1-Cre/*loxP* system, with the *loxP* sites flanking the coding exons of the catalytic domain of Tgm2. After PolyIC-mediated induction, a more than 95% knockout efficiency was observed in purified LT-HSCs and the protein expression of Tgm2 was confirmed to be vanished in the purified LT-HSCs from conditional Tgm2-KO mice. Conditional knockout mice are viable and show no aberrant organ functions.

In steady state condition, the distribution of mature blood cell lineages and immunophenotypically-defined HSPC populations within the BM, the mitochondrial potential of HSPCs reflected by the non-invasive cationic dye JC-1, as well as the cell cycle status of HSPCs mirrored by the intracellular Ki67 staining did not show any significant variations upon loss of Tgm2. However, the *in vitro* continuous observation of prospectivly isolated LT-HSCs by time-lapse microscopy-based cell tracking revealed a delayed entry into cell cycle with a two fold increased apoptosis rate after knocking out Tgm2, indicating Tgm2 expression might be essential for survival of LT-HSCs. Moreover, while the absence of Tgm2 in LT-HSCs did not influence differentiation and lineage choice *in vitro*, overexpression of Tgm2 in LT-HSCs resulted in an increase of the most immature subpopulation upon cultivation. All these features were not observed in Tgm2-deleted MPPs, suggesting Tgm2 playing a specific function at the level of LT-HSCs. Upon stress hematopoiesis, induced by the administration of 5-fluorouracil (5-FU), there was a trend towards delayed recovery of LT-HSCs lacking Tgm2. Although Tgm2 express specificly in LT-HSCs, two rounds of competitive BM serial transplantation displayed an equal overall engraftment and multi-lineage reconstitution of LT-HSCs from Tgm2-WT and Tgm2-KO mice in peripheral blood (PB), BM and spleens. Interestingly, LT-HSCs from Tgm2-KO mice reconstituted to more myeloid cells and fewer B cells in the first four weeks after primary transplantation, which disappeared at later time points.

Gene expression profiling and simultaneous single cell proteo-genomic profiling indicated that HSPCs and LT-HSCs from Tgm2-KO mice were transcriptionally more active. A heterogeneity of Tgm2 expression within Tgm2-WT LT-HSCs was revealed by single cell data. Commonly up-regulated genes in Tgm2-KO LT-HSCs and MPPs were significantly involved in regulation of transcription from RNA polymerase II promoter in response to stress, positive regulation of cell death as well as negative regulation of mitogen-activated protein kinase (MAPK) signaling pathways. In Tgm2-KO LT-HSCs, 136 up-regulated genes demonstrated an enrichment of genes involved in apoptosis, as well as negative regulation of MAPK signaling pathway.

Taken together, this dissertation shows that Tgm2 protein is highly specifically expressed in LT-HSCs, but not in subsequent progenitor populations. However, Tgm2 is not essential for differentiation and maturation of myeloid lineages, the proliferation and the long-term multi-lineage reconstitution potential of LT-HSCs after transplantation. Tgm2 might be involved in accurate stress response of LT-HSCs and the transition from LT-HSCs into MPPs, meaning that the absence of Tgm2 results in poor survival, myeloid bias upon transplantation, as well as slower recovery upon chemotherapeutic treatment.

Zusammenfassung

Die Hämatopoese beginnt in der Embryonalentwicklung und versorgt das Blutsystem während der gesamten Lebensspanne eines Organismus. Alle Blutzelltypen, einschließlich Erythrozyten, Leukozyten und Thrombozyten, entstehen aus Langzeit-repopulierenden hämatopoetischen Stammzellen (Englisch: long-term repopulating hematopoietic stem cells; LT-HSC), die sich im Knochenmark (Englisch: bone marrow; BM) befinden. LT-HSC stehen an der Spitze der hämatopoetischen Differenzierungshierarchie. In Homöostase befinden sie sich hauptsächlich in Quieszenz, d.h. ausserhalb des Zellzyklus. Sie sind jedoch die wirksame Population bei der Regeneration des Blutes unter Stressbedingungen, wie beispielsweise nach der Transplantation hämatopoetischer Stammzellen. Für eine Regeneration des Blutsystems verlassen ruhende LT-HSC die Quieszenz, sie entwickeln sich zu aktiv teilenden LT-HSC, um sich schnell zu vermehren und zu differenzieren. Im Anschluss kehren LT-HSC wieder in die Ruhephase zurück. Der Wechselprozess der LT-HSC zwischen Selbsterneuerung und Differenzierung wird streng reguliert, um sowohl die Erzeugung benötigter differenzierter Blutzellen als auch die Aufrechterhaltung der Zahl an HSC im Körper zu ermöglichen. Die Teilung von LT-HSC wird als Selbsterneuerung bezeichnet, wenn mindestens eine der Tochterzellen eine Stammzelle bleibt. LT-HSC verlieren die Fähigkeit zur Selbsterneuerung, sobald sie differenzieren, und wandeln sich in kurzzeit (Englisch: short-term; ST) repopulierende HSC und multipotenten Progenitorzellen (Englisch: multipotent progenitors; MPPs) um. MPP differenzieren sich in oligopotente Vorläuferzellen, zu denen Granulozyten-Monozyten-Vorläuferzellen (Englisch: granulocyte-monocyte progenitors; GMPs), gemeinsame myeloische Vorläuferzellen (Englisch: common-myeloid progenitors; CMPs), gemeinsame lymphoide Vorläuferzellen (Englisch: common-lymphoid progenitors; CLPs), sowie megakaryozyt-erythroide Vorläuferzellen (Englisch: megakaryocyte-erythroid progenitors; MEPs) u.a. gehören. Diese Vorläuferzellen entwickeln sich schließlich zu allen reifen Blutzelllinien und unterstützen die ständige Regeneration und Rekonstitution des Blutsystems.

Das hämatopoetische System der Maus ist wahrscheinlich das am besten verstandene adulte Stammzellsystem. Die prospektive Isolierung und Identifizierung von murinen LT-HSC, sowie anderer Progenitorzellpopulationen, wurde in den letzten fünf Jahrzehnten schrittweise mit der Identifizierung mehrerer Oberflächenmarker und Markergene etabliert. Die erste Errungenschaft bei der Identifizierung unreifer Populationen innerhalb von murinem BM ist das LSK-Kompartiment (Lineage-Sca1+cKit+), das vermehrt CD117 (cKit) und Stammzellantigen 1 (Englisch: stem cell antigen 1; Sca1) exprimiert, aber keine Marker für reife Blutzellen

aufweist. LT-HSC machen etwa 10 % des LSK Kompartiments aus. Aktuell erreicht die Markerkombination aus LSK und CD150+ CD34-/low CD48- die höchste Reinheit von LT-HSC in der sortierten Fraktion.

Frühere Studien haben in Transkriptionsprofilen und quantitativen PCR-Analysen (qPCR) gezeigt, dass Transglutaminase 2 (Tgm2) eines der am stärksten hochregulierten Gene in ruhenden LT-HSC ist, im Vergleich zu aktivierten HSC, mobilisierten HSC, ST-HSC, MPP, sowie leukämischen Stammzellen (Englisch: leukemic stem cells; LSCs). Warum Tgm2 in ruhenden LT-HSC der Maus stark hochreguliert ist und welche Rolle Tgm2 in LT-HSC spielt, ist jedoch noch nicht untersucht worden. Die Rolle von Tgm2 in der Hämatopoese ist weitgehend unbekannt. Dementsprechend ist das Ziel dieser Dissertation, die Rolle von Tgm2 in der murinen Hämatopoese, insbesondere in murinen LT-HSC, zu untersuchen.

Tgm2, das vom *Tgm2*-Gen kodiert wird, ist ein multifunktionales Protein aus der Familie der Transglutaminasen. Tgm2 ist sowohl innerhalb als auch außerhalb der Zelle lokalisiert und gilt als ubiquitär exprimiertes Protein. Es besteht aus vier Domänen: einem NH2-terminalen β-Sandwich, einem α/β-katalytischen Kern, der die katalytische Triade (Cys277, His335 und Asp358) für die Acyl-Transfer-Reaktion enthält, und zwei COOH-terminalen β-Fass-Domänen mit GTP-Bindungsstelle. Durch das Verschieben der beiden β-Fass-Domänen, um entweder die katalytische Domäne für die Ca2+-Bindung freizulegen oder zu maskieren, existieren bei Tgm2 zwei sich gegenseitig ausschließende funktionelle Formen. Diese bezeichnet man als offene bzw. geschlossene Konformation. Die offene Transamidase-aktive Konformation wird durch erhöhte Kalziumkonzentrationen gefördert, während die geschlossene GTP-gebundene Konformation in Bereichen mit verringerter Kalziumkonzentration, aber erhöhtem GTP-Gehalt, dominiert. Neben der bekanntesten enzymatischen Aktivität der Transglutaminase für Transamidierung, Desaminierung und Vernetzung von Proteinen fungiert Tgm2 auch als GTPase/ATPase, Kinase, Adhäsions-/Gerüstprotein sowie als Disulfid-Isomerase. Es wurden insgesamt vier verschiedene Spleißvarianten von Tgm2 beschrieben, bei denen die Sequenzen am C-Terminus verkürzt sind, sodass ein Teil der gesamten GTP-Bindungsstelle fehlt. Der Verlust des C-terminalen Endes wirkt sich auf ihre GTPase/ATPase-Aktivitäten, ihre Fähigkeit, Komplexe mit anderen Proteinen zu bilden, sowie auf ihre Stabilität und Position aus.

Die sich häufenden Daten aus verschiedenen Zelltypen sowie aus Studien an Krebs deuten darauf hin, dass Tgm2 an der Zellproliferation, Differenzierung, dem Überleben und der Apoptose von Zellen beteiligt ist. Die Rolle von Tgm2 in der Hämatopoese ist jedoch noch weitgehend unbekannt. Dementsprechend ist das Ziel dieser Dissertation, die Rolle von Tgm2 in der murinen Hämatopoese, insbesondere in murinen LT-HSC, zu untersuchen.

In dieser Arbeit wurde zuerst die Expression von Tgm2 in hochrein-sortierten murinen hämatopoetischen Stamm- und Vorläuferzellpopulationen (HSPC) analysiert. Low-Input-Massenspektrometrie und eine WES-Proteinanalyse bestätigten die hochspezifische Proteinexpression von Tgm2 in LT-HSC. Bereits im MPP-Stadium war das Tgm2-Protein fast nicht detektierbar. Diese Ergebnisse deuten darauf hin, dass Tgm2 ein spezifischer Proteinmarker für LT-HSC ist, was die zukünftige Generation einer fluoreszierenden Reporter-Mauslinie basierend auf endogenem Tgm2-Tagging rechtfertigt.

Um die funktionelle und molekulare Rolle von Tgm2 in LT-HSC zu beschreiben, wurde ein konditionales Tgm2-Knockout-Mausmodell unter Verwendung des Mx1-Cre/*loxP*-Systems generiert. Die *loxP*-Stellen flankieren die kodierenden Exons der katalytischen Domäne von Tgm2 und führen nach Deletion zum Verlust der Tgm2 Expression. Der Mx-1-Promotor wird nach der Injektion von Polyinosinsäure:Polycytidylsäure (Englisch: polyinosinic:polycytidylic acid; polyIC) Interferon-abhängig aktiviert und führt zur nachgeschalteten Expression der Cre-Rekombinase. Zur Erzeugung der konditionalen Knockout-Linie wurden jeden zweiten Tag drei Runden der PolyIC-Injektion durchgeführt, und alle Experimente wurden am zehnten Tag nach der letzten PolyIC-Injektion durchgeführt. Nach PolyIC-vermittelter Induktion wurde bei gereinigten LT-HSC eine Knockout-Effizienz von mehr als 95 % in LT-HSC gemessen. Konditionale Knockout-Mäuse sind lebensfähig und zeigt keine abweichenden Organfunktionen oder physiologische Veränderungen.

In Homöostase zeigte die Verteilung reifer Blutzelllinien und immunphänotypisch definierter HSPC-Populationen keine signifikanten Veränderungen. Der nicht-invasive, kationische Farbstoff JC-1, der das mitochondriale Potenzial widerspiegelt, zeigte ebenfalls keine Steigerung des mitochondrialen Potentials nach Tgm2-Deletion. Durch intrazelluläre Ki67-Färbung konnten keine Veränderungen des Zellzyklus-Status und des Anteils an quieszenten Zellen von LT-HSC und MPP nach Verlust der Tgm2-Funktion gemessen werden. In-vitro-Funktionsanalysen mittels Zeitraffermikroskopie und Einzelzelltracking mit prospektiv sortierten LT-HSC demonstrierten jedoch einen verzögerten Eintritt in den Zellzyklus mit einer zweifach erhöhten Apoptoserate nach dem Ausschalten von Tgm2. Der Zellzyklus von späteren Generationen oder von sortierten MPP blieb unverändert, was darauf hindeutet, dass die Tgm2-Expression für das Überleben von LT-HSC nach Differenzierungsinduktion wesentlich sein könnte. Darüber hinaus führte die Überexpression von Tgm2 in LT-HSC unter Verwendung von pseudotypisierten lentiviralen Partikeln des Vesikulären Stomatitis-Virus-G (VSVG) zu einem zweifachen Anstieg undifferenzierter HSPC bei In-vitro-Kultivierung. All diese Ergebnisse wurden bei sortierten MPP nicht beobachtet, was darauf hindeutet, dass Tgm2 in LT-HSC eine wichtige Rolle spielt. Die RNA-Sequenzierung deutet auf ein

unterschiedliches Genexpressionsprofil von LT-HSC oder MPP von Tgm2-WT- und Tgm2-KO-Mäusen hin. Die Analyse der differentiellen Expressionsgene (Englisch: differential expression genes; DEGs) hat gezeigt, dass die Zellen von Tgm2-KO-Mäusen transkriptionell stärker aktiviert sind und mehr Gene hochreguliert werden. Häufig hochregulierte Gene in Tgm2-KO LT-HSC und MPP (70 von 337 DEGs) sind maßgeblich an der Regulierung der Transkription vom RNA-Polymerase-II-Promotor als Reaktion auf Stress, an der positiven Regulierung des Zelltods, sowie an der negativen Regulierung der Mitogen-aktivierten Proteinkinase (Englisch: mitogen-activated protein kinase; MAPK)-Signalwege beteiligt. LT-HSC von Tgm2-KO Mäusen haben 136 hochregulierte Gene im Vergleich zu WT-LT-HSC. Prozess- und Signalweg-Anreicherungsanalysen dieser Gene zeigten eine signifikante Induktion von Apoptose, sowie eine negative Regulation des MAPK-Signalwegs. Darüber hinaus umfassen die signifikant angereicherten Signalwege von 271 hochregulierten Genen in Tgm2-KO-MPP eine positiv regulierte Gefäßsystementwicklung und Zellmigration. Dies bestätigt die unterschiedliche Funktion von Tgm2 in LT-HSC und MPP. Simultane proteogenomische Einzelzellsequenzierungsanalysen mittels des BD Rhapsody Systems von Tgm2-WT und Tgm2-KO LT-HSC und LSK haben eine Heterogenität der Tgm2-Expression innerhalb von Tgm2-WT LT-HSC gezeigt. LT-HSC mit hoher Tgm2-Expression zeigten auch eine hohe Expression von bekannten LT-HSC Genen wie Vwf und Mllt3. LT-HSC, die anfangen die Tgm2-Expression zu verlieren, zeigten eine erhöhte Genexpression, welche mit denen aus dem Genexpressionsprofil von Tgm2-KO LT-HSC und MPP übereinstimmt.

Knochenmarktransplantation, Infektion und Entzündung, chemotherapeutische Behandlung und Alterung lösen den hämatopoetischen Stresszustand aus. Ruhende LT-HSC werden durch Stressinduktion in den Eintritt des Zellzyklus getrieben, um die Produktion reifer myeloischer Zellen zu erhöhen. Bei der Stress-Hämatopoese haben Tgm2-WT- und Tgm2-KO-Mäuse gezeigt, dass sie ähnlich auf die Behandlung mit 5-Fluoruracil (5-FU) reagieren. Innerhalb verschiedener Kompartimente unreifer Stamm- und Vorläuferzellen wurden keine signifikanten Unterschiede zwischen Tgm2-WT- und Tgm2-KO-Mäusen über 15 Tage nach der Behandlung gezeigt. Die Messung an Tag 4 nach der Behandlung hat jedoch eine Tendenz zur verzögerten Erholung von LT-HSC ohne Tgm2 gezeigt. Obwohl Tgm2 spezifisch in LT-HSC exprimiert wird, zeigten zwei Runden kompetitiver serieller Knochenmarktransplantationen ein gleichmäßiges Angewachsen und langzeitliche Blutzellrekonstitution in peripherem Blut, BM und Milzen nach Transplantation von LT-HSC aus Tgm2-WT- und Tgm2-KO-Mäusen. Interessanterweise bildeten LT-HSC von Tgm2-KO-Mäusen in den ersten vier Wochen nach der Primärtransplantation mehr myeloische Zellen und weniger B-Zellen, Unterschiede, die zu späteren Zeitpunkten verschwanden.

Insgesamt zeigt diese Dissertation, dass das Tgm2-Protein hochspezifisch in LT-HSC exprimiert wird, aber nicht in nachfolgenden Vorläuferpopulationen. Tgm2 ist jedoch nicht essentiell für die Differenzierung und Reifung myeloider Linien, die Proliferation und das langfristige Rekonstitutionspotenzial von LT-HSC nach der Transplantation. Die Daten zeigen, dass Tgm2 an der Stressreaktion von LT-HSC und dem Differenzierungsübergang von LT-HSC zu MPP eine wichtige Rolle spielen kann. Dies bedeutet, dass das Fehlen von Tgm2 zu einem schlechteren Überleben von HSC nach Differenzierungsinduktion, einem Überhang an myeloischer Zelldifferenzierung nach Transplantation sowie einer langsameren Erholung nach einer chemotherapeutischen Behandlung führt.

1. Introduction

1.1. The hematopoietic system

Hematopoiesis – the formation of blood cells – starts during embryonic development and replenishes the blood system during the entire lifespan. Blood is a special type of connective tissue that is formed by plasma and different types of blood cells. The primitive hematopoiesis starts from embryonic day (E) 7.5, with the first primitive erythroid cell being given rise in yolk sac. Definitive blood initiates also in the yolk sac with the appearance of erythroid-myeloid progenitors and immune-restricted progenitors by E8.5 (Böiers et al. 2013; McGrath et al. 2015). By E10.5, the definitive hematopoietic stem cells (HSCs) that have the ability to fully repopulate the hematopoietic system are detected. They are first generated in the aorta-gonad-mesonephros (AGM) region (Medvinsky and Dzierzak 1996; Rybtsov et al. 2011). Interestingly, the locations of definitive HSCs are constantly changing throughout development. They migrate to the placenta and fetal liver soon after being generated in the AGM. Afterwards, they migrate to the spleen, and around birth to the bone marrow (BM), which remain the major sites of adult hematopoiesis (Bowie et al. 2007; Rieger and Schroeder 2012).

Approximately one trillion cells are regenerated daily in adult human BM (Doulatov et al. 2012). As many mature blood cell types are short lived, they have to be constantly replenished by new cells in order to balance the numbers of different blood cells in the circulation. Therefore, blood is one of the most regenerative and plastic tissues. Blood plasma (55% of the blood volume) contains all the dissolved nutrients, hormones, gases, wastes and ions as well as proteins. The rest of the blood volume consists of various hematopoietic cell types with different functions. Erythrocytes (red blood cells, RBCs) provide transportation of oxygen (O_2) and carbon dioxide (CO_2) through the whole circulation. Leukocytes (white blood cells, WBCs) comprise of granulocytes, monocytes and lymphocytes. Granulocytes consist of neutrophils, eosinophils and basophils that are responsible for infectious and allergic reactions. Monocytes replenish macrophages and dendritic cells. Lymphocytes are T-cells, B-cells and NK-cells that are involved in innate and adaptive immune responses. Platelets are also one type of blood cells that are generated from megakaryocytes. They can adhere to the endothelial cell lining of damaged blood vessels and help for blood clotting and wound healing. All blood cell types arise from HSCs, which are at the apex of the hematopoietic differentiation hierarchy. They differentiate through increasingly lineage-restricted progenitor cell intermediates which undergo a gradual fate restriction and lineage choice that finally generate the diverse mature functional blood cell types (Rieger and Schroeder 2012; Doulatov et al. 2012; Ng and Alexander 2017).

1.1.1. Identification of murine hematopoietic stem and progenitor cells

The murine hematopoietic system is probably the best understood adult stem cell system. The first discovery of murine hematopoietic stem and progenitor cell (HSPC) compartments goes back to 1956, when scientists realized that injecting unirradiated BM cells could recover animals from BM failure after lethal doses of irradiation (FORD et al. 1956; MCCULLOCH and TILL 1960) and these transplanted animals were restored in all blood cell types by the injected BM cells (H. S. Micklem and John F. Lontit 1966).

Clonal tracing, transplantation experiments as well as single cell RNA sequencing with prospective isolation of cells via flow cytometry have established the lineage-restricted hierarchies of HSCs (Wu et al. 1968; Kondo et al. 1997; Akashi et al. 2000; Nakorn et al. 2003). The initial achievement of identifying immature populations within murine BM is the immature multipotent cells express high CD117 (cKit) and stem cell antigen 1 (Sca1) (Spangrude et al. 1988b; Spangrude et al. 1988a; Uchida and Weissman 1992; Morrison and Weissman 1994; Osawa et al. 1996) but lack of BM mature lineage markers (Muller-Sieburg et al. 1986). This procedure identified an immature population called LSK. After that, stepwise identification of multiple surface markers and marker genes enabled the prospective identification and isolation of defined HSPCs using fluorescence-activated cell sorting (FACS)-based methods.

1.1.2. Murine hematopoietic hierarchy

As the starting population of hematopoiesis, HSCs represent about 10% of the LSK (Lineage$^-$ Sca1$^+$ cKit$^+$) compartment, which comprises multipotent HSPC populations at different degree of differentiation. The most immature stem cells are called long-term (LT) repopulating HSCs that reside in the BM and remain largely dormant. However, they are the operative population in blood repopulation upon stress-inducing conditions such as hematopoietic stem cell transplantation. They are the main contributors to long-term reconstitution of the whole blood system, and simultaneously maintain hematopoiesis after transplantation. A variety of strategies have been proposed to improve prospective LT-HSC identification, for instance, lack of FMS-like receptor tyrosine kinase-3 (Flt3, CD135) (Adolfsson et al. 2001; Adolfsson et al. 2005), expression of Endothelial protein C receptor (EPCR, CD201) (Kent et al. 2009), fluorescent dyes with efflux properties such as DNA-binding dye Hoechst 33342 (Goodell et al. 1996) as well as mitochondrial-binding dye rhodamine 123 (Kim et al. 1998). Currently, the marker combination of LSK CD150$^+$ CD34$^{-/low}$ CD48$^-$ reaches the highest purity of LT-HSCs in the sorted fraction (Osawa et al. 1996; Kiel et al. 2005; Yamamoto et al. 2013).

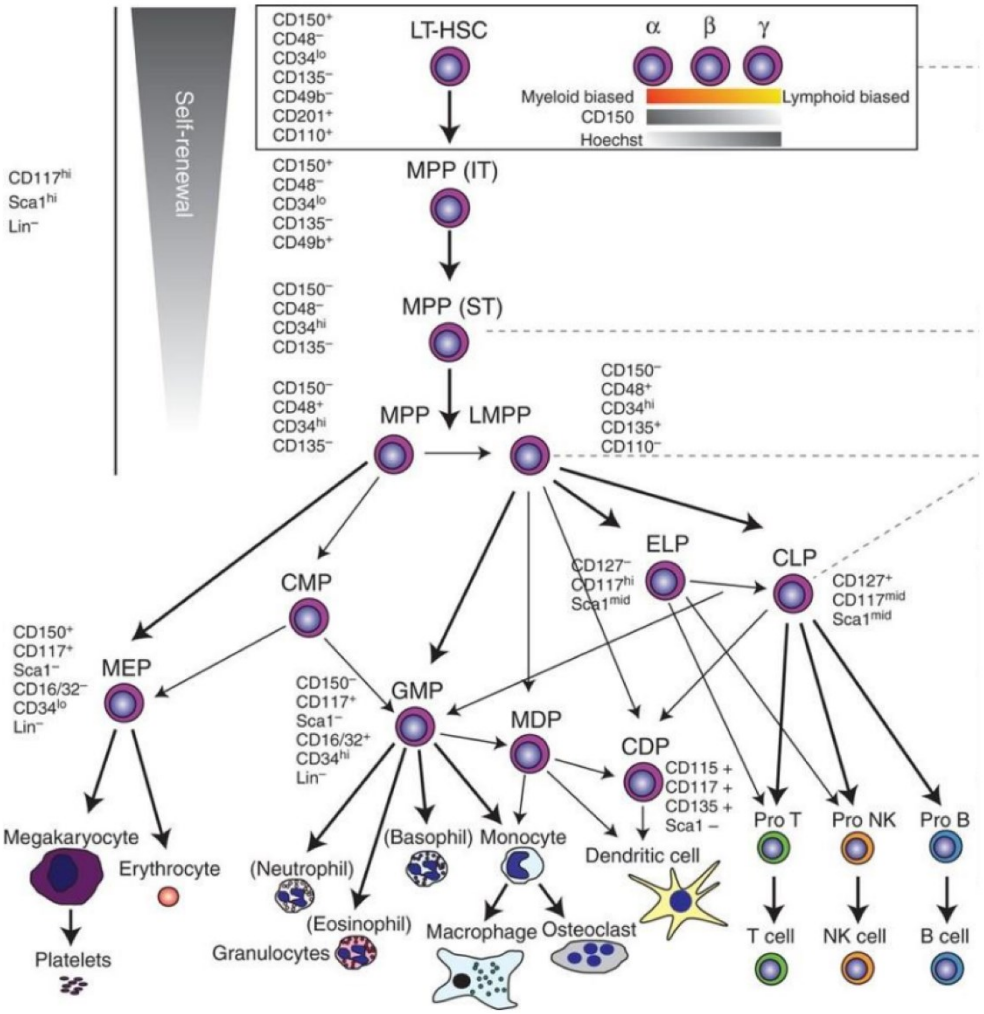

Figure 1 Differentiation hierarchy of murine hematopoiesis.

A detailed murine hematopoiesis is displayed. Hematopoiesis is a hierarchical process with LT-HSCs at the top. LT-HSCs produce MPPs which can further differentiated into lineage-restricted progenitors and consequently mature lineage cells. Different cell subsets can be distinguished and prospectively isolated base on their unique expression profiles of different combination of cell surface markers.

LT-HSC: long-term hematopoietic stem cell; MPP: multipotent progenitor; IT-: intermediate-term repopulating; ST-: short-term repopulating; LMPP: lymphoid-primed MPP; ELP: early lymphoid progenitor; CLP: common lymphoid progenitor; CMP: common myeloid progenitor; GMP: granulocyte–macrophage progenitor; MEP: megakaryocyte–erythrocyte progenitor; CDP: common dendritic progenitor; MDP: monocyte–dendritic cell progenitor; NK: natural killer cell. **Adapted and modified from (Rieger and Schroeder 2012)**

Dormant LT-HSCs can exit quiescence and progress to active LT-HSCs, which rapidly expand and differentiate to regenerate the blood system or return back to quiescence (Li and Bhatia 2011). The LT-HSCs' decision of processing self-renewal or differentiation is tightly regulated to enable both the generation of differentiated cells and the maintenance of the body HSC number (Rieger and Schroeder 2012). An LT-HSC division is called self-renewal, when at least one of the daughter cells remains a stem cell. The LT-HSCs lose the capacity for self-renewal once committed to differentiation and develop into short-term (ST) repopulating HSC and multipotent progenitors (MPPs). MPPs have been phenotypically characterized as LSK

CD150$^-$ CD34$^+$ cells. MPPs differentiate into oligopotent lineage-restricted progenitors which include cell types such as granulocyte-monocyte progenitors (GMPs), common-myeloid progenitors (CMPs), common-lymphoid progenitors (CLPs), as well as megakaryocyte-erythroid progenitors (MEPs) (Akashi et al. 2000; Yamamoto et al. 2013). These progenitor cells eventually commit to different mature lineage blood cells and support the regeneration and replenishment of the blood system (**Figure 1**).

1.1.3. Heterogeneity of murine HSPCs

Both LT-HSC and MPP compartments are functionally heterogeneous with regard to repopulating activity, self-renewal capacity and *in vitro* colony forming activity (Müller-Sieburg et al. 2002; Uchida et al. 2003; Muller-Sieburg et al. 2004; Sieburg et al. 2006; Wilson et al. 2008). Stem cell transplantation of FACS-isolated LT-HSCs exhibit erythroid-, myeloid- or lymphoid- biased lineage reconstitution patterns (Uchida et al. 2003; Muller-Sieburg et al. 2004; Sieburg et al. 2006; Dykstra et al. 2007). By using Hoechst dye efflux, myeloid-biased LT-HSCs and lymphoid-biased LT-HSCs could be purified (Challen et al. 2010). Different levels of CD150 expression may allow discrimination of LT-HSC sub-populations. Decreased expression of CD150 is associated with reduced erythroblast/megakaryocyte differentiation potential, while CD150 high cells displays barely detectable myeloid engraftment in primary-recipient mice but full reconstitution capability in the secondary-recipient mice (Morita et al. 2010). Similarly, transplantation of the LSK CD135$^+$ cells shows efficient but restricted lymphoid reconstitution potential, whereas the LSK CD135$^-$ cells support multi-lineage reconstitution (Adolfsson et al. 2001). More recently, a subset of LT-HSCs has been described as megakaryocyte-lineage primed HSCs (Rodriguez-Fraticelli et al. 2018), in line with previous transplantation studies on platelet-biased HSC subsets (Yamamoto et al. 2013; Haas et al. 2015).

MPPs have been also described with specific reconstitution potential and lineage restriction based on a stepwise gain of CD34, CD48, and CD135 as well as loss of CD150 expression (Adolfsson et al. 2001; Wilson et al. 2008; Cabezas-Wallscheid et al. 2014; Pietras et al. 2015). Recently, MPPs have been further described to be subdivided into MPP1-6 populations (MPP1: LSK CD34$^+$ CD135$^-$ CD150$^+$ CD48$^-$; MPP2: LSK CD34$^+$ CD135$^-$ CD150$^+$ CD48$^+$; MPP3: LSK CD34$^+$ CD135$^-$ CD150$^-$ CD48$^+$; MPP4: LSK CD34$^+$ CD135$^+$ CD150$^-$ CD48$^+$; MPP5: LSK CD34$^+$ CD135$^-$ CD150$^-$ CD48$^-$; MPP6: LSK CD34$^-$ CD135$^-$ CD150$^-$ CD48$^-$) (Sommerkamp et al. 2021). MPP1 is produced by LT-HSCs and in parallel differentiate into MPP2-4 with different kinetics and at variable levels depending on hematopoietic demands. Myeloid-biased MPP subsets MPP2 and MPP3 work together with lymphoid-primed MPP4 for blood production (Cabezas-

Wallscheid et al. 2014; Pietras et al. 2015). MPP5 have a close relationship with MPP1 as they both exhibit balanced lineage contribution upon transplantation and capability of generating MPP1-4 but not HSCs, while MPP6 cells represent with even higher multi-lineage potential compared to MPP5 (Sommerkamp et al. 2021). Notably, these different subdivided MPP1-6 most likely overlap with the previously described ST-HSCs and MPP subpopulations from different groups (Challen et al. 2021).

To address the heterogeneity and hierarchy of HSC and MPP subpoulations, multi-omics analysis including RNA sequencing and mass spectrometry have been applied for the investigation of finding reliable surface markers or marker genes. Intrinsic differences in gene expression profiles (*vWf*, *Rhob*, *Pld3*) selectively reflect discrepancies in LT-HSC self-renewal durability (Kent et al. 2009). Multipotent LT-HSCs with erythroid-megakaryocyte-lineage differentiation potential are expected to express *GATA-1* and *SCL/TAL-1* (Adolfsson et al. 2005). Consistently, MPP2 shows high expression levels of *Gfi1b*, *Gata1*, and *Fog1* indicating an active erythroid-megakaryocytic differentiation feature (Pietras et al. 2015).

1.1.4. Transcriptomic data reveals transglutaminase 2 (Tgm2) as a marker gene of murine LT-HSC

Previous studies have shown the strongly elevated and restricted Tgm2 gene expression in murine LT-HSCs. The transcription profiles of highly purified LT-HSCs, ST-HSCs and MPPs have revealed Tgm2 as one of the most upregulated genes in LT-HSCs (Forsberg et al. 2005). Later, they have further identified changes of gene expression in the HSC vs. MPP, mobilized vs. non-mobilized HSC, and leukemic (LSC) vs. non-leukemic (non-LSC) datasets and verified these results with quantitative PCR (qPCR). Tgm2 gene expression has been shown to be downregulated upon HSC differentiation, mobilization and leukemic transformation (Forsberg et al. 2010). Transforming growth factor β (TGF-β) signaling has been implicated in HSC quiescence. Tgm2, as one of the inducers of the TGF-β pathway, is elevated with increasing GFP label retention levels where TGF-β signaling is overrepresented in the GFP Hi upregulated gene sets. This work is done by using a GFP- label-retaining cell (LRC) system, in which high GFP in HSCs indicates a lower replication/division history (Qiu et al. 2014). Cabezas-Wallscheid et.al have identified a dormant HSCs (dHSCs) sub-population by a long-term label-retaining cell (LRC) approach with extremely low in vivo proliferation history and highest long-term reconstitution potential. By performing the whole transcriptome RNA sequencing analysis of dHSCs (LRCs), active HSCs (aHSC, non-LRCs), and MPP1, retinoic acid (RA)-induced signaling has been found to be highly enriched in dHSCs with Tgm2 as one of the target gene in RA pathway (Cabezas-Wallscheid et al. 2014). Moreover, Tgm2 has been

shown to be upregulated upon RA signaling agonist all-trans retinoic acid (ATRA) treatment (Cabezas-Wallscheid et al. 2017), which as a metabolite of Vitamin A is supportive for increasing the hematopoietic stemness in mice. A proteomic analysis of differential protein expression in HSCs and MPP1s has also been presented, in which Tgm2 has been shown to be significantly higher expressed in HSCs than in more differentiated MPP1 (Cabezas-Wallscheid et al. 2014).

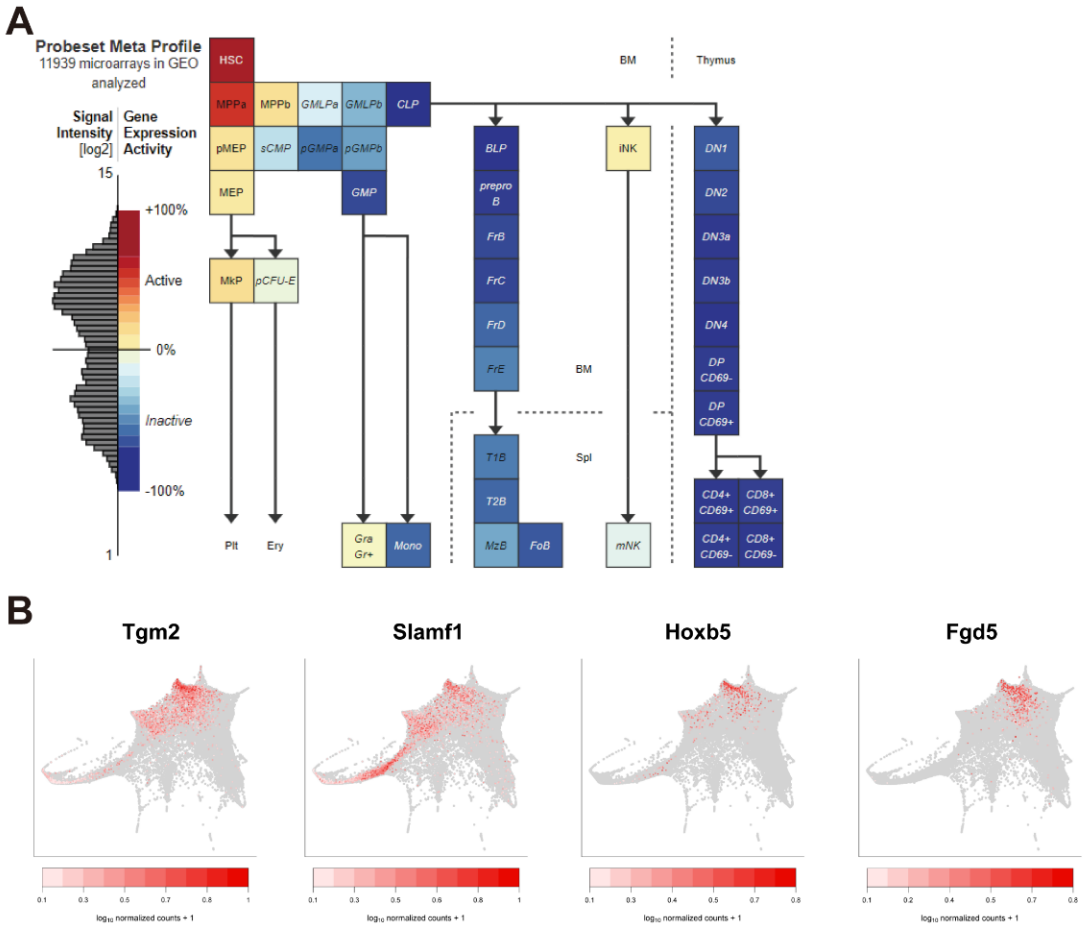

Figure 2 HSCs exhibit high Tgm2 expression at gene level.
(A) Expression levels of Tgm2 in murine hematopoietic system determined by the Gene Expression Commons (https://gexc.riken.jp/) (Seita et al. 2012). **(B)** Visualization of HSC marker gene expression patterns in the force-directed graph layout of the single-cell profiles (Dahlin et al. 2018).

In agreement with above mentioned studies, gene expression level has appeared to be the highest in HSCs when using the Gene Expression Commons (Seita et al. 2012) to search for Tgm2. Less amount of the gene has been expressed in the MPPs and MEPs, while the other progenitors and mature lineage cells have expressed almost non-detectable amount of the gene (**Figure 2A**). Furthermore, Dahlin et al. has generated a single-cell transcriptional landscape of 44,802 individual HSPCs including LSKs and LKs using a droplet-based sequencing method (Dahlin et al. 2018). *Fgd5* and *Hoxb5* have been described as HSC marker genes that specifically expressed within the HSC compartment (Gazit et al. 2014; Acar et al.

2015; Chen et al. 2016). Visualization of Tgm2 together with Slamf1 (coding for CD150), Hoxb5 and Fgd5 in the force-directed graph layout of the single-cell profiles (**Figure 2B**) displays an overlap, confirming a high Tgm2 gene expression in HSCs at single cell resolution.

However, the reason why Tgm2 is strongly upregulated in mouse dormant LT-HSCs and what the role of Tgm2 is in LT-HSCs has not been investigated yet.

1.2. Transglutaminase family

Transglutaminases (Tgase, TGs; EC2.3.2.13) represent a family of nine gene products, of which eight, factor XIII-A (FXIII-A) and transglutaminase 1-7, have enzymatic function, and one, Protein 4.2 (Band 4.2), is enzymatically inactive. The catalytic function of Tgase was first discovered in 1957 from guinea pig liver (Sarkar et al. 1957). All enzymatic active Tgases have an active catalytic triad, consisting of a cysteine, histidine and aspartate residue, and catalyze post-translational modification of proteins in a Ca^{2+} dependent manner. Despite all forms of Tgases have perceptible structural homology and similar function, their distributions, localizations as well as the mechanisms of action are different from each other. Over the last decades, the enzymes from this family have been extensively investigated to elucidate their structures and catalytic activities, tissular and cellular distributions and relevance to cell biology and diseases. Transglutaminase 2 (Tgm2) has been found to be present in the nucleus, cytoplasm, plasma membrane, and mitochondria, as well as outside the cell in the extracellular matrix (ECM) and exosome (Tatsukawa and Hitomi 2021). It is a multi-functional enzyme that involves in multiple biological processes.

1.2.1. The structure of Tgm2

Tgm2, encoded by the *Tgm2* gene, is a 76-kDa monomeric protein. The entire gene is composed of 13 exons and 12 introns (Mehta 2005). The human *TGM2* gene localizes at chromosome 20 while murine *Tgm2* gene localizes at chromosome 2, which is syntenic to human chromosome 20 (D'Amato et al. 1999). Availability of the protein's crystal structure (Liu et al. 2002; Pinkas et al. 2007; Han et al. 2010) facilitate the understanding of the reversible conformational changes of Tgm2 during the regulation of its activity. Tgm2 protein consists of four domains: an NH_2-terminal β-sandwich, an α/β catalytic core that contains the catalytic triad (Cys277, His335, and Asp358) for acyl-transfer reaction (Murthy et al. 2002), and two COOH-terminal β-barrel domains with GTP-binding site (**Figure 3**).

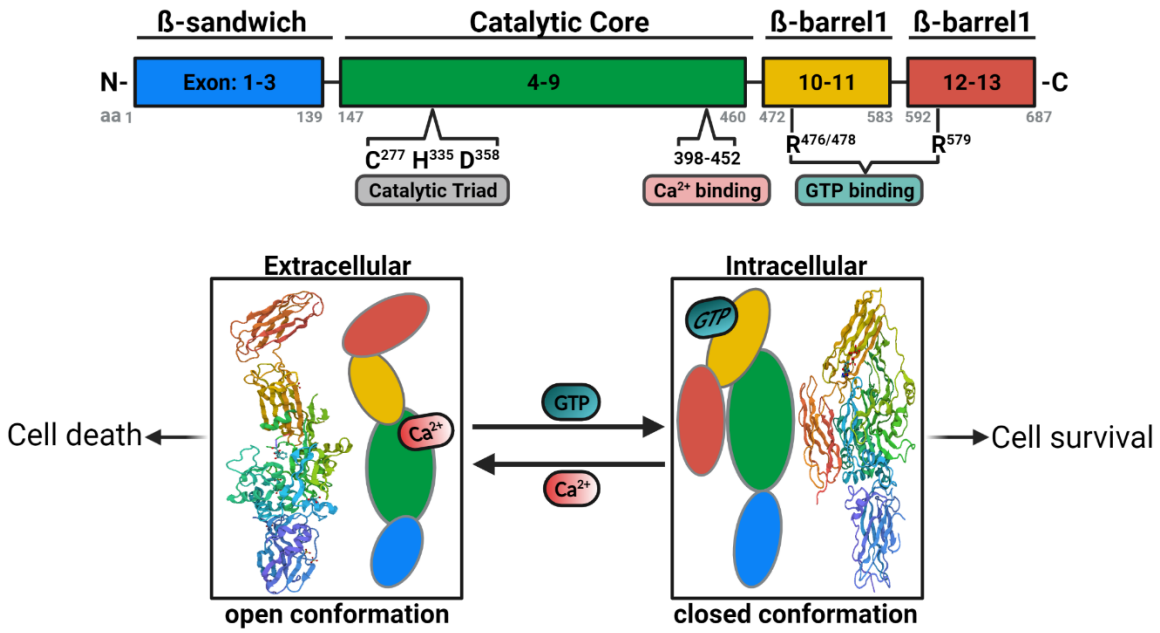

Figure 3 Structure of Tgm2.

The N-terminal β-sandwich is colored in blue. The catalytic core region is colored in green. Two C-terminal β- barrels are colored in yellow and red. (Upper) Exons and functional domains of Tgm2 are shown. Tgm2 gene encoding Tgm2 protein consists of 13 exons. The catalytic triad residues (C277, H335, and D358), Ca^{2+} binding site as well as GTP binding sites are displayed. (Below) 3D models and conformational changes of Tgm2 are indicated. The extracellular and intracellular activities of Tgm2 are regulated by Ca^{2+} and GTP concentration. Binding of Ca^{2+} results in the opened conformation and triggers transamidase activity that always results in cell death. Conversely, binding of GTP renders Tgm2 in the closed conformation which is often associated with cell survival. Figure generated in BioRender.

By moving the two β-barrel domains to expose or mask the catalytic domain for Ca^{2+} binding, Tgm2 exists in two mutually and functionally exclusive forms, so called open/closed conformations. The open transamidase-active conformation is favored in the elevated calcium concentration areas, while the closed GTP bound conformation is dominant in the decreased calcium concentration but increased GTP levels. Under physiological conditions, high levels of GTP and low Ca^{2+} keep Tgm2 in its closed conformation that masks the active site of transamidation (Gundemir et al. 2012). However, a calcium ion influx due to extreme stress or cell damage reduces the Tgm2-binding affinity for GTP or GDP (Datta et al. 2007), causing the exposure of the active site (Pinkas et al. 2007) and induces the open conformation. Considerably, the extracellular matrix normally has a lower GTP level and relatively higher Ca^{2+} level in comparison to the intracellular environment. As the switch between open and closed conformation is highly dependent on intracellular and extracellular GTP/GDP and calcium levels, the transamidase site is inactivated in the GTP bound form and GTP binding is inactivated in the calcium-bound form (Eckert 2019).

1.2.2. Multi-functional activity of Tgm2

Like the other family members, the most well-known function of Tgm2 is acting as transamidase in a Ca^{2+}-dependent manner. Under high calcium concentration condition, the structural conformation of Tgm2 is altered from closed to an open form that exerts crosslinking and transamidase activities (Begg et al. 2006). The catalytic reaction of Tgm2 is a two-step procedure. During the first step, a thioester bond is formed through the nucleophilic attack of the sulfur of the active site cysteine (C277) on an acyl-donor (the γ-carboxamide group of a protein glutamine residue). An ammonia molecule is released at this step as a byproduct. During the second step, a primary amine or water (which is the acyl-acceptor) attacks the thioester bond and results in either transamidation or deamidation. If the attacking group is a primary amine (either a small biological amine or the ε-group of a protein lysine residue), the reaction is called transamidation; if a water molecule serves as the acyl acceptor, it is called deamidation (Gundemir et al. 2012; Tatsukawa and Hitomi 2021). Transamidation leads to the formation of a covalent intra- or inter-molecular N^{ε}-(γ-glutamyl) lysine isopeptide bond and results in either amine incorporation, in which a primary amine is incorporated onto the glutamine side chain, or protein cross-linking, in which the glutamine residue is cross-linked to a lysine residue. The deamidation reaction leads to the conversion of the site-specific acyl-donor glutamine to a glutamate residue.

Besides the primary transglutaminase enzymatic activity, Tgm2 acts as a GTPase/ATPase that binds and hydrolyzes GTP and ATP when the intracellular Ca^{2+} concentration is low. Its GTPase activity participates in the transmembrane signaling of phospholipase Cδ as a component of α1B/α1D adrenergic, thromboxane A2, and oxytocin receptor (Nurminskaya and Belkin 2012). The transamidase and GTPase activities are mutually exclusive, whereas ATP binding is surprisingly resistant to Ca^{2+} and has no effect on the transamidase activity. The ATPase activity of Tgm2 is found predominantly in the regulation of mineralization of the ECM in osteoblasts (Nurminskaya and Belkin 2012).

Tgm2 has been described with an unexpected enzymatic function which results in phosphorylation of insulin-like growth factor binding protein (IGFBP)-3 on the surface of breast cancer cells (Mishra and Murphy 2004). Further investigations have revealed an intrinsic serine/threonine kinase activity to phosphorylate p53 tumor suppressor protein (Mishra and Murphy 2006), histone H1-4 (Mishra et al. 2006), and retinoblastoma (Rb) protein (Mishra et al. 2007).

As a protein that can be secreted to the cell surface and extracellular space, Tgm2 has been reported to promote the stabilization and deposition of ECM proteins through its crosslinking

activity. This is a function of Tgm2 which binds non-covalently to proteins and serves as enzymatic substrates for transamidation or cross-linking. For instance, Tgm2 forms a heterocomplex with fibronectin and interacts with intergrin and heparin surfate proteoglycans in a direct non-covalent interaction manner. Therefore, in addition to its enzymatic functions, the non-covalent interactions of Tgm2 implicate it in adapter/scaffold functions. Moreover, Tgm2 has been reported to demonstrate a protein disulfide isomerase (PDI) activity, which has been implicated in mitochondrial-dependent apoptosis (Hasegawa et al. 2003; Malorni et al. 2009).

1.2.3. Regulation of Tgm2 expression and its activity

The expression of Tgm2 is controlled mainly at transcriptional level. Tgm2 promoter contains response elements to inflammation and hypoxia that leading to an increased expression of Tgm2 (Jang et al. 2010). Tgm2 gene expression is also misregulated in cancer (Malkomes et al. 2021), where Tgm2 is often found to be overexpressed in cancer cells resistant to chemotherapy or with high metastatic potential. RA induces the expression of Tgm2 and promotes the cellular differentiation of neutrophil granulocytes through the heterodimer retinoid acid receptor (RAR)/retinoid X receptor (RXR) and transcription factor Sp1. Being described as a positive feedback loop, Tgm2 influences TGF-β activation and signaling, and in turn, TGF-β1 increases the expression of Tgm2 (Ritter and Davies 1998). Micro-RNA19 (miR-19) is shown to directly downregulate Tgm2 expression and enhance the invasion of colorectal cancer cells (Cellura et al. 2015). Furthermore, cytokines such as interleukin (IL)-1, IL6, nuclear factor-kB (NFkB) and tumor necrosis factor (TNF)-α also increase the expression of Tgm2 in various cell types (Kuncio et al. 1998; Johnson et al. 2001; Park et al. 2009; Jang et al. 2010; Frisdal et al. 2011).

Besides the above mentioned Ca^{2+} and GTP, which are known as a competitive activator and a suppressor of the change of Tgm2 conformation, other factors have also been shown to regulate the activity of Tgm2. Extracellular space is suitable for Tgm2 activity since the extracellular Ca^{2+} concentration is high and the GTP concentration is low. However, it has been reported that Tgm2 is kept to be catalytically inactive under a highly oxidative state due to the formation of disulfide bonds (Stamnaes et al. 2010), which can be reversed by thioredoxin (Jin et al. 2011). The interaction between Tgm2 and membrane lipid sphingosylphosphocholine reduces the Ca^{2+} requirement for Tgm2 activation (Lai et al. 1997). Last, SUMOylation can stabilize Tgm2 by inhibiting Tgm2 ubiquitination and enhances protein activity (Luciani et al. 2009). On contrary, S-nitrosylation has been reported to negatively regulate the activity of extracellular Tgm2, indicating that nitric oxide is a potential inhibitor of Tgm2 activation (Lai et

al. 2001). Tgm2 acetylation has been also reported to suppress its activity *in vitro* (Lai et al. 2010).

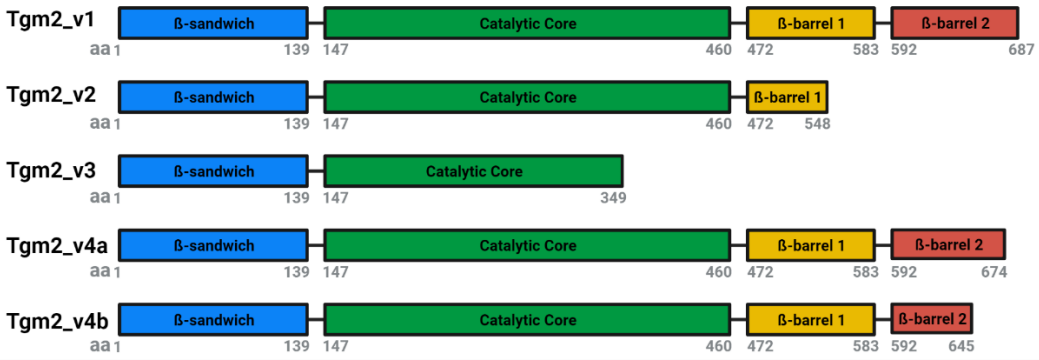

Figure 4 Schematic representation of different spliced isoforms of Tgm2.

Tgm2_v1 represents the full-length version, while Tgm2_v2, Tgm2_v3, Tgm2_v4a and Tgm2_v5b represent the four different spliced forms of Tgm2. The N-terminal β-sandwich is colored in blue. The catalytic core region is colored in green. Two C-terminal β- barrels are colored in yellow and red. The number represents the amino acid residues. Figure generated in BioRender.

Alternative splicing of Tgm2 is also involved in the regulation of the transamidase activity. Alternative splicing is an important mechanism for modulating gene functions and often causes a single gene to have multiple functions. Several splicing variants of Tgm2 are described with truncated and shortened sequences at the C-terminal, resulting in lacking part of the entire GTP-binding site (Lai and Greenberg 2013). Besides full length Tgm2, there have been in total four different spliced forms of Tgm2 reported (**Figure 4**). Gentile et al. (Gentile et al. 1991) reported the full-length Tgm2 transcript that encodes a polypeptide of 687 amino acids. Two alternative transcipts encoding Tgm2 protein isoforms were subsequently cloned from RA-induced human erythroleukemia cells, revealing open reading frames coding for a polypeptide of 548 amino acids (Fraij et al. 1992) and a polypeptide of 349 amino acids (Fraij and Gonzales 1996). Loss of the C-terminal GTP binding domain is the main feature of these two Tgm2 variants. Two further alternatively spliced forms of Tgm2 were detected and characterized in human ubilical vein endothelial cells (HUVEC), vascular smooth muscle cells and leukocytes (Lai et al. 2007). These two Tgm2 variants are generated through an atypical alternative splicing event resulting in proteins of similar mass to full-length Tgm2 but with alternative C-terminus. The C-terminal not only contains the GTP binding domain but also found to bind to the binding sites for G protein-coupled receptors (GPCRs) as well as the nuclear export signal peptide sequences that is important for intracellular localization. Thus, the loss of C-terminal residues affects their GTPase/ATPase activities, protein instability, their abilities to form complexes with other proteins as well as their locations. However, the roles of different spliced forms of Tgm2 remain unclear.

1.2.4. Tgm2 mouse model

Different mouse models have been generated to elute the *in vivo* function of Tgm2 (Iismaa et al. 2009). To investigate the role of Tgm2 in intracellular signaling pathways relevant to cardiac hypertrophy, a transgenic mouse model overexpressing rat Tgm2 cDNA in the heart under the control of the murine α-myosin heavy chain promoter has been generated (Small et al. 1999). Tgm2 has acted in the heart as transglutaminase and the overexpression of cardiac Tgm2 has resulted in a unique hypertrophy phenotype. Another transgenic mouse model overexpressing human Tgm2 in neurons and heart using the murine prion promoter has been more recently generated to study the role of Tgm2 in neurodegenerative conditions (Tucholski et al. 2006). This transgenic model has developed more intensive hippocampal neuronal damage under kainic acid treatment, which indicates for the first time that Tgm2 may play an active role in excitatory amino acid-induced neuronal cell death.

Two Tgm2 knockout mouse models have been reported by two different groups simultaneously. One model is developed by replacing part of exon 5 and all of exon 6, where the catalytic domain is localized, with a neomycin resistance gene (Laurenzi and Melino 2001). The other model is using the Cre/*loxP* system with *loxP* sites flanking introns 5 and 8 for deletion of exons 6 to 8 of the catalytic core (Nanda et al. 2001) to generate a conditional model. Both knockout models showed absence of Tgm2 protein in homozygote progeny.

Tgm2 knockout mice have been shown with decreased NFkB activation after lipopolysaccharide-induced septic shock (Falasca et al. 2008), reduced infiltration of macrophages and myofibroblasts, decreased collagen synthesis, reduced TGF-β activation, as well as decreased hepatic transglutaminase activity but normal liver fibrosis (Shweke et al. 2008). Furthermore, Tgm2 knockout mice have been described with a delayed corneal wound closure (Tong et al. 2013) and reduced hepatocyte apoptosis and Sp1 cross-linking following ethanol treatment (Tatsukawa et al. 2009). However, no lethal effect has been proposed in Tgm2 knockout models.

1.2.5. Tgm2 in cellular processes

Although Tgm2 knockout mouse models show no obvious abnormal phenotype, accumulating data suggest the involvement of Tgm2 in cell proliferation, differentiation, survival and apoptosis. In hamster fibrosarcoma cells, Tgm2 is found to affect the progression through the cell cycle from S phase to G2/M phase on the GTPase dependent activity (Mian et al. 1995). In endothelial cells, downregulation of Tgm2 expression leads to cell cycle arrest associated with increased cyclin E expression and decreased cyclin B levels (Nadalutti et al. 2011). Tgm2

has been demonstrated to amplify cell growth by down-regulating the tumor suppressor phosphatase PTEN and causing the activation of Akt1 pathway (Verma et al. 2008).

Tgm2 is playing a role in cell survival and apoptosis, which is debated in the field. It is well acknowledged that Tgm2 is acting either as a facilitator or attenuator of the apoptotic process (Fésüs and Szondy 2005). Many groups have been reported that Tgm2 sensitizes cells to apoptosis when its transamidating activity is turned on; in contrast, it is protective when its transamidating activity is inactive (Antonyak et al. 2001; Tucholski and Johnson 2002; Milakovic et al. 2004). Studies on the oxidative stress-induced cell death have shown that high reactive oxygen species (ROS) level triggers Ca^{2+} influx resulting in Tgm2 activation and cell death (Fésüs and Szondy 2005; Iismaa et al. 2009). Conflictingly, Tgm2 has been shown to be upregulated in various cancer cell types and the overexpression of Tgm2 supports cancer progression, cell survival and drug resistance (Agnihotri and Mehta 2017). For example, Tgm2 overexpression increases Akt1 activity and promotes cell survival, motility, and associated with drug resistance in cancer cells (Verma and Mehta 2007). Tgm2 exhibits a pro-survival effect in hypoxic cancer cells by mediating inhibition of cross-linked caspase-3 as well as mitochondria membrane depolarization in response to Ca^{2+} overload (Cho et al. 2010). Similarly, Tgm2 depletion in endothelial cells resulted in cell-cycle arrest and apoptosis (Nadalutti et al. 2011). Study from our laboratory has observed an induction of Caspase-3-driven apoptosis after Tgm2 ablation in colorectal carcinoma cells (Malkomes et al. 2021). Therefore, the complex regulation between the pro-survival and pro-apoptotic activities of Tgm2 is dependent from the conformation, cell types as well as stressor types.

Increased Tgm2 expression promotes differentiation of stem cells toward certain lineages. For example, overexpressing Tgm2 in BM-derived mesenchyme stem cells (MSCs) promotes progression into cardiomyocyte-like cells (Song et al. 2007). Deficient of Tgm2 expression in epidermal cancer stem cells results in an activation of apoptosis and reduction of cancer stem cell survival and migration (Fisher et al. 2015). Tgm2 expression has also been linked to the stem cell-like phenotype in ovarian cancer (Cao et al. 2012) and for mammary epithelium (Kumar et al. 2011). Thus, additional studies addressing the role of Tgm2 in stem cell phenotypes and differentiation are of high interest.

1.3. Tgm2 in hematopoiesis and HSCs

The role of Tgm2 in hematopoiesis remains largely unknown. The first evidence revealing potential functions of Tgase in hematopoiesis is investigated in crustaceans. It has been shown that Tgase, whose activity is affected by ROS level in hematopoietic tissue (HPT) cells of the crayfish *Pacifastacus leniusculus* (Junkunlo et al. 2016), is maintaining the HPT cells in an

undifferentiated stage (Lin et al. 2008). Blocking Tgase mRNA expression or inhibiting Tgase activity with cystamine injection promotes the HPT differentiation and the delivery of HPT progenitor cells into the peripheral circulation (Lin et al. 2008; Junkunlo et al. 2018). In the mammalian system, only a few studies focused on Tgm2 in blood cells. High level of Tgm2 is expressed and activated on the surface of macrophages and dendritic cells differentiated *ex vivo* from human peripheral blood mononuclear cells (PBMCs) during the differentiation process (Hodrea et al. 2010). Also, Tgm2 expression limits the physiological B cell response to an axegenous protein antigen and regulate humoral immune response (Kim et al. 2012). Moreover, Tgm2 has been demonstrated to present an increased expression on mouse splenic T cells from naïve T cells to activated T cells and the absence of Tgm2 leads to a decreased T-cell proliferation *in vitro* (Kim et al. 2014a). These suggests a role of Tgm2 in dendritic cell activation and B cell differentiation after immunization, as well as T cell activation and proliferation.

In malignant hematopoiesis, all-trans retinoic acid (ATRA) treated acute promyelocytic leukemia (APL) cells NB4 harbor induction of Tgm2 gene expression, which programs differentiating APL cells to an inflammatory stage (Jambrovics et al. 2018). Proteomic analysis on the effects of a range of leukemogenic oncogenes has shown that the Tgm2 is expressed at greater levels as a consequence of oncogenic transformation and its expression is higher at relapse than diagnosis in many cases. This may lead to the protection of the leukemic stem cell due to increased adhesion/reduced motility (Pierce et al. 2013). Therefore, Tgm2 may be a potential target in leukemia treatment.

Besides the fact that Tgm2 is highly elevated in murine HSCs at transcripts level, Tgm2 has recently been described to be involved in the HSC homeostasis by showing an impaired RhoA/ERK1/2 pathway in the absence of Tgm2, displaying a decreased rate of differentiation of BM HSCs in the Tgm2 knockout mice which is very likely due to the Tgm2-dependent impairment of autophagy (Oliverio et al. 2020). However, it has to be mentioned that the surface markers to identify HSC in this study are not the common markers combination described in **2.2.2.3**, which leaves some doubt of the cell population that they have actually analyzed.

1.4. Aim of the study

Our laboratory has a long-standing history in studying the function of Tgm2 in colorectal cancer. Therefore, many different genetic tools as well as technical approaches have been already established. In this project, the role of Tgm2 in murine hematopoiesis especially murine LT-HSCs is studied.

Firstly, the conditional Tgm2 knockout mouse model has been created with the Mx1-Cre/*loxP* system. A gene-targeting construct is generated, where *loxP* sites are inserted and flank the catalytic core domain of Tgm2. This mouse model is used for studying the loss of function of Tgm2 in hematopoiesis. Secondly, in order to investigate the physiological function of Tgm2, *in vitro* and *in vivo* experiments have been performed with gain or loss of Tgm2 function LT-HSCs as well as MPPs and analyze how these cells behave in cell proliferation, cell differentiation, and most importantly, the response in stress hematopoiesis. The Tgm2 overexpression is performed with a lentiviral plasmid for lentiviral gene transfer, coding for murine Tgm2 and the fluorescent reporter VENUSnucmem behind an internal ribosomal entry site (IRES) domain, driven by a spleen focus-forming virus (SFFV) promoter. Thirdly, as Tgm2 has various functions in cells, with the help of transcriptomic analysis, the molecular mechanism of Tgm2 in LT-HSCs and MPPs is investigated with the conditional knockout mice. Furthermore, due to the fact that the high Tgm2 mRNA expression leads to the specific Tgm2 protein expression in LT-HSCs, a reporter mouse line is being designed and the generation is ongoing, which might serve as a valuable tool for different aspects of Tgm2 related studies.

2. Materials and Methods

Most of the methods used in this project are established standard protocol from Prof. Dr. Michael Rieger's laboratory (Department of Medicine, Hematology/Oncology, Goethe University Hospital Frankfurt am Main, Germany). Methods adopted from published articles are cited accordingly.

2.1. Materials

2.1.1. Chemicals and Reagents

Table 1 Chemicals and reagents

Reagent	Company
Draq7™	BD Biosciences, Franklin Lakes, USA
HDGreen™ Plus DNA Stain	Intas,Göttingen, Germany
Poly(I:C) HMW	InvivoGen, San Diego, USA
5-Fluorouracil 50 mg/ml	Medac, Wedel, Germany
Ampicilin (sodium salt)	Roth, Karlsruhe, Germany
Isopropanol	Roth, Karlsruhe, Germany
Bovine serum albumin (BSA)	Sigma Aldrich, St.Louis, USA
Dimethyl sulfoxide (DMSO)	Sigma Aldrich, St.Louis, USA
Ethanol puriss. P.a., absolute ≥99.8% (GC)	Sigma Aldrich, St.Louis, USA
Sodium azide (NaN3) ≥99%, p.a.	Sigma Aldrich, St.Louis, USA
Sodium Chloride (NaCl)	Sigma Aldrich, St.Louis, USA
Calcein AM	Thermo Fisher Scientific, Waltham, USA
Pierce Protease and Phosphatase Inhibitor Mini Tablets	Thermo Fisher Scientific, Waltham, USA
Agarose, universal	VWR, Leuven, Belgium

2.1.2. Buffers and solutions

Table 2 Buffers and solutions

Buffer/Solution	Catalog No.	Company/Components
10% FBS Buffer	-	1x PBS + 10% FBS
FACS buffer	-	1xPBS, 10 % FBS, 1mM EDTA, 0.1% Sodium Azide, stored at 4°C

BSA stock solution (10%)	-	10 g BSA in 100 ml PBS, stored at 4°C
Alkaline lysis buffer	-	25mM NaOH, 0.2mM EDTA, pH=12.0, stored at room temperature (RT)
Neutralizing buffer	-	40mM Tris-HCl, pH=5.0, stored at RT
BD Horizon™ Brilliant Stain Buffer	563794	BD Biosciences, Franklin Lakes, USA
BD Pharm lyse™ Lysing Buffer	555899	BD Biosciences, Franklin Lakes, USA
BD Pharmingen™ Stain Buffer (FBS)	554656	BD Biosciences, Franklin Lakes, USA
HEPES solution 1M, pH 7.0-7.6	H0887	Sigma Aldrich, St.Louis, USA
Histopaque®-1083	10831	Sigma Aldrich, St.Louis, USA
Tris Actate-EDTA buffer, 10x concentrate	T9650	Sigma Aldrich, St.Louis, USA
StemSpan™ serum free expansion medium (SFEM)	09650	StemCell Technologies, Vancouver, Canada
16% Formaldehyde Solutio (w/v), Methanol-free	28908	Thermo Fisher Scientific, Waltham, USA
Gibco™ 10x phosphate-buffered saline (PBS) (without Mg2+ and Ca2+)	14080	Thermo Fisher Scientific, Waltham, USA
Gibco™ 1x phosphate-buffered saline (PBS) (without Mg2+ and Ca2+)	14190	Thermo Fisher Scientific, Waltham, USA
Gibco™ Fetal Bovine Serum	10270	Thermo Fisher Scientific, Waltham, USA
Gibco™ L-Glutamine 200mM (100 x)	25030	Thermo Fisher Scientific, Waltham, USA
Gibco™ Pen Strep	15140	Thermo Fisher Scientific, Waltham, USA
Gibco™ 0.25% Trpsin-EDTA (1 x)	25200	Thermo Fisher Scientific, Waltham, USA
Gibco™ Trypan Blue Stain (0.4%)	15250	Thermo Fisher Scientific, Waltham, USA
Invitrogen™ 10x Permeabilization Buffer	00-8333-56	Thermo Fisher Scientific, Waltham, USA
Invitrogen™ EDTA solution 0.5M, pH 8.0	AM9260G	Thermo Fisher Scientific, Waltham, USA
Invitrogen™ Fixation Per Diluent	00-5223-56	Thermo Fisher Scientific, Waltham, USA
Invitrogen™ Fixation/Permeabilization concentrate	00-5123-43	Thermo Fisher Scientific, Waltham, USA
Invitrogen™ UltraPure™ Distilled Water	10955	Thermo Fisher Scientific, Waltham, USA
M-PER™ Mammalian Protein Extraction Reagent	78501	Thermo Fisher Scientific, Waltham, USA

2.1.3. Kits

Table 3 Kits

Kit	Catalog No.	Company
High Sensitivity D1000 Reagent	5067-5585	Agilent Technologies, St.Clara, USA
High Sensitivity D1000 ScreenTape	5067-5584	Agilent Technologies, St.Clara, USA
BD Rhapsody™ Cartridge Kit	633733	BD Biosciences, Franklin Lakes, USA
BD Rhapsody™ Cartridge Reagent Kit	633731	BD Biosciences, Franklin Lakes, USA
BD Rhapsody™ cDNA kit	633773	BD Biosciences, Franklin Lakes, USA
BD Rhapsody™ WTA Amplification Kit	633801	BD Biosciences, Franklin Lakes, USA
BD™ single-Cell Multiplexing Kit Mouse Immune Sample Tag	633793	BD Biosciences, Franklin Lakes, USA
AMPure XP	A63881	Beckman Coulter, Brea, USA
NextSeq 2000 P3 Reagents (200 Cycles)	20040560	Illumina, San Diego, USA
NextSeq 500/550 High Output Kit v2.5 (150 Cycles)	20024907	Illumina, San Diego, USA
NucleoBond® Xtra Maxi EF	740424.50	Macherey-Nagel GmbH, Düren, Germany
NucleoSpin® Gel and PCR Clean-Up	740609.50	Macherey-Nagel GmbH, Düren, Germany
12-230 kDa Jess or Wes Separation Module, 8 x 25 capillary cartridges	SM-W004	Protein Simple, San Jose, USA
Anti-Rabbit Detection Module for Jess, Wes, Peggy Sue or Sally Sue	DM-001	Protein Simple, San Jose, USA
miRNeasy Micro Kit	74004	QIAGEN GmbH, Hilden, Germany
QIAamp DNA blood mini kit	51306	QIAGEN GmbH, Hilden, Germany
EasySep™ Mouse Biotin Positive Selection Kit II	17665	StemCell Technologies, Vancouver, Canada
SMART®-Seq HT Kit	634455	Takara, San Jose, USA
Invitrogen MitoProbe™ JC-1 Assay Kit	M34152	Thermo Fisher Scientific, Waltham, USA
Invitrogen UltraComp eBeads™ Compensation Beads	01-2222-42	Thermo Fisher Scientific, Waltham, USA
Phire™Tissue Direct PCR Master Mix	F-170L	Thermo Fisher Scientific, Waltham, USA
Phusion Blood Direct PCR Master Mix	F-175L	Thermo Fisher Scientific, Waltham, USA
Qubit™ Protein Assay Kit	Q33211	Thermo Fisher Scientific, Waltham, USA

Qubit™dsDNA HS Assay Kit	Q32851	Thermo Fisher Scientific, Waltham, USA

2.1.4. Primers

Table 4 Primers and sequences

Primer name	Sequence	Tm
Murine Tgm2 P1 forward	GTTTAACCATGAATCAGGATG	56 °C
Murine Tgm2 P2 forward	GGCAAGGTCTGAGAAAGCAC	63 °C
Murine Tgm2 P3 reverse	GACAAAGGAGCAAGTGTTAC	58 °C
Cre forward	AAATTGCCAGGATCAGGGTTAAAG	63 °C
Cre reverse	AGAGTCATCCTTAGCGCCGTAAAT	65 °C

2.1.5. Lentiviral plasmids

Table 5 Lentiviral plasmids and descriptions

No.	Plasmid name	Discription	Reference
495	pMD2.G.VSV-G	Expression plasmid for VSV-G (*env*); pseudotyping of lentiviral particles; CMV promoter	(Yee et al. 1994), also **Appendix Figure 42**
393	pMDLg.HIVGag-Pol.pRRE	Expression plasmid for structural genes (*gag/pol*) of HIV-1; for lentiviral particle assembly; CMV promoter	(Dull et al. 1998), also **Appendix Figure 42**
392	pRSV.HIV-REV	Expression plasmid for lentiviral reverse transcriptase (*rev*) of HIV-1; driven by RSV promoter	(Dull et al. 1998), also **Appendix Figure 42**
5105	pRRL.PPT.SFFV.MCS.IRES-VENUSnucmem.PRE	Plasmid vector with a 5' packaging signal for lentiviral gene transfer; coding for a fusion protein of hImportin and the fluorescent protein VENUS behind an IRES domain; driven by SFFV promoter	See **Appendix Figure 43**
5537	pRRL.PPT.SFFV.mTgm2.IRES.VENUSnucmem.PRE	Plasmid vector with a 5' packaging signal for lentiviral gene transfer; coding for murine Tgm2 and a fluorescent reporter VENUSnucmem behind an IRES domain; driven by SFFV promoter	Cloned from pRRL.PPT.SFFV.MCS.IRES.VENUSnucmem. PRE, also **Appendix Figure 43**
5538	pRRL.PPT.SFFV.mCherry-linker-mTgm2.IRES.VENUSnucmem.PRE	Plasmid vector with a 5' packaging signal for lentiviral gene transfer; coding for murine Tgm2 linked with mCherry fluorescent protein and a fluorescent reporter VENUSnucmem behind an IRES domain; driven by SFFV promoter	Cloned from pRRL.PPT.SFFV.MCS.IRES.VENUSnucmem.PRE, also **Appendix Figure 43**

VSV: vesicular stomatitis virus; VSV-G: Vesicularstomatitis virus G protein; CMV: Cytomegalovirus; RSV: Rous sarcoma virus; IRES: Internal ribosome entry side; PPT: polypurine tract; SFFV: spleen focus-forming virus; PRE: post-transcriptional regulatory element.

2.1.6. Conjugated Antibodies

Table 6 Fluorochrome-conjugated antibodies

Antibody	Clone	Fluorchrome	Company	Catalog No./Identifier
anti-mouse CD3e	145-2C11	Biotin	eBioscience™	Cat. #13-0031-82; RRID:AB_466319
anti-mouse CD3	17a2	AF647	Biolegend	Cat. #100209; RRID:AB_389323
anti-mouse CD19	eBio1D3 (1D3)	Biotin	eBioscience™	Cat. #13-0193-82; RRID:AB_657656
anti-mouse B220	RA3-6B2	Biotin	eBioscience™	Cat. #36-0452-85; RRID:AB_469753
	RA3-6B2	PE	Biolegend	Cat. #12-0452-82; RRID:AB_465671
anti-mouse CD11b/Mac1	M1/70	Biotin	eBioscience™	Cat. #13-0112-82; RRID:AB_466359
	M1/70	BV605	Biolegend	Cat. #101237; RRID:AB_11126744
anti-mouse Gr1	RB6-8C5	Biotin	eBioscience™	Cat. # 13-5931-86; RRID:AB_466802
	RB6-8C5	PE-Cy7	eBioscience™	Cat. #25-5931-82; RRID:AB_469663
anti-mouse Ter119	TER-119	Biotin	eBioscience™	Cat. #13-5921-82; RRID:AB_466797
	TER-119	APC-eF780	eBioscience™	Cat. #47-5921-82; RRID:AB_1548786
anti-mouse CD11a	M17/4	APC	Biolegend	Cat. #101120; RRID:AB_2562779
anti-mouse CD16/32	2.4G2	V450	BD Horizon™	Cat. #560539; RRID:AB_1645268
anti-mouse CD41a	eBioMWReg30	Biotin	eBioscience™	Cat. #13-0411-82; RRID:AB_763484
	eBioMWReg30	APC-eF780	eBioscience™	Cat. #47-0411-82; RRIE:AB_2573958
anti-mouse Sca-1	D7	PerCp-Cy5.5	eBioscience™	Cat. #45-5981-82; RRID:AB_914372
	D7	BV510	Biolegend	Cat. #108129 RRID:AB_2561593
anti-mouse CD48	HM48-1	FITC	Biolegend	Cat. #103404; RRID:AB_313019

	HM48-1	APC-Cy7	Biolegend	Cat. #103432; RRID:AB_2561463
anti-mouse CD117/cKit	2B8	PE-Cy7	Biolegend	Cat. #105814; RRID:AB_313223
	2B8	BV421	Biolegend	Cat. #105828; RRID:AB_11204256
anti-mouse CD150	TC15-12F12.2	PE	Biolegend	Cat. #115904; RRID:AB_313683
	TC15-12F12.2	PE-Cy7	Biolegend	Cat. #115927; RRID:AB_11204248
anti-mouse CD34	clone RAM34	eF660	eBioscience™	Cat. #50-0341-82; RRID:AB_10596826
Fixable viability dye	-	eF506	eBioscience™	Cat. #65-0866-14
	-	eF780	eBioscience™	Cat. #65-0865-14
anti-mouse CD201	eBio1560	PE	eBioscience™	Cat. #16-2012-83 RRID:AB_657696
anti-mouse CD45.1	A20	eF450	eBioscience™	Cat. #48-0453-82; RRID:AB_ 1272189
anti-mouse CD45.2	104	PerCP-Cy5.5	eBioscience™	Cat. #45-0454-82; RRID:AB_953590
	104	BV650	Biolegend	Cat. #109835; RRID:AB_11203374
Streptavidin	-	APC-eF780	eBioscience™	Cat. #47-4317-82
	-	BV711	BD Horizon™	Cat. #563262; RRID:AB_2869478
Ki67	SolA15	PE-Cy7	eBioscience™	Cat. #25-5698-82; RRID:AB_11220070
7-AAD	-	-	BD Pharmingen™	Cat. #559925 RRID:AB_2869266

2.1.7. BD™ AbSeq Antibody-oligonucleotide conjugates

Table 7 AbSeq oligonucleotides

AbSeq	Clone	Sequence ID	Barcode sequence
Rat Anti-Mouse CD1d	1B1	AMM2067	GTGAGCGGTAGGTTAGTAAATCGGTATGTGGAAGTC
Rat Anti-Mouse CD2	RM2-5	AMM2251	GTTGAATGGCGGAATGTTGGACTTAGCTTGGTATGC
Rat Anti-Mouse CD3 Molecular Complex	17A2	AMM2117	ATTCGGCGAGAGATTATGTGTTGCGTGTGGTTAGGT
Hamster Anti-Mouse CD3	145-2C11	AMM2001	GAGATAGGCTAGTTGGATAATTGCGCGGTGAGAGTC

Rat Anti-Mouse CD4	RM4-5	AMM2002	GTTTAGCGTAGGGTGCATTAGAG CGAGTTAGCGAGT
Rat Anti-Mouse CD5	53-7.3	AMM2043	TCGGAGTTGCGGTAATTAGTATAT CTTTCGGAGGCC
Rat Anti-Mouse CD6	J90-462	AMM2228	CCGTAAGATGGGTTTCGCGATAG AGAGTTTGTAAGG
Rat Anti-Mouse CD9	KMC8	AMM2096	GTAGGGTATCCGGAGAAGCGTAA AGTATGACATGGG
Rat Anti-Mouse CD11a	M17/4	AMM2147	AAGGGATTTAGTAGGTTTAGGAT AGGTGATTCGTGG
Rat Anti-Mouse CD14	rmC5-3	AMM2070	CAGCAATGGTAGTCACGTAGGGA GTTAATAGGGAGT
Rat Anti-Mouse CD16/CD32	2.4G2	AMM2003	GTTGAGATATGCGTTTAGAGTAG CGTGAGTTAGACC
Rat Anti-Mouse CD19	1D3	AMM2007	AAGCATGTCGTTTGTGGCGTACT ATTAAGGTGAAGC
Rat Anti-Mouse CD24	M1/69	AMM2040	TTATATACGTAGTCGGAATGTTGA GTCGGGCGGTGG
Hamster Anti-Mouse CD28	37.51	AMM2016	CGTGGGTTGATTAGCGATTATTAT TCCGTTGTTGTC
Rat Anti-Mouse CD44	IM7	AMM2010	CATGGGTTGTCTCGTTGTAAGTA GTATAGTTGCTGC
Rat Anti-Mouse CD45R/B220	RA3-6B2	AMM2006	GTGGGTTAGGACGTTATGATCGA GTATTAGGGAGGC
Mouse Anti-Mouse CD45.1	A20	AMM2029	GATGTTCGGCGGGTATTCGTGGT TATTTATTCGGCT
Mouse Anti-Mouse CD45.2	104	AMM2014	TGGTAACGTAGCTCGGGAATAAG TAATGCGGAAGTC
Rat Anti-Mouse CD47	miap301	AMM2224	GGAGAACGTAAATATAGTGGAGT AGCGGAAGATGGT
Hamster Anti-Mouse CD48	HM48-1	AMM2064	TTCTGGGCGTTTGGTAGTCGGCT GATTTATATGAGT
Rat Anti-Mouse CD49d	R1-2	AMM2075	TGCGCGTTTGAGAGTCGGGATAT TTCGTTAGGTTCG
Hamster Anti-Mouse CD69	H1.2F3	AMM2022	TTAGAATGATTAGCGGTATATGTC GTGATGCAGCGT
Mouse Anti-Mouse CD72 a, b, and d Alloantigens	K10.6	AMM2229	GGTGGTTAGTTGTGGCGTTATTT GGCGATGGAGTTC
Hamster Anti-Mouse CD79b	HM79b	AMM2227	GAGGTTCGAGGTAGGTATAATAA GATGGTTGAGAGC
Hamster Anti-Mouse CD80 (B7-1)	16-10A1	AMM2037	TGAGAGGGTATATTAGGCGTGCG TAGGAGTTAGTTG
Hamster Anti-Mouse CD81	Eat2	AMM2199	CAGAGATTAGTGGTTCGGTGTTT GGTTATTCGTAGC

Rat Anti-Mouse CD83	Michel-19	AMM2151	GAGGTAGTTTAGAGCCGTTAGATGGATAGTCAGGTG
Rat Anti-Mouse CD84	1D3/CD84	AMM2237	TAGTGTTGGCGCGGTAATTTAAGAGTCGATGGAAGT
Rat Anti-Mouse CD86	GL1	AMM2025	AGTTTAGTGTTCGCGTGTTGCCGTTATTTGATTGTC
Mouse Anti-Mouse CD90/Mouse CD90.1	HIS51	AMM2044	CAGTTGCCGGATTAGAGAAGTACGATAGAAAGAAGT
Rat Anti-Mouse CD93 (Early B Lineage)	AA4.1	AMM2099	GTAACGTGACGAAGAGTAATGATATGAGGGCCTGGT
Rat Anti-Mouse CD115 (CSF-1R)	T38-320	AMM2094	ACGATTGTATGCGAGTGAGGCGAAAGTAGATGGGCT
Rat Anti-Mouse CD117	2B8	AMM2023	TTGTATCGGTAGTAGGTTATGAATTCGCGGGTGAGG
Rat Anti-Mouse CD180	RP/14	AMM2259	TGAGCGACGGTAATGGCATGATAAGGTGATAGACGG
Rat Anti-Mouse CD184	2B11/CXCR4	AMM2047	CGTGGTAATAAGGTGAATAGGTCGCGAGAAGTAAGT
Rat Anti-Mouse CD200	OX-90	AMM2104	AAGTAAATGGAGTAAGCACGTAGTATGGCGGCAGTT
Mouse Anti-Mouse CD244.2	2B4	AMM2161	ACGATCAGGACGAATAGGTAGGTGGAGCATAATAGC
Rat Anti-Mouse CD274	MIH5	AMM2038	ACATGAGAGTAGGTTAATTGGTCGAGCAGTATAGTC
Rat Anti-Mouse CD276	MIH32	AMM2225	GGACACAAAGAATTCGGACGTATATGATGCTAGGCG
Rat Anti-Mouse TER-119	TER-119	AMM2028	GTCGTGGTCGGATAGCGTGTAGGTTTAAAGTAGAGG
Rat Anti-Mouse Pre-B Cell Receptor	SL156	AMM2107	CCGTAGTGCGATTTGGCGTGTATATTGGTTAGTGGC
Rat Anti-Mouse Siglec-H	440c	AMM2154	GAGCGTTGCGAGATTAATAGGCCATAGTAGAAGTTT
Rat Anti-Mouse Ly-6G and Ly-6C	RB6-8C5	AMM2015	CATTGCGAGGAGTAAGGCGATATCTAGTTGTGCTGG
Rat Anti-Mouse Ly-6A/E	D7	AMM2026	GTGGATAGGAGTGTTAGATACGGACGAATTGATGTT
Mouse Anti-Mouse NK-1.1	PK136	AMM2017	GGTCTGGGATTCGTATAGTTCGCGGTAGTTGAGCTT
Hamster Anti-Mouse Vγ 2 T-Cell Receptor	UC3-10A6	AMM2155	CGAATGTCAGGTTAATAGCGAGAATGGAATAGTGTC
Rat Anti-Mouse Vβ 6 T-Cell Receptor	RR4-7	AMM2185	GGAGATAAGTAAGGAGCGATTGCATAGAGGGTTGGC

Rat Anti-Mouse Vβ 11 T-Cell Receptor	RR3-15	AMM2190	TATGGTCTTACTGAGGGCGGAAT TAGGTTGTTGGGC

2.1.8. Unconjugated primary antibodies

Table 8 Unconjugated primary antibodies

Antibody	Clone	Source	Company
Anti Tgm2	D11A6	Rabbit monoclonal	Cell Signaling Technology
Anti α-Tubulin	11H10	Rabbit monoclonal	Cell Signaling Technology

2.1.9. Cytokines

Table 9 Cytokines

Cytokine	Catalog Number	Company
Recombinant mutine SCF	250-03-100UG	Propotech
Recombinant murine TPO	315-14-100UG	Propotech
Recombinant murine IL3	213-13-100UG	Propotech
Recombinantmurine IL6	216-16-100UG	Propotech

2.1.10. Cell culture medium

Table 10 Cell culture medium

Medium	Components
LT-HSC restricted culture medium	SFEM; 100 ng/ml murine SCF, 100 ng/ml murine TPO, and 1% Pen Strep
MPP permissive culture medium medium	SFEM; 100 ng/ml murine SCF, 100 ng/ml murineTPO, 20 ng/ml murine IL3, 20 ng/ml murine IL6, and 1% Pen Strep

2.1.11. Consumables

Table 11 Consumables

Consumable	Company
Loading Tip	Agilent Technologies, St.Clara, USA
Optical Cap, 8x Strip	Agilent Technologies, St.Clara, USA
Optical Tube, 8x Strip	Agilent Technologies, St.Clara, USA
Injekt® 5 ml Syringe	B. Braun SE, Melsungen, Germany
Solofix® Blood lancet	B. Braun SE, Melsungen, Germany
BD Microlance™ 3 23G-Nr.16 Needle	BD Biosciences, Franklin Lakes, USA
Costar® Stripette (5, 10, 25 and 50 ml)	Corning, New York, USA
Falcon® Nylon cell strainer (40, 70, 100 µm)	Corning, New York, USA
Falcon® 14 ml Polypropylene round bottom tube	Corning, New York, USA

Falcon® 5 ml Polystyrene round-bottom tube with cell-strainer cap	Corning, New York, USA
Falcon® Tissue Culture Dish 35 x 10mm Style	Corning, New York, USA
DNA LoBind Tube (1.5 and 5.0 ml)	Eppendorf, Hamburg, Germany
Eppendorf tube (1.5 and 2.0 ml)	Eppendorf, Hamburg, Germany
Feather Disposable Scalpel No.10	Feather, Osaka, Japan
Diamond® Tipack (DF10ST, DF30ST, DF200ST, DF1200ST)	Gilson, Villiers-le-Bel, France
Tipack™ D5000 5000 µL Tips for Pipetman®	Gilson, Villiers-le-Bel, France
Cell culture dish (5 and 10cm)	Greiner Bio-One, Frickenhausen, Germany
Cell Culture Plate (24-well, 96-well)	Greiner Bio-One, Frickenhausen, Germany
Cellstar® sterile centrifuge tubes (15 and 50 ml)	Greiner Bio-One, Frickenhausen, Germany
Microtest plate (Terasaki Plate)	Greiner Bio-One, Frickenhausen, Germany
Polypropylene FACS tubes sterile (5 ml)	Greiner Bio-One, Frickenhausen, Germany
25 micro-inserts 4 well for self-insertion	IBIDI, Munich, Germany
C-Chip Disposable Hemocytometer (Neubauer Improved)	NanoEntek, Waltham, USA
Pasteur pipettes (glas)	Roth, Karlsruhe, Germany
8-Lid chain, flat	Sarstedt, Nümbrecht, Germany
Microvette® 100 K3 EDTA	Sarstedt, Nümbrecht, Germany
Multiply®-µStrip 0.2 ml chain	Sarstedt, Nümbrecht, Germany
Polystyrene FACS tubes (5 ml)	Sarstedt, Nümbrecht, Germany
NUNC tissue culture plates (24-well)	Thermo Fischer Scientific, Waltham, USA

2.1.12. Machines and equipments

Table 12 Machines and equipments

Instrument	Company
Tape Station 4150	Agilent Technologies, St.Clara, USA
BD FACRAria™ III	BD Biosciences, Franklin Lakes, USA
BD LSRFortessa™	BD Biosciences, Franklin Lakes, USA
BD Rhapsody Hemocytometer Adapter	BD Biosciences, Franklin Lakes, USA
BD Rhapsody ™ P1200M pipette	BD Biosciences, Franklin Lakes, USA
BD Rhapsody ™ P5000M pipette	BD Biosciences, Franklin Lakes, USA
BD Rhapsody™ Express	BD Biosciences, Franklin Lakes, USA
BD Rhapsody™ Scanner	BD Biosciences, Franklin Lakes, USA
TSc ThermoShaker	Biometra GmbH, Jena, Germany
BioRad T100 Thermal Cycler	BioRad, Hercules, USA
UV-Transillumination GelDoc 2000	Bio-Rad, Hercules, USA

Axiovert 25 Microscope	Carl Zeiss AG, Oberkochen, Germany
CellObserver 430 optical microscope	Carl Zeiss AG, Oberkochen, Germany
Eppendort ThermoMixer C	Eppendorf, Hamburg, Germany
Biobeam 2000	Gamma-Service Medical GmbH, Leipzig, Germany
Gilson Pipetman Neo 8x200	Gilson, Villiers-le-Bel, France
Centrifuge Micro 220R	Hettich, Tuttlingen, Germany
Centrifuge Rotana 460R	Hettich, Tuttlingen, Germany
Sequencer NextSeq 2000	Illumina, San Diego, USA
Sequencer NextSeq 550	Illumina, San Diego, USA
Intergra Vacusafe	Integra Biosciences, Gernwald, Germany
Freezer -20°C and refrigerators	Liebherr, Bulle, Switzerland
DNA Gel Chamber Typ Maxi	NEO Lab, Heidelberg, Germany
DNA Gel Chamber Typ Midi	NEO Lab, Heidelberg, Germany
DNA Gel Chamber Typ Mini	NEO Lab, Heidelberg, Germany
6-Tube Magnetic Separation Rack	New England BioLabs, Ipswich, USA
NEBNext® Magnetic Separation Rack	New England BioLabs, Ipswich, USA
ProteinSimple WES	Protein Simple, San Jose, USA
Vortex-Genie®	Scientific Industries, USA
EasySep™ Magnet	StemCell Technologies, Vancouver, Canada
EasySep™ Magnet “The Big Easy”	StemCell Technologies, Vancouver, Canada
Freezer -80°C, Heraeus	Thermo Fisher Scientific, Waltham, USA
HERAcell 150i CO_2 incubator	Thermo Fisher Scientific, Waltham, USA
HERASafe 2030i working bench	Thermo Fisher Scientific, Waltham, USA
Nano-Drop 1000 spectrophotometer	Thermo Fisher Scientific, Waltham, USA
Q Exactive HF Orbitrap Mass Spectrometer	Thermo Fisher Scientific, Waltham, USA
Qubit 4 Fluorometer	Thermo Fisher Scientific, Waltham, USA
Large magnetic separation stand with 15 ml tube adapter	V&P Scientific, San Diego, USA

2.1.13. Software and algorisms

Table 13 Software and algorisms

Software	Developer
Adobe Illustrator 2022	Adobe Inc, San Jose, USA
AxioVision 4.8 software	Carl Zeiss AG, Oberkochen, Germany
bcl2fastq2 v2.20	Illumina, San Diego, USA
Biorender	https://biorender.com
Citavi 6	Swiss Academic Software GmbH, Wädenswil, Switzerland
Clone manager 9	Sci Ed Software, Colorado, USA
Compass SW V5.0.0	Protein Simple, San Jose, USA
DESeq2 v1.18.1	(Michael Love, Simon Anders, Wolfgang Huber 2017)

FACSDiva 8.1	BD Biosciences, Franklin Lakes, USA
FlowJo software V10.8.0	BD Biosciences, Franklin Lakes, USA
GraphPad Prism V9.3.0	GraphPad Software, San Diego, USA
MaxQuant V2.1.0	https://www.maxquant.org/maxquant
Metascape	http://metascape.org (Zhou et al. 2019)
Microsoft Office 2013	Microsoft, Washington, USA
Perseus 1.6.15.0	https://www.maxquant.org/perseus (Tyanova et al. 2016)
Seurat V3.0	Satija Lab and Collaborators
SeqGeq software V1.7.0	BD Biosciences, Franklin Lakes, USA
Snapgene V6.0	GSL Biotech LLC, San Diego, USA
SRplot	http://www.bioinformatics.com.cn/en, an online platform for data analysis and visualization
STAR 2.6.1d	https://github.com/alexdobin/STAR
Subread Package	http://subread.sourceforge.net
Trimmomatic v0.39	http://www.usadellab.org/cms/?page=trimmomatic
Venny 2.1	Oliveros, J.C. (2007-2015) Venny. An interactive tool for comparing lists with Venn's diagrams. https://bioinfogp.cnb.csic.es/tools/venny/index.html
VolcaNoseR	https://huygens.science.uva.nl/VolcaNoseR (Goedhart and Luijsterburg 2020)
The Tracking Tool TTT	Schroeder Lab, https://bsse.ethz.ch/csd/software/ttt-and-qtfy.html

2.2. Methods

2.2.1. Animal experiments methods

2.2.1.1. Animals

All animals were kept and bred according to the guidelines of the Federation of European Laboratory Animal Science Associations (FELASA) in the animal husbandry facility of Georg-Speyer-Haus (Frankfurt am Main, Germany). The animals were kept in individually ventilated cages (IVC) at a maximum of 6 animals per cage with a 12 hour light-dark interval. General health status of all animals was monitored daily by the scientist, the animal caretakers or the veterinarian. Mouse strains C57BL/6J, B6.SJL, Mx1-Cre^{-}Tgm2$^{loxP/loxP}$ and Mx1-Cre^{+}Tgm2$^{loxP/loxP}$ were used in the project. C57BL/6J and B6.SJL mouse strains were purchased from Charles River Laboratory (Sulzfeld, Germany) or bred in MFD Diagnostics GmbH (Wendelsheim, Germany). All mice were used at 8-16 weeks of age if not specifically stated. All the *in vivo* animal experiments were performed in accordance with German animal welfare legislation and were approved by the relevant local authorities (Regierungspräsidium Darmstadt).

2.2.1.2. Generation of Mx1-Cre^{+}Tgm2$^{loxP/loxP}$ conditional knockout mice

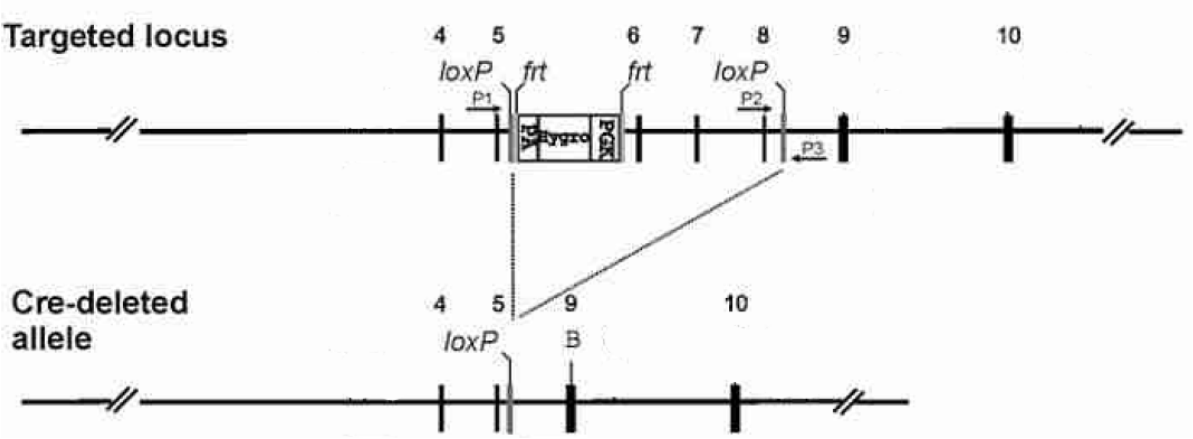

Figure 5 Targeted construct of Tgm2.

Targeted locus showing exons 4–10, with inserted *loxP* sites flanking the catalytic domain of Tgm2 from exons 6 to 8. The locations of primers used for genotyping are indicated. *loxP* sequences can be recognized by Cre recombinase. **Adapted and modified from (Nanda et al. 2001).**

PGK: phosphoglycerate kinase I promoter; hygro: hygromycin resistance gene; PA, SV40 poly(A) tail.

Generation of Mx1-Cre^{+}Tgm2$^{loxP/loxP}$ conditional knockout mouse line was performed referring to the description from Nanda (Nanda et al. 2001). Chimeric mice were generated and back-crossed with C57BL/6 mice to obtain heterozygous floxed (flanked by *loxP* sites) Tgm2 mice. Knockout animals were generated by crossing heterozygous (Tgm$^{WT/loxP}$) or homozygous (Tgm2$^{loxP/loxP}$) mice with transgenic mice expressing Cre recombinase in the germline under the control of the the type I interferon-inducible Mx1 promoter (transgene referred as Mx1-Cre). Genotyping of Mx1-Cre was performed using 5'-AAATTGCCAGGATCAGGGTTAAAG-3' and 5'-AGAGTCATCCTTAGCGCCGTAAAT-3' as described in **2.2.4.6**.

To activate Cre expression *in vivo* in order to generate conditional Tgm2 knockout mice, 5 µg/gram body weight of polyinosinic:polycytidylic acid (polyIC; Invivogen, USA) was intraperitoneally (i.p) injected three times every second day. Knockout genotyping was performed on the 4th day after the last polyIC injection and all the experiments in this project were performed on the 10th day after the last polyIC injection. Efficient excision of floxed allele was confirmed with peripheral blood (PB) DNA as described in **2.2.4.5** using 5'-CATGAATCAGGATGCACGTG-3', 5'-GGCAAGGTCTGAGAAAGCAC-3' and 5'-GACAAAGGAGCAAGTGTTAC-3'.

The following nomenclature was used: PolyIC treated Mx1-Cre^{-}Tgm2$^{loxP/loxP}$ mice were defined as **Tgm2-WT** whereas Mx1-Cre^{+}Tgm2$^{loxP/loxP}$ mice were defined as **Tgm2-KO** in this project.

2.2.1.3. PB withdraw from mouse

To obtain blood from mice, vena facialis bleeding was performed with a Solofix®Blood lancet (B. Braun SE, Germany) and about 100 µl blood was collected per mouse into an EDTA

Microvette® tube (Sarstedt, Germany). Erythrocytes were lysed using the 1x BD Pharm lyse™ Lysing Buffer (BD Biosciences, USA) in a fresh 1.5 ml Eppendorf tube (Eppendorf, Germany) for 15 min in dark. Leukocytes cell pellet was spin down with centrifugation (400 x g, 5 min, RT). Cell pellet was further washed twice with 1 ml 1x PBS (400 x g, 5 min, 4°C). Thereafter, the remaining leukocytes were used for PB DNA isolation (**2.2.4.5**) or stained with fluorochrome-labeled antibodies for FACS analysis (**2.2.3.3**).

2.2.1.4. 5-FU administration of Mx1-Cre^{+}Tgm2$^{loxP/loxP}$ mice

On the 10th day after the last polyIC injection of the Mx1-Cre^{-}Tgm2$^{loxP/loxP}$ and Mx1-Cre^{+}Tgm2$^{loxP/loxP}$ mice, 150 mg/kg 5-Fluorouracil (Medac, Germany) was administered intravenously (i.v). BM cell count and HSPC distributions were analyzed from ficoll-enriched bone marrow mononuclear cells (BMMNCs) at the indicated time points post-treatment.

2.2.2. Perspective isolation and purification of murine BM HSPCs

2.2.2.1. Murine BM cell isolation via crushing and lineage depletion

The femurs, tibias, coxae and sternum from 8-16 weeks old mice of indicated mouse strains were removed and cleaned to remove muscles and fibrous tissues. The isolated cleaned bones were crush with mortar and pestle in 10% FBS with a final volume of 50 ml. Total BM cells were stained with biotin-labeled antibodies CD3e, CD11b, CD19, CD41, B220, Gr-1 and Ter119 against mature blood cells. To obtain a better enrichment of HSPC populations, a cell depletion of lineage positive cells was performed using the EasySep™ Mouse Biotin Positive Selection Kit II (Stemcell Technologies, Canada) and Easysep™ magnet (Stemcell Technologies, Canada) after washing with 1x PBS (290 x g, 7 min, 4 °C). A detailed experimental protocol were described in the previous publication (Yu et al. 2022).

2.2.2.2. Murine BM cell isolation via flushing and Ficoll enrichment

Alternatively, femurs, tibiae and coxae were removed from each mouse separately for single mouse analysis and cleaned to remove excess muscles and fibrous tissues. BM cells were extracted by flushing out from the bones with 3 ml cold 1x PBS using a 5 ml syringe (B. Braun SE, Germany) applied with a 23G needle (BD Biosciences, USA). To enrich for BMMNCs, the 3 ml cell suspension was carefully loaded on top of 3 ml Histopaque® 1083 (Sigma, USA) and seperated by density gradient centrifugation (400 x g, 30 min, RT), without setting the breaks. The interphase was collected and washed twice with 1 x PBS (290 x g, 7 min, 4 °C). A detailed experimental protocol were described in the previous publication (Yu et al. 2022).

2.2.2.3. Staining and FACS sorting of isolated HSPCs

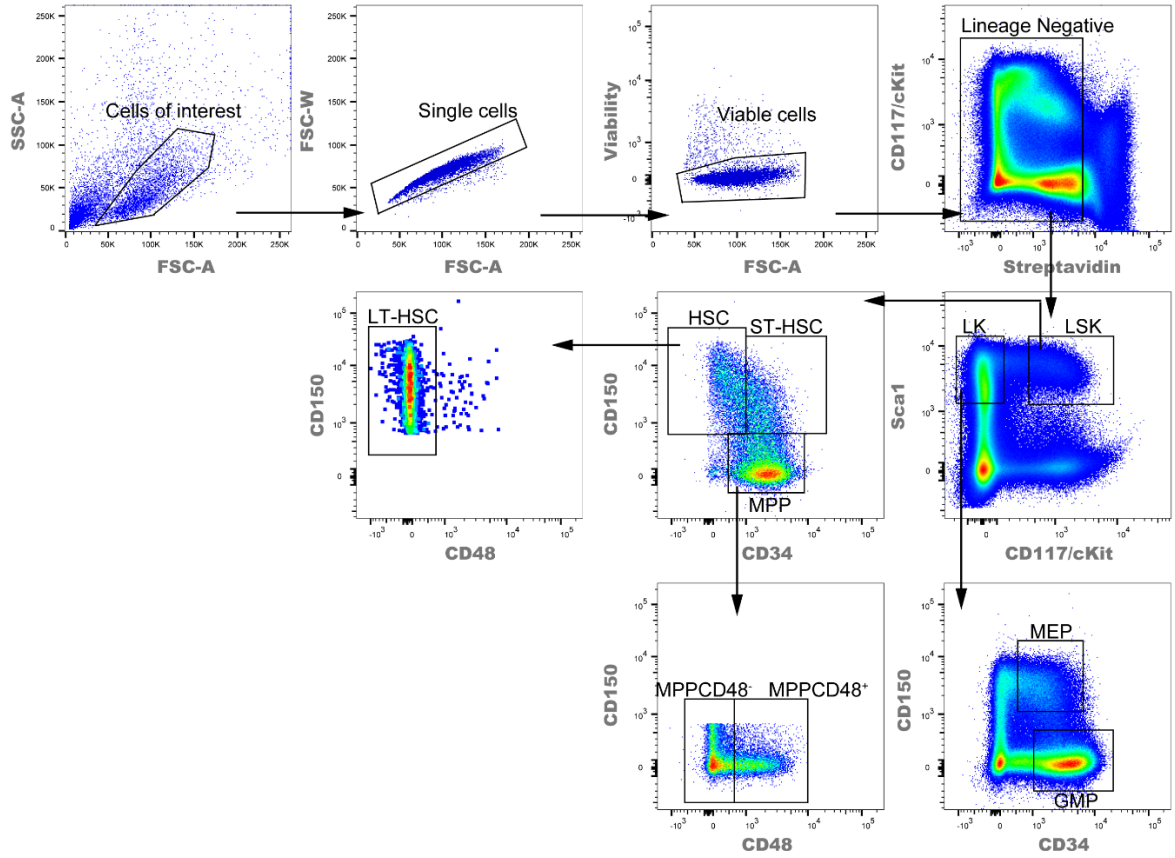

Figure 6 FACS gating schemes to phenotype HSPC subpopulations.

BM lineage marker-negative cells are stained with the selected fluorochrome-conjugated antibodies. Biexponential transformation is applied to visualize all events in each plot. Quality cells are gated using a scatter gate followed by the exclusion of doublets and dead cells. By excluding the lineage marker positive cells, LSK (Lin^- $CD117^+$ $Sca1^+$) and LK (Lin^- $CD117^+$ $Sca1^-$) populations are gated out according to the expression of CD117 and Sca1. LT-HSC (LSK $CD150^+$ $CD34^{-/low}$ $CD48^-$), ST-HSC (LSK $CD150^+$ $CD34^+$) and MPP (LSK $CD150^-$ $CD34^+$) are further gated from LSK, whereas GMP (LK $CD150^-$ $CD34^+$) and MEP (LK $CD150^+$) are gated from LK.

The lineage depleted lineage negative cells were stained with fluorochrome-labeled antibodies against progenitor markers, streptavidin against biotin-labeled antibodies and the fixable viability dye. The cells were incubated for 30 min on ice in dark before the cells were washed once with 1x PBS (290 x g, 7 min, 4 °C) to remove excessive antibodies. Stained cells were analyzed via LSR Fortessa (BD Biosciences, USA) or sorted via FACS Aria III (BD Biosciences, USA). Both cytometers were controlled with the software FACSDiva 8.1 (BD Biosciences, USA). A representative FACS plot for the distinctive HSPCs is shown in **Figure 6**. Dead cells were excluded by Fixable Viability Dye. Remaining lineage positive progenitors were excluded based on Streptavidin binding to biotin-labeled antibodies. From lineage negative population, the following populations were identified: LSK (Lin^- $CD117^+$ $Sca1^+$), LT-HSC (LSK $CD150^+$ $CD34^{-/low}$ $CD48^-$), ST-HSC (LSK $CD150^+$ $CD34^+$), MPP (LSK $CD150^-$ $CD34^+$), LK (Lin^- $CD117^+$ $Sca1^-$), GMP (LK $CD150^-$ $CD34^+$) and MEP (LK $CD150^+$). Sorted cells were counted with trypan blue exclusion either manually with Neubauer proved Hemocytometer (**2.2.8.2**) or

Terasaki plates (**2.2.8.3**) in case of very low cell number. Data analysis was performed with FACSDiva 8.1 (BD Biosciences, USA) or FlowJo software v10 (BD Biosciences, USA).

2.2.2.4. JC-1 staining

JC-1 dye (5,5',6,6'-tetrachloro1,1',3,3'-tetraethylbenzimidazolocarbocyanine iodide; Thermo Fisher Scientific, USA) staining was performed to separate cell populations mito-low (green fluorescence emission ~529 nm) or mito-high (green fluorescence emission ~529 nm and red fluorescence emission shift ~590nm) according to the measurement of mitochondrial membrane potential. Before staining the cells with surface markers, lineage negative cells were incubated with 2µM JC-1 at 37°C, 5% CO_2 for 30 min. Cells were then washed, stained with fluorochrome-labelled antibodies and analyzed via FACS. Data analysis was performed with FACSDiva 8.1 (BD Biosciences, USA) or FlowJo software v10 (BD Biosciences, USA).

2.2.2.5. Ki67 staining

Ki67 staining was performed according to the manufacturer's protocol. Cells stained with different fluorochrome-labeled antibodies were fixed in 1x fixation buffer (Thermo Fisher Scientific, USA) for 45 min, washed with 1x permeabilization buffer (Thermo Fisher Scientific, USA) and stained with fluorochrome-labeled Ki67 antibody for 30 min at RT. After washing with 1x PBS, cells were incubated with 20µl of 7-AAD (BD Biosciences, USA) for at least 10 min in dark. Cells were resuspend in FACS buffer and measured via FACS. Data analysis was performed with FACSDiva 8.1 (BD Biosciences, USA) or FlowJo software v10 (BD Biosciences, USA).

2.2.3. Competitive repopulation assay

2.2.3.1. Primary transplantation: transplantation of donor LT-HSCs

6-8 weeks old B6.SJL ($CD45.1^+$) were lethally irradiated with 8.5 Gy using a Biobeam 2000 (Gamma-Service Medical GmbH, Germany) with a Cs137 gamma irradiation source at least 4 hours prior to transplantation. 200 freshly FACS sorted LT-HSCs from 10-week-old Tgm2-WT and Tgm2-KO mice ($CD45.2^+$) together with 5 x 10^5 ficoll-enriched BMMNCs from C57BL/6J mice as competitor recipient cells were injected intravenously (i.v) into lethally irradiated B6.SJL ($CD45.1^+$) recipient mice (5-6 mice per group). Engraftment and multi-lineage reconstitution were monitored over 20 weeks by pheripheral blood analysis. After 20 weeks, primary transplanted mice were sacrificed and the BM cells isolated from femurs, tibias and coxae as well as the spleen were collected for the following described secondary transplantation, and end point analysis.

2.2.3.2. Secondary transplantation

BMMNCs were collected by ficoll enrichment (**2.2.2.2**) with isolated BM cells from individual primary transplantation recipient mouse. 1 x 10^6 BMMNCs from each mouse were one to two transplanted into lethally irradiated B6.SJL ($CD45.1^+$) secondary recipient mice (8-10 mice per group). Engraftment and multi-lineage reconstitution of secondary transplantation were monitored over 20 weeks by PB analysis. Afterwards, secondary transplanted mice were sacrificed and the BM cells isolated from femurs, tibias and coxae as well as the spleen were collected for the end point analysis.

2.2.3.3. PB analysis

Multi-lineage reconstitution was determined every 4 weeks post transplantation in PB. Pheripheral blood was withdrawn and RBC were lysed as described (**2.2.1.3**) every 4 weeks. Leukocytes were stained with fluorochrome-labeled antibodies CD45.1, CD45.2, Ter119, CD11b, Gr1, B220 and CD3e. Fixable Viability Dye was also added for dead/live cell exclusion.

2.2.3.4. End point BM analysis

50 µl of flushed BM cells were kept in a fresh Eppendorf tube (Eppendorf, Germany) for total BM cell counting and lineage cell determination by staining with fluorochrome-labeled antibodies CD45.1, CD45.2, Ter119, CD11b, Gr1, B220, CD3e and Fixable Viability Dye. The remaining flushed BM cells were proceed with density gradient centrifugation (**2.2.2.2**). Ficoll-enriched BMMNCs isolated from each recipient mouse were stained with biotin-labeled antibodies CD3e, CD11b, CD19, CD41, B220, Gr-1 and Ter119 against mature blood cells. After washing with 1x PBS (290 x g, 7 min, 4 °C), cells were stained with fluorochrome-labeled antibodies CD45.1, CD45.2, Streptavidin, Sca1, CD117, CD48, CD150, CD34 and Fixable Viability Dye to determine different HSPCs as mentioned in **2.2.2.3**.

2.2.3.5. End point spleen analysis

The spleens from recipient mice were collected and weighted. Spleen cells were isolated by meshing the spleen through a 100 µm Falcon® Nylon cell strainer (Corning, USA). 1 x 10^7 spleen cells were stained with fluorochrome-labeled antibodies CD45.1, CD45.2, Ter119, CD11b, Gr1, B220, CD3e and Fixable Viability Dye to analyze lineage cells.

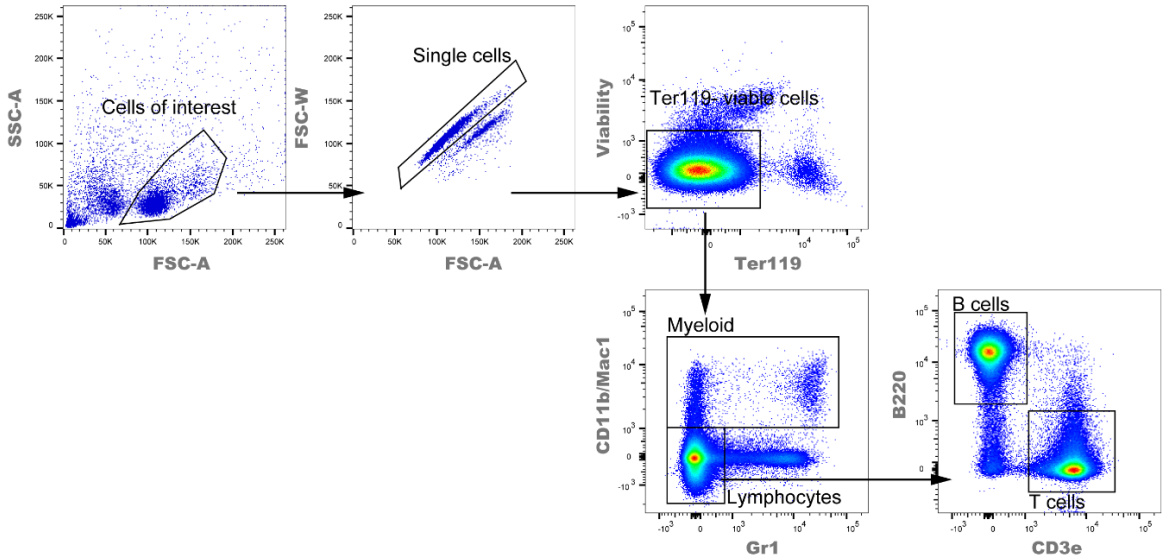

Figure 7 FACS gating schemes of mature lineage populations.

Total BM, lysed PB or spleen cells are stained with the selected fluorochrome-conjugated antibodies. Biexponential transformation is applied to visualize all events in each plot. Quality cells are gated using a scatter gate followed by the exclusion of doublets and dead cells. By excluding the remaining RBCs with the expression of Ter119, Myeloid ($CD11b^+/Gr1^+$) cells and lymphocytes ($CD11b^-Gr1^-$) are obtained from the leucocytes. B cells ($B220^+$) and T cells ($CD3e^+$) are further gated from the lymphocytes.

2.2.4. Molecular and biochemistry methods

2.2.4.1. Competent cells

DH5α chemically competent *Escherichia coli* (*E. coli*) from Thermo Fischer Scientific (Thermo Fischer Scientific, USA) are used for cloning applications. Genotype: F– φ80lacZΔ M15 Δ (*lacZYA-argF*) U169 *recA1 endA1 hsdR17 (rK– mK+) phoA supE44 λ- thi–1 gyrA96 relA1*.

2.2.4.2. Transformation

100 µl aliquoted chemically competent DH5α cells were thawed on ice and mixed with 5-50 ng DNA in 10 µl. After 30 min on ice incubation, DNA uptake was mediated by heat shock for 90 sec at 42°C followed by 2 min incubation on ice. 440 µl sterile LB medium (without ampicilin) was added to the cells and incubated at 37°C for 1 h with shaking at 200 x g. 50 µl of bacteria suspension was plated on LB-Agar plates supplemented with ampicillin and incubated overnight at 37°C. The remaining bacterial suspension was pelleted down by centrifucation (10000 x g, 1 min), 450 µl of medium was discarded. The residual volume (50 µl) was used to resuspend the pelleted competent cells and plated on LB-Agar plates supplemented with ampicillin and incubated overnight at 37°C as well. At least three single bacteria colonies grown on LB-Agar plates were picked and expanded in 3 ml LB-medium supplemented (without ampicilin) and cultivated at 37°C with continuous shaking at 200 x g. The best culture was transferred to a 200 ml LB medium (50 µg/ml ampicillin) and shaked at 37°C overnight with

200 x g for plasmid preparation. A negative control of competent cells without adding DNA was always included.

2.2.4.3. Plasmid preparation (Maxi prep)

Plasmid DNA was purified from 200 ml bacteria culture using the NucleoBond® Xtra Maxi EF kit (Macherey-Nagel GmbH, Germany) following the manufacturer's protocol. The plasmid DNA was eluted using TE-EF buffer from the kit. The concentration of the plasmid DNA was determined using NanoDrop 1000 Spectrophotometer (Thermo Fisher Scientific, USA) and the plasmid DNA was stored at -20°C.

2.2.4.4. Simple DNA extraction with HotSHOT protocol (Truett et al. 2000)

PB leukocytes pellet obtained from **2.2.1.3** or cultivated single LT-HSC colonies was lysed with 20 µl homemade Alkaline lysis buffer at 95°C for 20min. 20 µl homemade Neutralizing buffer was added to the cell lysate on ice followed by vortexing. The final DNA product was stored at -20°C.

2.2.4.5. Genotyping of murine PB DNA

Genotyping of successive Tgm2 knockout was performed with three-primer-system using DNA products from PB or cultivated single LT-HSC colonies. PCR was performed in a 20 µL reaction volume using Phusion Blood Direct PCR Master Mix (Thermo Fisher Scientific, USA) according to the manufacturer's protocol with modification. In order to obtain a better efficiency of amplification in this project, 2 µL of DNA (**2.2.1.3**) was used as templates instead of using 1 µL of whole blood.

2.2.4.6. Genotyping of murine tissues DNA

Genotyping of Mx1-Cre was performed with mouse tissue. PCR for specific amplification of DNA double strands was performed in a 20 µL reaction volume using Phire™Tissue Direct PCR Master Mix (Thermo Fisher Scientific, USA) Dilution & Storage protocol according to the manufacturer's protocol.

2.2.4.7. Agarose gel electrophoresis

Agarose gel electrophoresis was performed after the PCR genotyping. 2% (w/v) agarose (VWR, Belgium) was heat dissolved in 1x TAE buffer. After cooling to roughly 60°C, 7 µl/ 120 ml HDGreen™ Plus DNA Stain (Intas, Germany) was added enabling visualization of DNA under UV light. Polymerized gels were then placed into an electrophoresis chamber, covered by 1x TAE buffer and the samples were loaded directly as premixed gel loading dyes were contained in the previously mentioned PCR Master Mix. To determine DNA fragment size, O'GeneRuler Express DNA Ladder, which was included in the PCR Master Mix kits, was

loaded on the gels. DNA fragments were separated for 30min applying 110V. DNA gel was visualized and documented by the UV-Transillumination GelDoc 2000 (Bio-Rad, USA).

2.2.4.8. DNA extraction and purification from agarose gel

In order to isolate DNA from an agarose gel after visualizing, relevant gel pieces were excised from the gel and stored in a 1.5 ml Eppendorf tube (Eppendorf, Germany). The NucleoSpin® Gel and PCR Clean-Up kit (Macherey-Nagel GmbH, Germany) was used to extract and clean plasmid DNA fragments from agarose gels following the manufacturer's protocol. The extracted DNA concentration was determined using NanoDrop 1000 Spectrophotometer (Thermo Fisher Scientific, USA).

2.2.4.9. DNA sequencing

Identity of the purified DNAs were confirmed by Sanger based DNA sequencing. Sequencing was performed with GATC Services at Eurofins Genomics (Ebersberg, Germany). The sequencing sample was prepared in an Eppendorf tube (Eppendorf, Germany) with 5 µl of DNA template (50-100 ng/µl plasmid DNA or 5 ng/µl 300-1000 bp purified PCR products) and 5 µl of a 5 µM primer. The results were analyzed using the Clone Manager 9 software (Sci Ed Software, USA).

2.2.4.10. Lentivirus transduction vector generation

In our laboratory, the third generation lentivirus vector derived from human immunodeficiency virus (HIV) with biosafety features was used for gene transduction into cell lines and primary cells. The open reading frame (ORF) of the VENUS fluorescent reporter protein (VENUS-hImportin subunit α1 (AA2-67)) was cloned into the lentiviral vector pRRL.PPT.SFFV.IRES.eGFP.PRE by replacing the ORF of eGFP (Schambach et al. 2006). A multiple cloning site (MCS) was inserted after the SFFV promoter.

2.2.4.11. Generation of lentiviral expression vector for murine Tgm2 and mCherry-linker-mTgm2

Murine full-length Tgm2 constructs were produced and cloned into the MCS position of our lentiviral expression vectors (General Biosystems, USA) (**Appendix Figure 43B**).

2.2.4.12. Preparation of protein lysates

Cells were lysed on ice with lysis buffer prepared by M-PER™ Mammalian Protein Extraction Reagent (Thermo Fisher Scientific, USA) and Pierce Protease and Phosphatase Inhibitor Mini Tablets (Thermo Fisher Scientific, USA) according to the manufacturer's protocol. Low cell number lysates, e.g. 2000 FACS sorted LT-HSCs, were prepared by sorting the cells directly into 7 µl lysis buffer. Cultured cell lysates, e.g. lentivirus transduced 3T3 cultured cells, were

prepared by lysing 5 x 10^6 cells with 100 µl lysis buffer. Protein concentration of cultured cell lysate was determined using Qubit™ Protein Assay Kit (Thermo Fisher Scientific, USA).

2.2.4.13. Protein expression analysis with WES System (Protein Simple, San Jose, USA)

0.4 mg/ml of cultured cell protein lysate or whole FACS sorted cell lysate was used for protein detection. Cartridge preparation, sample processing and applying on the capillary was performed according to the manufacturer's protocol of the 12-230 kDa Jess or Wes Separation Module, 8 x 25 capillary cartridges kit (Protein Simple, San Jose, USA). If multiplexing of several antibodies within one capillary was not feasible, i.e. due to cross-reaction of used antibodies or similar protein molecular weight, same sample was used twice in the same run, once for detection of protein of interest and once serves as loading control. Default run settings were used. The primary antibody dilution was 1:30. α-Tubulin (αTub) was used as a loading control. Protein detection was validated using High-Dynamic-Range (HDR) multi-image analysis for every tested sample and analysis was performed with the software Compass SW V5.0.0 (Protein Simple, San Jose, USA).

2.2.5. Low input label-free mass spectrometric proteomics

Low input label-free mass spectrometric proteomics analysis was performed in collaboration with Dr. Kuan-Ting Pan (Clinical Proteomics, Frankfurt Cancer Institute, Germany).

2.2.5.1. Sample preperation

5000 LT-HSCs or 10000 MPPs were sorted into four reaction vessels that contained 15 µL 0.1 % RapiGest (water) prepared with 50 mM triethylammonium bicarbonate (TEAB; Thermo Fisher Scientific, USA). 0.3 µL BondBeaker (Thermo Fisher Scientific, USA) and 0.3 µL 1 M iodoacetamide (IAA; Sigma Aldrich, USA) were added to each vessel and incubated 30 min at 37 °C. 1 µL 50 mM TEAB containing sequencing grade trypsin (25 ng for LT-HSC and 50 ng for MPP samples; Promega, USA) was added and incubated at 37 °C for 4 h in a humidity chamber. 0.8 µL 7.5 % trifluoroacetic acid (TFA; Thermo Fisher Scientific, USA) was added to each sample and incubated at 37 °C for 45 min to initiate lysis. Samples were spun at 15,000 x g for 10 min and the supernatant was transferred to fresh vessels. Samples were then dried down in an Eppendorf Concentrator (Eppendorf, Germany) under vacuum until complete dryness and stored at – 20 °C until mass spectrometric measurement.

2.2.5.2. Mass spectrometric measurement

Samples were reconstituted with 6 µL 5 % acetonitrile (ACN), 0.1 % formic acid (FA), sonicated, spun down briefly and transferred into HPLC sample vials. Samples were injected

twice as equally distributed for technical replicates. Mass spectrometric analysis was performed on a Q Exactive HF Orbitrap (Thermo Fisher Scientific, USA) interfaced with an Ultimate 3000 nano-HPLC system (Thermo Fisher Scientific, USA). Samples were separated on an inhouse-made analytical column (ReproSil-Pur 120 C18-AQ, 1.9 µm pore size, 75 µm inner diameter, 30 cm; Dr. Maisch GmbH, Germany) using an one-hour gradient at a flow rate of 300 nL/min. Mobile phase A and B were 0.1 % (vol/vol) FA and 80 % ACN, 0.08 % FA, respectively. The gradient started at 5 % B at 3 min, increased to 50 % B in 42 min, and then to 70 % B in 4 min. After washing with 90 % B for 6 min, the column was re-equilibrated with 5 % B for the remainder of the run time.

2.2.5.3. Proteomic data analysis

Raw files were searched using MaxQuant 2.0.1 with default settings and an updated mouse data base retrieved from uniport containing only reviewed entries. Match between runs was used to boost identifications. Proteingroups.txt output file was processed using Perseus 1.6.15.0 filtering out reverse hits, potential contaminations and hits only identified by site. Data was then transformed (Log2) and the column median was subtracted from the individual values of the respective column (median normalization). Identified proteins were then filtered for 50 % valid quantifications over all samples. Two-sided t-test (5 % FDR) was performed to identify significantly regulated proteins.

2.2.6. Bulk RNA sequencing analysis

Total RNA of 500 FACS-sorted LT-HSCs or MPPs from Tgm2-WT and Tgm2-KO mice was isolated by miRNeasy micro Kit (Qiagen, Germany) using low input DNase protocol. RNA and library preparation integrity were verified with LabChip Gx Touch 24 (Perkin Elmer, USA). Approximately 1-5 ng of total RNA was used as starting material for SMART®-Seq HT Kit (Takara, USA). Sequencing was performed in collaboration with Dr. Stefan Günther (Max-Planck-Institute for Heart- and Lung Research, CPI - DNA & RNA Technologies, DZHK - Advanced Molecular Analytics Platform RheinMain, Bad Nauheim, Germany) on the NextSeq500 sequencer (Illumina, USA) using v2 chemistry with 1 × 75 bp single-end setup. The resulting raw reads were assessed for quality, adapter content, and duplication rates with FastQC (Andrews S. 2010). Trimmomatic version 0.39 was employed to trim reads after a quality drop below a mean of Q20 in a window of 20 nucleotides. Only reads between 15 and 75 nucleotides were cleared for further analyses. Trimmed and filtered reads were aligned against the Ensembl mouse genome version mm10 (GRCm38) using STAR 2.6.1d with the parameter “–outFilterMismatchNoverLmax 0.1” to increase the maximum ratio of mismatches to mapped length to 10%. The number of reads aligning to genes was counted with

featureCounts 1.6.5 tool from the Subread package. Only reads mapping at least partially inside exons were admitted and aggregated per gene. Reads overlapping multiple genes or aligning to multiple regions were excluded. Differentially expressed genes were identified using DESeq2 version 1.18.1. Only genes with a minimum fold change of ±1.5 (log2 ± 0.59), a maximum Benjamini–Hochberg corrected p-value of 0.05, and a minimum combined mean of 5 reads were deemed to be significantly differentially expressed. The Ensemble annotation was enriched with UniProt data (release 24.03.2017) based on Ensembl gene identifiers.

2.2.7. Single cell RNA sequencing with BD Rhapsody™ (BD Biosciences, USA)

2.2.7.1. Single cell capture and cDNA synthesis with BD Rhapsody™ system

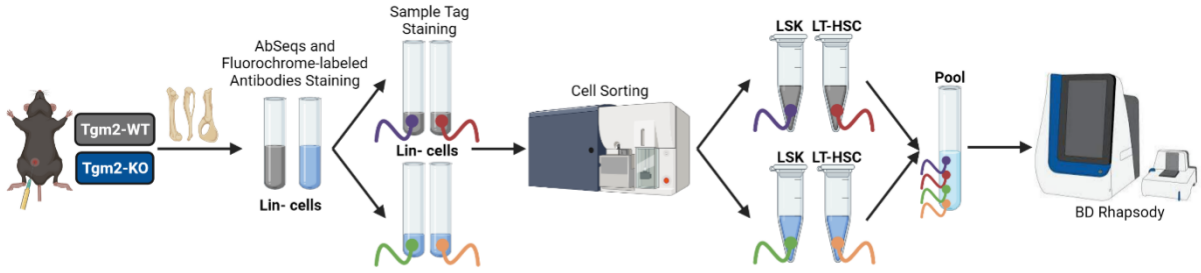

Figure 8 Experimental scheme of cell preperation for scRNAseq.

Lineage negative cells from Tgm2-WT and Tgm2-KO mice BM are stained with fluorochrome-labeled antibodies and AbSeqs. Antibody stained lineage negative cells are split into two vials for staining with two different Sample Tags. One vial of Sample Tag labeled lineage negative cells from Tgm2-WT/Tgm2-KO mice is used for sorting LSKs and the other vial is used for sorting LT-HSCs. All four sorted populations are pooled and proceeded for single cell capture with BD Rhapsody. Figure generated in BioRender.

Lineage negative cells from Tgm2-WT and Tgm2-KO mice were isolated as described in **2.2.2.1**. Sample pooling scheme is shown as **Figure 8**. Lineage negative cells from Tgm2-WT or Tgm2-KO mice were incubated with fluorochrome-labeled antibody mixtures and AbSeqs Ly-6A/E, CD48, CD117. Stained samples were washed once with 1x PBS (290 x g, 7 min, 4 °C). Afterwards, AbSeq antibody mixtures (BD Biosciences, USA, **Table 7**) were added to the samples and the cells were incubated for 40min on ice and washed twice with Stain Buffer (BD Biosciences, USA). Antibody stained lineage negative cells were split into two vials for incubation with two different Sample Tags (BD Biosciences, USA; in total 4 Sample Tags were used) independently for 20 min at RT. Sample Tag labeled lineage negative cells were washed twice with 1x PBS (290 x g, 7 min, 4 °C) and resuspended in 100 µl FACS buffer. One vial of Sample Tag labeled lineage negative cells from Tgm2-WT/Tgm2-KO mice was used for sorting LSKs and the other vial was for sorting LT-HSCs. Sorted cells were pooled and resuspended in 620 µl of cold Sample Buffer (BD Biosciences, USA), counted with Calcein AM (Thermo Fisher Scientific, USA) and Draq 7 (BD Biosciences, USA) staining according to the

manufacturer's protocol. The single cell capture and subsequent cDNA synthesis were performed exactly following the manufacturer's protocol provided by BD Biosciences.

2.2.7.2. Whole transcriptome amplification library preparation and sequencing

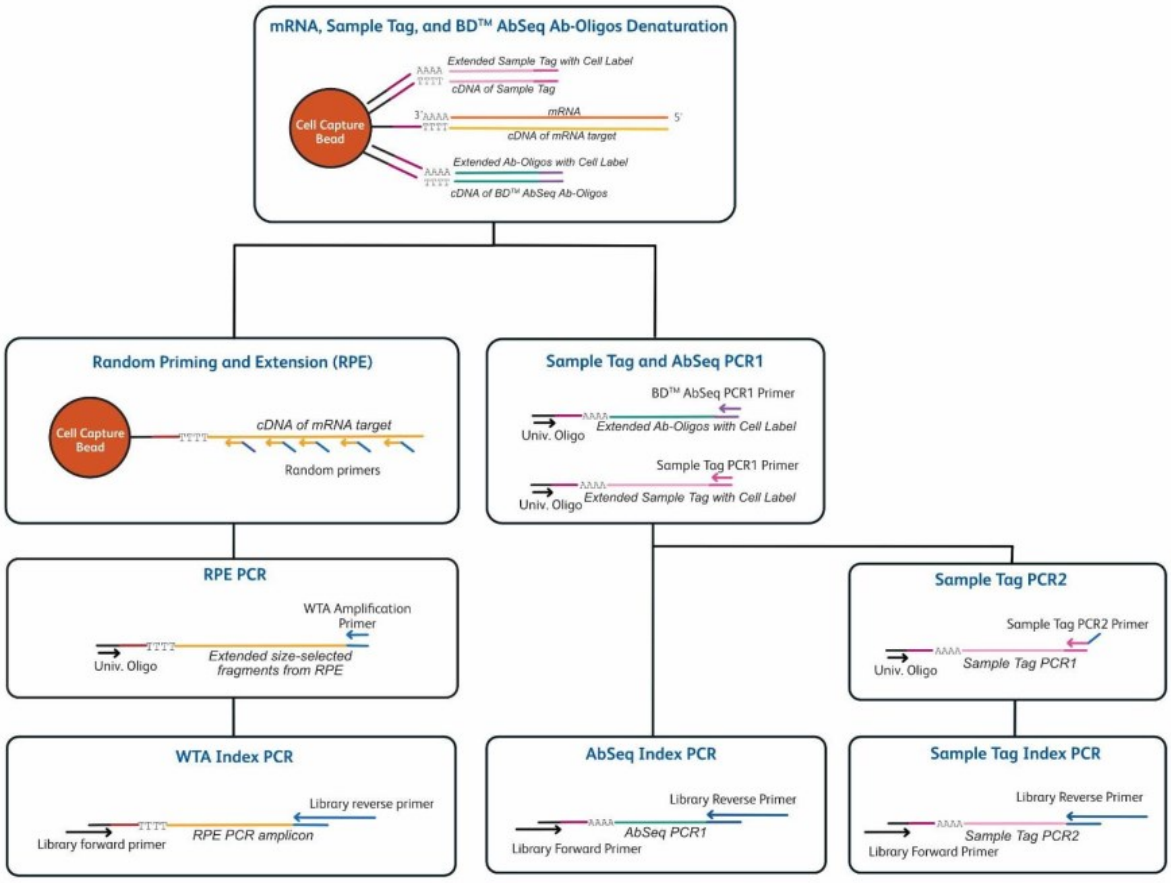

Figure 9 Whole transcriptome amplification library preparation workflow.

Single-cell cDNA library preparation was performed exactly according to the mRNA Whole Transcriptome Analysis (WTA), AbSeq, and Sample Tag library preparation protocol provided by BD Biosciences. The concentration, size and integrity of the resulting PCR products and final libraries were assessed using both Qubit™ dsDNA HS assay kit (Thermo Fisher Scientific, USA) and the Agilent Tape Station 4150 (Agilent, USA). Sequencing was performed in collaboration with Dr. Stefan Günther (Max-Planck-Institute for Heart- and Lung Research, CPI - DNA & RNA Technologies, DZHK - Advanced Molecular Analytics Platform RheinMain, Bad Nauheim Germany). Finished libraries were diluted to equimolar ratios and a final concentration of 1nM final libraries was prepared (~82/16/2% WTA/AbSeq/Sample tag ratio) and spiked with 20% Phix control DNA to increase sequence complexity. Sequencing was performed with P3 flowcell and 2 x 75bp paired end setup and sequenced with 2 x 75bp paired-end on NextSeq 2000 instrument (Illumina, USA). Raw counts were demultiplexed by bcl2fastq (2.20.).

2.2.7.3. Single cell RNAseq Data analysis

The FASTQ files obtained from sequencing were analysed following the BD Biosciences Rhapsody pipeline (BD Biosciences) via SevenBridges platform (SevenBridges, USA). Read pairs with low quality were removed based on read length, mean base quality score and highest single nucleotide frequency. The remaining high-quality R1 reads were analysed to identify cell label and unique molecular identifier (UMI) sequences. The remaining high-quality R2 reads were aligned to the reference panel sequences (mRNA and AbSeq). Reads with the same cell label, same UMI sequence and same gene were collapsed into a single molecule. The obtained counts were adjusted by BD Biosciences developed error correction algorithms – recursive substitution error correction (RSEC) and distribution-based error correction (DBEC) – to correct sequencing and PCR errors. Cell counts were then estimated, using second derivative analysis to filter out noise cell labels, based on the assumption that putative cells have much more reads than noise cell labels. Barcoded oligo-conjugated antibodies (single-cell multiplexing kit; BD Biosciences) were used to infer origin of sample (e.g. sorted cell population) and multiplet rate by the BD Rhapsody analysis pipeline. The RSEC-adjusted molecule counts obtained from the Rhapsody pipeline were imported and the expression matrices were further analysed using SeqGeq (BD Biosceineces, USA) implemented with a Seurat Plugin (V4.0.3) generated base on Seurat 3.0.

2.2.8. Cell culture methods

2.2.8.1. Cultivation of adherent cell lines

The cell line NIH-3T3 (murine embryonic fibroblasts) was cultivated in DMEM medium supplemented with 10 % FBS, 20 mM HEPES and 3.5 mM L-glutamine and incubated at 37°C, 5% CO_2. Cells were detached with 0.25% Trypsin-EDTA (Thermo Fisheer Scientific, USA) and split every 2 – 3 days.

2.2.8.2. Conventional cell counting with Neubauer proved Hemocytometer

Cell density was determined by manual cell counting. Cells were diluted with 1x PBS and mixed with 1 to 2 diluted Trypan Blue Stain (Thermo Fischer Scientific, USA). 10 µl of the cell mixture was loaded on the Hemocytometer (NanoEntek, USA). The cell concentration was calculated by multiplication of the average amount of counted cells within the four counted squares with the dilution factor and the chamber factor (10^4). Total cell count was obtained by multiplication with the volume of the cell suspension.

2.2.8.3. Cell counting using Terasaki culture plates

For very low cell numbers (e.g. sorted LT-HSCs or cultured LT-HSCs), Terasaki plates (Greiner Bio-One, Germany) were used to determine cell number. 10 µl of diluted or undiluted culture sample was mixed with 1 to 10 diluted Trypan Blue Stain (Thermo Fischer Scientific, USA) and loaded onto the mini-well of the Terasaki plate followed by centrifugation (290 x g, 5 min). All visible cells on the bottom of the well were counted and multiplied with the dilution factor and the total volume of the cultured sample to obtain the total cell number.

2.2.8.4. Lentivirus particles production

Vesicular Stomatitis Virus-G (VSVG)-pseudotyped lentiviral particles were routinely produced in a split genome approach by calcium-phosphate-mediated transient transfection of human embryonic kidney HEK293T producer cells (Dull et al. 1998) by technical assistant in our lab. After 48 hours, supernatant was collected, filtered (45µm), and enriched by ultracentrifugation at 50,000 x g for 1h at 4 °C. Viral titers were determined by transduction of NIH-3T3 cells with different concentrations of virus supernatant and measured via FACS.

2.2.8.5. Lentivirus transduction

30,000 NIH-3T3 cells were seeded in a 24-well cell culture plate (Greiner Bio-One, Germany) and transduced with lentiviral particles using a multiplicity of infection (MOI) of 0.1 - 0.5. Cells were cultured in 100 µl DMEM medium at 37°C, 5% CO_2 for 48 hours. After 48 hours, medium were exchanged to 500 µl fresh DMEM and cultured until 80% confluency for further usage.

2.2.8.6. *In vitro* expansion and differentiation assay of primary hematopoietic cells

Freshly sorted LT-HSCs and MPPs were counted and 200 LT-HSCs or 1000 MPPs were seeded into 96-well culture plates in 200 µl SFEM (StemCell Technologies, Canada) supplemented with 100 ng/ml murine-SCF and murine-TPO. Additional 20 ng/ml IL3 as well as 20 ng/ml IL6 was added in to the medium for MPPs cultivation. Cells were cultured at 37°C, 5% CO_2 for 7 days. For Tgm2 overexpression, 200 LT-HSCs or 1000 MPPs were transduced with lentiviral particles using a MOI of 100 and cultured in 200 µl medium at 37°C, 5% CO_2 for 7 days.

All individual conditions were plated as triplicates. At the indicated days of analysis, the cells were harvested and 10 µl of cell suspension was used for cell counting. The remaining cells were spin down (290 x g, 7min, 4°C) and resuspend in 50 µl Brilliant Stain Buffer (BD Biosciences, USA). Cells were stained with fluorochrome-labeled antibodies against CD41, CD48, CD117, CD16/32, CD11a, CD11b and Fixable Viability Dye to determine differentiation status by FACS measurement. Data analysis was performed with FACSDiva 8.1 (BD Biosciences, USA) or FlowJo software v10 (BD Biosciences, USA).

2.2.8.7. Time-lapse imaging and single cell tracking

Cells were imaged using video-microscopy and tracked as previously described (Rieger et al. 2009; Thalheimer et al. 2014). 50 - 100 FACS sorted LT-HSCs or MPPs were seeded in a 24-well NUNC tissue culture plate (Thermo Fisher Scientific, USA) equipped with 4 well micro-inserts (IBIDI, Germany). Plates were gas-tight sealed with adhesive tape after 5% CO_2 saturation and placed inside a CellObserver 430 microscope (Zeiss, Germany) equipped with a 37°C temperature module to maintain cell culture. Phase contrast images were acquired every 2 min using a 10x phase contrast objective, and an AxioCamHRm camera (at 1388x1040 pixel resolution) with a self-written VBA module remote controlling Zeiss AxioVision 4.8 software. Cells were imaged for 7 days and manually tracked using a self-written computer program (The Tracking Tool TTT) developed by Timm Schroeder (Rieger et al. 2009) until the fate of all progenies in the third cell generation was determined. The generation time of an individual cell was defined as the time span from cytokinesis of its mother cell division to its own division. Dead cells were depicted by their shrunk, non-refracting with immobility. The current analysis did not rely on data generated by an unsupervised computer algorithm for automated tracking.

2.2.9. Statistical analysis

Statistical analysis was performed with GraphPad Prism V9.3.0. Statistical significance was determined via t-test (two-tailed, unpaired nonparametric Mann-Whitney test), Two-way ANOVA for grouped analysis comparing mean between rows or columns (Bonferroni correction), Two-way ANOVA for grouped analysis comparing regardless of row and columns (Turkey correction). Alpha threshold and confidence level is set to 0.05. *P value<0.05, **P value<0.01, ***P value<0.001 and ****P value<0.0001.

3. Results

3.1. Tgm2 expression is enriched in LT-HSCs not only at mRNA but also protein level

In order to verify the correlation between mRNA and protein expression levels, low input label-free mass spectrometric proteomics analysis on FACS sorted LT-HSCs and MPPs was performed. 5000 LT-HSCs and 10,000 MPPs were sorted as biological triplicates and lysed for quantitative mass spectrometry-based analysis. In total, 1000 proteins were detected. Among the detected proteins, 25 proteins were unique for HSCs and 275 proteins were unique for MPPs. Tgm2 was one of the most up-regulated protein in LT-HSCs in comparison to MPPs (**Figure 10A**).

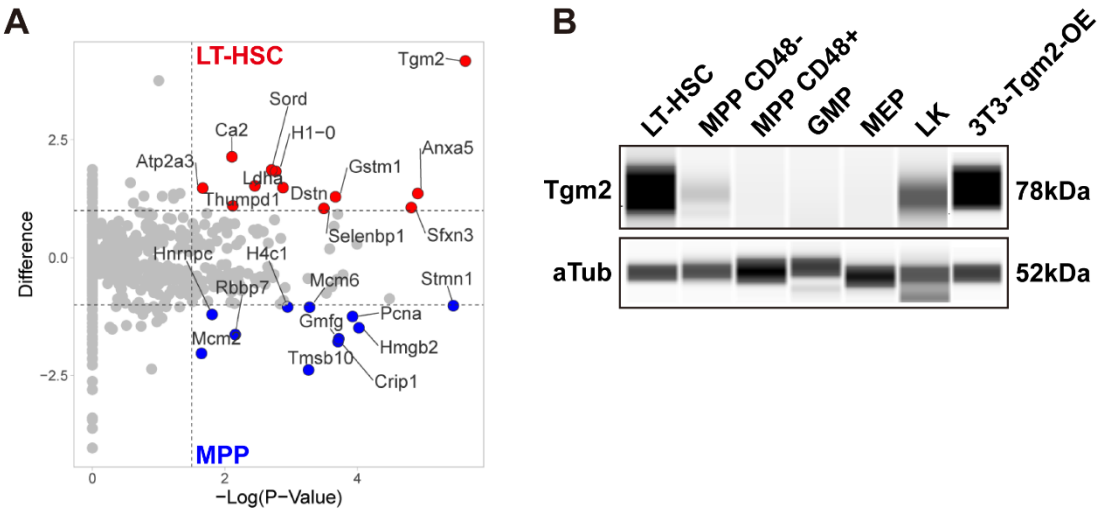

Figure 10 HSCs exhibit high *Tgm2* expression at protein level.

(A) Differential protein expression. Proteins expressed significantly higher in LT-HSCs and MPPs are shown in red and blue, respectively. The upper right corner shows proteins exclusively detected in LT-HSCs. **(B)** Protein expression analysis via WES. Protein expression of Tgm2 in FACS sorted LT-HSCs, CD48$^-$ MPPs, CD48$^+$ MPPs, GMPs, MEPs as well as LKs are detected. 3T3 cells transduced with murine Tgm2 overexpression construct serves as a positive control for Tgm2 expression. αTub expression serves as a loading control.

Tgm2 protein expression in 2000 FACS sorted LT-HSCs, CD48$^-$ MPPs, CD48$^+$ MPPs, GMPs, MEPs as well as LKs were lysed and analyzed by the highly sensitive capillary western system WES. Strikingly, a strong Tgm2 protein expression was detected in LT-HSCs. A weak Tgm2 expression was detected in CD48$^-$ MPPs but not in CD48$^+$ MPPs while the other populations express either low level or undetectable level of Tgm2. A detectable amount of Tgm2 protein was express in LKs but neither in GMPs nor MEPs (**Figure 10B**). Although LKs consists of MEPs (around 8%) and GMPs (around 50%), indicating the expression of Tgm2 was mainly contributed by the remaining progenitors from LKs such as common myeloid progenitors (CMPs) or common lymphoid progenitors (CLPs).

3.2. Conditional knock-out of Tgm2 is successfully generated with polyIC treated Mx1-Cre^{+}Tgm2$^{loxP/loxP}$ mice

In order to investigate the function of Tgm2 in LT-HSCs, a conditional Tgm2 knockout mouse model was generated. Most conditional knockout models are generated by flanking the gene of interests with *loxP* sites, which enables gene knockout in a tissue/cell specific manner by the expression of Cre recombinase (Kim et al. 2018). The most commonly used deleter strain for recombination in HSCs is the Mx1-Cre model, in which the Mx dynamin-like GTPase 1 promoter is activated in an interferon-dependent manner following by the injection of polyinosinic:polycytidylic acid (polyIC), and results in downstream expression of Cre recombinase (Kühn et al. 1995) that can remove the flanked *loxP* sites and generate the conditional knockout model. In the conditional knockout model (Nanda et al. 2001), Tgm2 was flanked by inserted *loxP* sites from exons 6 to 8, where encodes the Tgm2 catalytic domain.

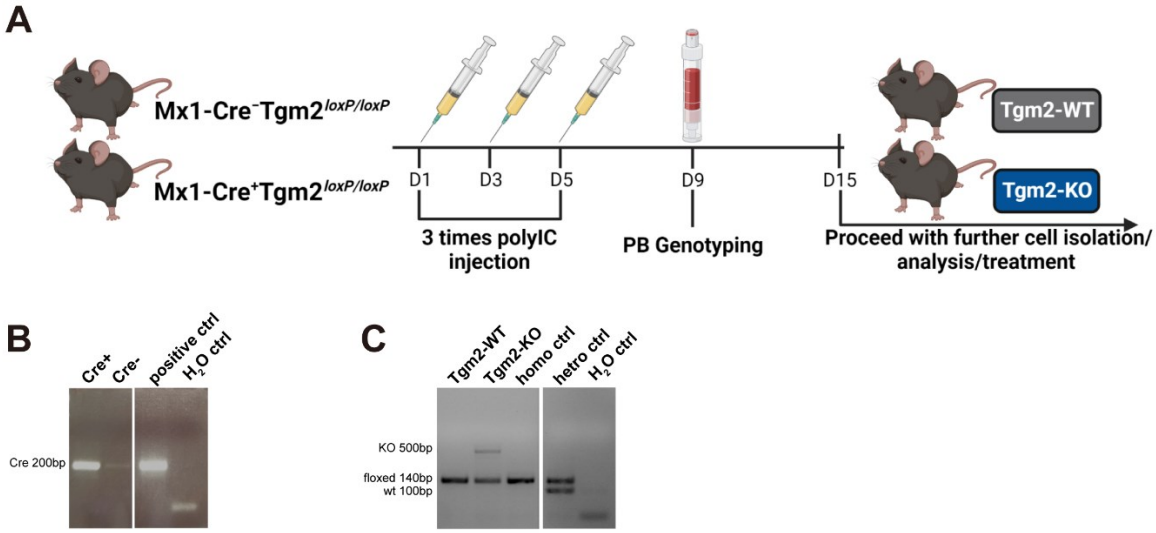

Figure 11 Schematic representation of generating conditional Tgm2-KO mice.
(A) Mx1-Cre^{-}Tgm2$^{loxP/loxP}$ and Mx1-Cre^{+}Tgm2$^{loxP/loxP}$ mice are genotyped for Mx1-Cre. I.p injection with 5 µg/gram body weight of polyIC on day (D)1, D3 and D5 is performed to achieve a three-round injection. PB is collected from treated mice on D9 for genotyping. PolyIC treated Mx1-Cre^{-}Tgm2$^{loxP/loxP}$ mice = Tgm2-WT; PolyIC treated Mx1-Cre^{+}Tgm2$^{loxP/loxP}$ =Tgm2-KO. All the experiment in this project are performed on D15. Figure generated in BioRender. **(B)** DNA gel electrophoresis of Mx1-Cre genotyping (primers Cre forward and Cre reserve) with mouse tissue. The expected size of the product is around 200bp. H_2O negative control is included. **(C)** DNA gel electrophoresis of Tgm2 knockout genotyping (primer murine Tgm2 P1, P2 and P3) with PB DNA. P2 and P3 allow to distinguish between wild type (100 bp) and floxed (140 bp) allele, whereas P1 and P3 determine deleted allele (500 bp). Homocygote control (homo ctrl: Tgm2$^{loxP/loxP}$), hetrocygote control (hetro ctrl: Tgm$^{wt/loxP}$) and H_2O negative control are included.

The Mx1-Cre was determined by genotyping with primers 5'-AAATTGCCAGGATCAGGGTTAAAG-3' and 5'- AGAGTCATCCTTAGCGCCGTAAAT-3' amplifying a 200-bp PCR product (**Figure 11B**). Afterwards, an appropriate number of mice

according to the experimental plan with either Mx1-Cre$^+$ or Mx1-Cre$^-$ genotype were transported to Georg-Speyer-Haus (Frankfurt am Main, Germany). 3 rounds polyIC injection was performed every second day (**Figure 11A**) and around 50 µl of PB of each mouse was withdrawn for knockout genotyping using primers P1: 5'-CATGAATCAGGATGCACGTG-3', P2: 5'-GGCAAGGTCTGAGAAAGCAC-3' and P3: 5'-GACAAAGGAGCAAGTGTTAC-3'. P2 and P3 allowed to distinguish between wild type (100 bp) and floxed (140 bp) allele, whereas P1 and P3 determined deleted allele (500 bp) (**Figure 11C**). The successive generation of conditional knockout mice were viable and showed no aberrant organ functions.

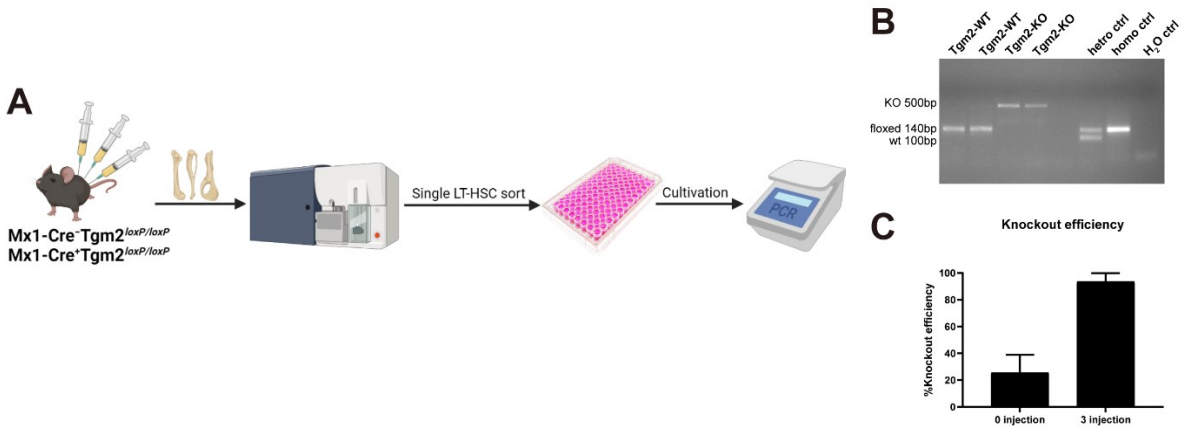

Figure 12 Knockout efficiency of FACS sorted single LT-HSCs.

(A) Single LT-HSCs from non-polyIC treated and three-round polyIC treated Mx1-Cre$^+$Tgm2$^{loxP/loxP}$ mice are sorted in to 96-well plate for cultivation (three plates per condition). DNA extracted from each growth single colony is genotyped (primer murine Tgm2 P1, P2 and P3). Figure generated in BioRender. **(B)** DNA gel electrophoresis of Tgm2 knockout genotyping (primer murine Tgm2 P1, P2 and P3) with cultured LT-HSCs. Image of four selected colonies are presented as an example here. P2 and P3 allowed to distinguish between wild type (100 bp) and floxed (140 bp) allele, whereas P1 and P3 determined deleted allele (500 bp). Homocygote control (homo ctrl: Tgm2$^{loxP/loxP}$), hetrocygote conytol (hetro ctrl: Tgm$^{wt/loxP}$) and H_2O negative control are included. **(C)** Knockout efficiency is calculated for each 96-well plate: $\mathbf{knockout\ efficiency} = \frac{\mathbf{Number\ of\ genotyped\ KO\ colonies}}{\mathbf{Number\ of\ total\ colonies}}$.

In order to examine the knockout efficiency of LT-HSCs after generating conditional knockout mice with 3 rounds polyIC injection, single LT-HSC from non-polyIC treated and 3-rounds polyIC treated Mx1-Cre$^+$Tgm2$^{loxP/loxP}$ was sorted into 96-well plate and cultured with 100 µl SFEM medium supplemented with 100 ng/ml SCF and TPO for 7-10 days until a colony was formed (**Figure 12A**). DNA was extracted from 354 single colonies and PCR for Tgm2 knockout verification was performed as described in **2.2.4.4**. Around 30% spontaneous deletion of the flanked fragment prior to polyIC injection was observed, which has been described in other publications (Kühn et al. 1995; Kemp et al. 2004), whereas 3 rounds polyIC injection has been resulting in over 95% deletion efficiency of individual LT-HSCs (**Figure 12B**).

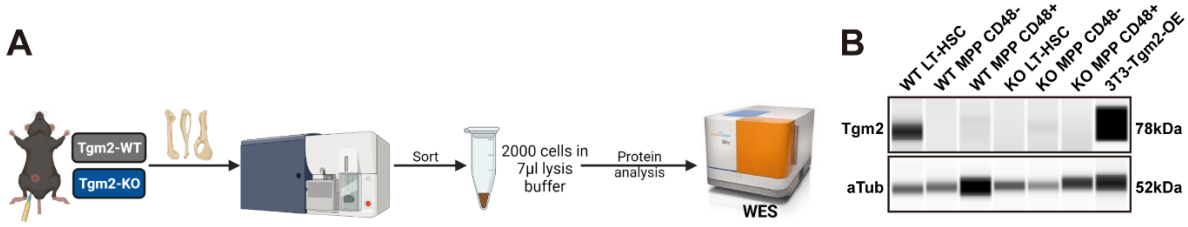

Figure 13 Protein expression analysis via WES.

(A) In order to obtain a concentrated protein lysates with rare cell populations, 2000 cells of interests from Tgm2-WT and Tgm2-KO mice are sorted directly into 7 µl lysis buffer. Figure generated in BioRender. **(B)** Protein expression of TG2 in 2000 FACS sorted LT-HSCs, $CD48^-$ MPPs and $CD48^+$ MPPs from Tgm2-WT and Tgm2-KO mice are detected. 3T3 cells transduced with murine Tgm2 overexpression construct serves as a positive control for Tgm2 expression. αTub expression serves as a loading control.

Tgm2 protein expression was detected in order to confirm the conditional knockout at protein level. Protein lysates of 2000 FACS sorted LT-HSCs, $CD48^-$ MPPs and $CD48^+$ MPPs from Tgm2-WT and Tgm2-KO mice were analyzed via WES analysis (**Figure 13A**). As expected, Tgm2 expression could be only detected in Tgm2-WT LT-HSCs, while LT-HSCs and MPPs from Tgm2-KO mice were lacking the expression of the protein (**Figure 13B**).

All these data indicated a successful Tgm2 deletion in the hematopoietic system was generated upon the treatment. Therefore, further experiments of this project were performed with 3 rounds of polyIC injection, using Mx1-$Cre^-$$Tgm2^{loxP/loxP}$ and Mx1-$Cre^+$$Tgm2^{loxP/loxP}$ mice to generate Tgm2-WT and Tgm2-KO mice, respectively.

3.3. Tgm2 conditional knockout does not alter the BM HSPC distributions, cycling status, and mitochondrial potential

To access the requirement of Tgm2 expression in steady-state hematopoiesis, the distribution of mature blood cells as well as HSPC distributions within hematopoietic organs were analyzed with Tgm2-WT and Tgm2-KO mice. Total BM cells were isolated according to the described methods in **2.2.2.2**.

Myeloid cells, B cells and T cells population were analyzed from total BM. No differences could be detected in B cells and T cells, while the myeloid cell population appeared to be slightly decreased in the BM of Tgm2-KO mice (**Figure 14A**). BMMNCs were enriched from the total BM cells via gradient centrifugation and LT-HSCs, ST-HSCs, MPPs, GMPs and MEPs distribution were analyzed via FACS. There was no differences in the HSPC cellular distribution between Tgm2-WT and Tgm2-KO mice (**Figure 14B**).

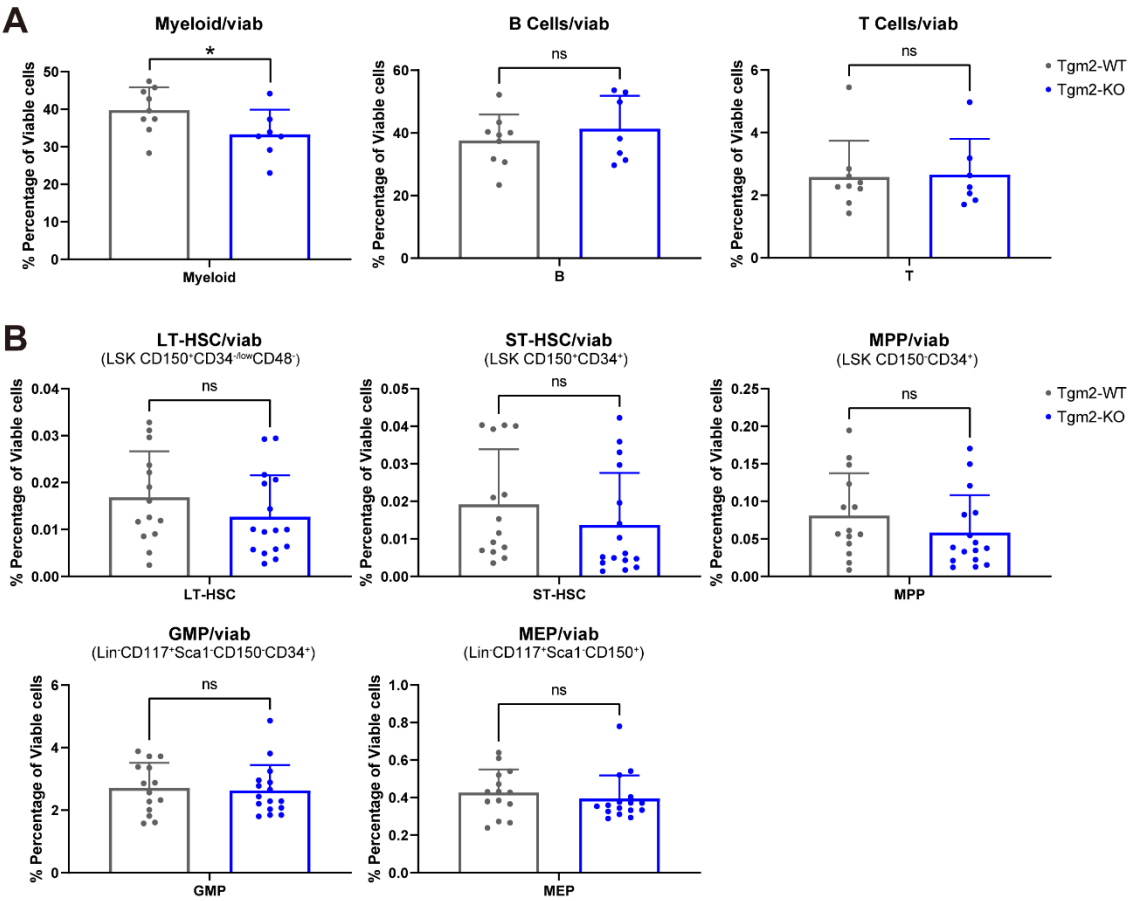

Figure 14 Analysis of BM leukocytes and HSPCs.

(A) Distribution of BM leukocytes including myeloid cells (CD11b$^+$/Gr1$^+$), B cells (CD11b$^-$ B220$^+$) and T cells (CD11b$^-$ CD3e$^+$) from Tgm2-WT and Tgm2-KO mice. Percentage is calculated from total viable cells. **(B)** Distribution of BM HSPCs including LT-HSC (LSK CD150$^+$ CD34$^{-/low}$ CD48$^-$), ST-HSC (LSK CD150$^+$ CD34$^+$), MPP (LSK CD150$^-$ CD34$^+$), GMP (LK CD150$^-$ CD34$^+$) and MEP (LK CD150$^+$) from Tgm2-WT and Tgm2-KO mice. Percentage is calculated from total viable cells. The mean ± SD is displayed. *P value<0.05.

To further delineate the importance of Tgm2 expression for the dormancy of LT-HSCs, the cell cycle status of HSPCs was analyzed using intracellular Ki67 staining. The concomitant use of 7-amino-actinocycin D (7-AAD) and Ki67 allows the measurement of G0, G1, S/G2/M (mitosis) phase. Ki67 is a nuclear protein associated with cellular proliferation, which is expressed during the cell cycle but absent in non-cycling cells. Ki67 is commonly used as a proliferation marker because it is not detected in G0 cells, but increases steadily from G1 through M. Normally, the majority of the LT-HSCs is quiescent in G0 phase to maintain their numbers and functions, the MPPs exhibit around 50% in G0 phase, whereas most of the GMPs and MEPs are in the G1 phase **(Figure 15A)**. In this analysis, Ki67 staining revealed an unaltered cell cycle status of Tgm2-WT and Tgm2-KO LT-HSCs and progenitors **(Figure 15B)**.

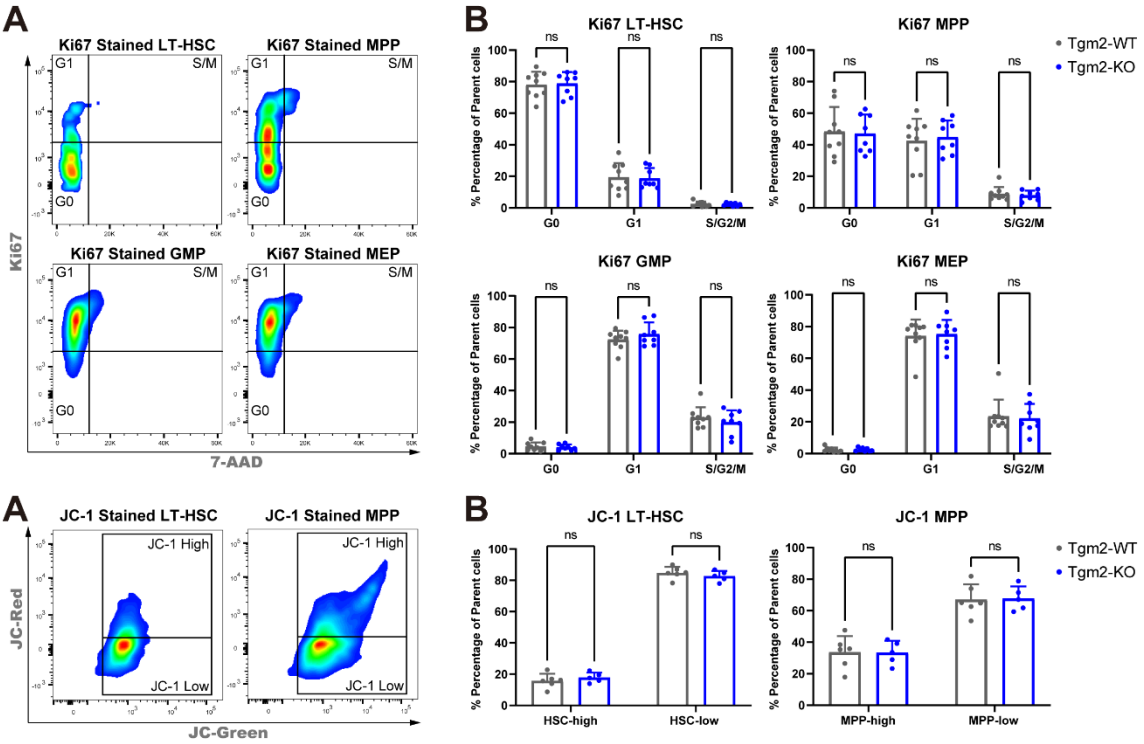

Figure 15 Ki67 expression of BM HSPCs.

(A) FACS representation of Ki67 staining of LT-HSC, MPP, GMP and MEP. **(B)** Frequencies of G0, G1, S/G2/M phase of LT-HSCs, MPPs, GMPs and MEPs from Tgm2-WT and Tgm2-KO mice. Percentage is calculated from parental population. The mean ± SD is displayed.

As Tgm2 is a highly Ca^{2+} dependent enzyme, the knockout of Tgm2 might result in alterations of calcium concentration in LT-HSCs. Intracellular calcium level is associated with mitochondrial membrane potential. To obtain an overall picture of the mitochondrial membrane potential changes within LT-HSCs and progenitors upon Tgm2 knockout, lineage-marker negative BM cells were stained with the JC-1 dye and prospective surface markers that have been well established in our lab. JC-1 is a cationic carbocyanine dye that accumulates in the mitochondria, indicated by a fluorescence emission shift from green (~525 nm) to red (~590 nm). The potential-sensitive color shift is due to concentration-dependent formation of red fluorescent J-aggregates. The ratio of green to red fluorescence of JC-1 is only dependent on the membrane potential but not the other factors such as mitochondrial size, shape, or density. Under steady conditions, around 13% of LT-HSCs displayed high mitochondrial potential while approximately 30% of MPPs exhibited high mitochondrial potential (Fawaz et al, unpublished data, **Figure 16A**). JC-1 stained LT-HSCs and progenitors did not show any differences between Tgm2-KO and Tgm2-WT (**Figure 16B**), indicating the mitochondrial potential remained unchanged upon Tgm2 knockout.

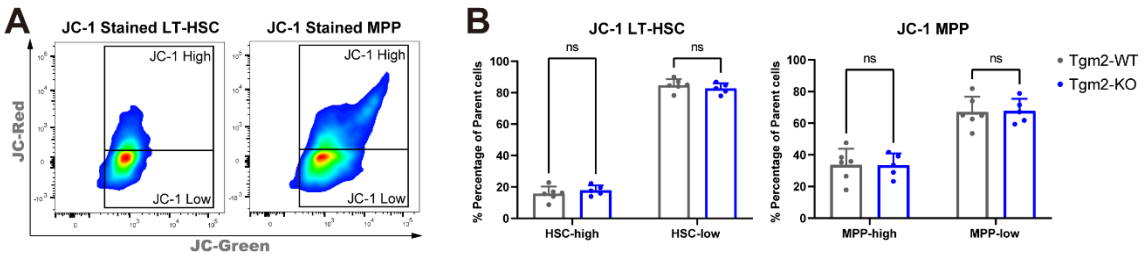

Figure 16 Mitochondria potential of LT-HSCs and MPPs.

(A) FACS representation of JC-1 staining of LT-HSC and MPP. **(B)** Frequencies of JC-1 high (mito-high) and JC-1 low (mito-low) in LT-HSCs and MPPs from Tgm2-WT and Tgm2-KO mice. Percentage is calculated from parental population.

Taken together, the analysis of LT-HSCs and progenitors of Tgm2-WT and Tgm2-KO mice showed that Tgm2 was not associated with the cellular distributions, cell cycle status and mitochondrial potential in the hematopoietic system *in vivo*.

3.4. *In vitro* characterization of LT-HSCs and MPPs upon conditional Tgm2 knockout

Besides analyzing the *in vivo* changes of Tgm2-KO HSPCs under steady state, the *in vitro* functional analysis of Tgm2-KO LT-HSCs and MPPs were also conducted.

3.4.1. Tgm2 conditional knockout LT-HSC shows delayed entry into cell cycle

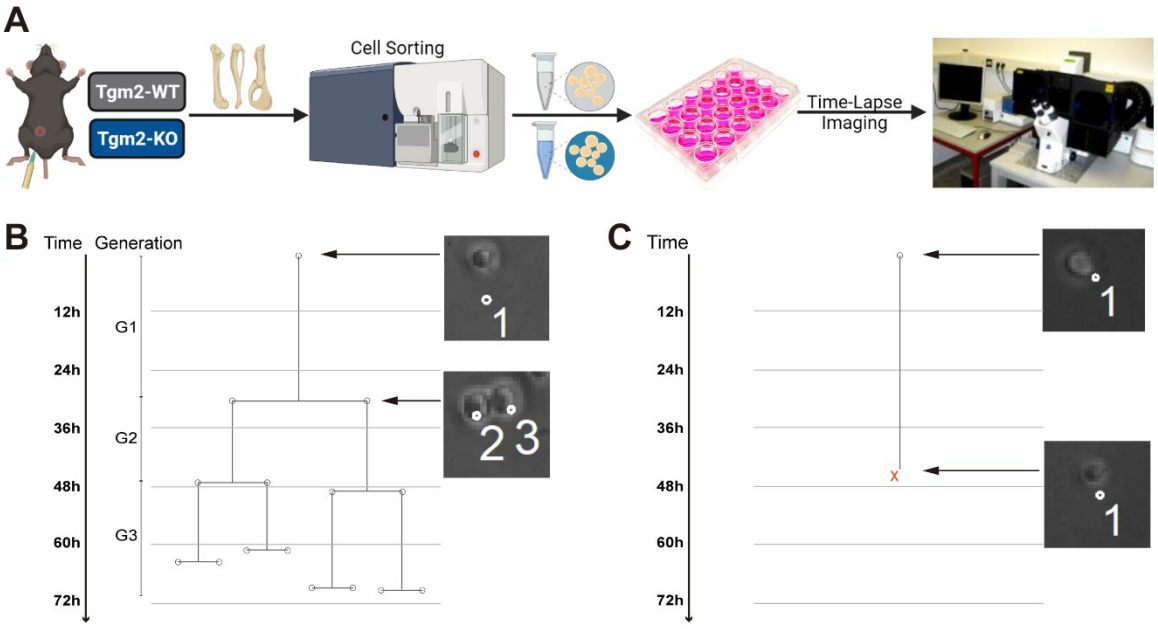

Figure 17 Time-lapse microscopy-based single cell tracking.

(A) Experimental scheme of time-lapse microscopy-based single cell tracking. Figure generated in BioRender. **(B)** Representative pedigree of an individual LT-HSC and its progeny up to the 3rd generation over 72 hours. Cell images of the indicated time points corresponding to the pedigree are displayed on the right. G1: first generation; G2: second generation; G3: third generation. **(C)** Representative pedigree of an individual LT-HSC going into apoptosis. Cell images are displayed on the right.

To investigate the proliferation and fate of HSPCs at single cell level, the time of first division and time of consecutive generations, Tgm2-WT and Tgm2-KO LT-HSCs and MPPs were continuous observed via time-lapse microscopy-based single cell tracking (**Figure 17A**). Freshly sorted Tgm2-WT and Tgm2-KO LT-HSCs and MPPs were plated into 24-well plates equipped with silicon culture inserts, which prevent the migration of the cells out of the camera field. Cells were incubated in self-renewal promoting conditions with SCF and TPO, additionally with IL-3 and IL-6 for MPPs and the time-lapse imaging was subsequently started allowing the real time observation of the behavior of the single cell. After observing the cells for 7 days, the image data was analyzed by tracking individual cells using a self-written computer program (Timm´s Tracking Tool; TTT) which can determine and record multiple parameters of individual cells at each time point. Single cells were tracked until the third generation. The mother generation was designated as G1. The generation time of an individual cell was defined as the time span from cytokinesis of its mother cell to its own division (**Figure 17B**). Dead cells could be recognized by their shrunken, non-refracting appearance and immobility (**Figure 17C**). This method allowed the observation of cellular changes such as apoptosis, generation time, or cell fate over time.

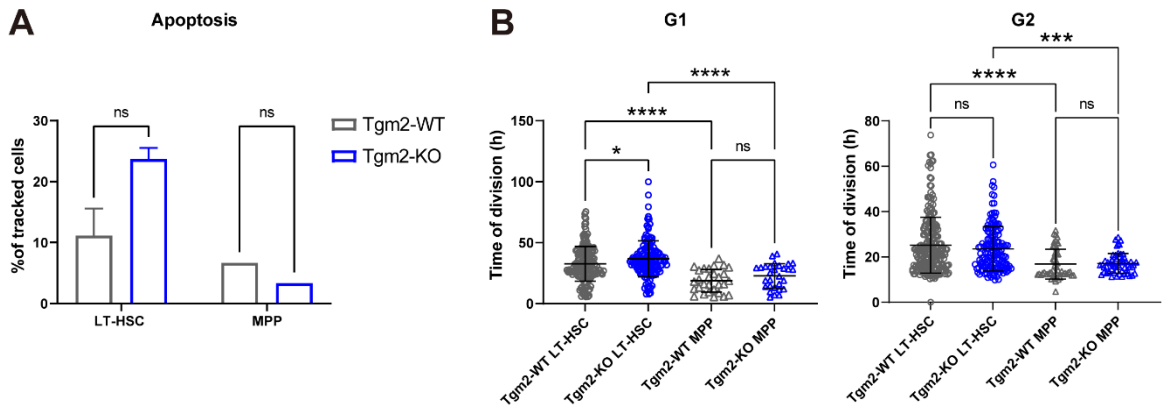

Figure 18 Time-lapse microscopy-based single cell tracking of Tgm-WT and Tgm2-KO LT-HSCs and MPPs. **(A)** Apoptosis rate before the first cell division of tracked cells. **(B)** Time of first division (left, G1) and generation time (right, G2) of Tgm-WT and Tgm2-KO LT-HSCs and MPPs. 135 Tgm2-WT LT-HSCs, 131 Tgm2-KO LT-HSCs and their progenies were tracked from three independent movies. The mean ± SD is displayed. *P value<0.05, **P value<0.01, ***P value<0.001 and ****P value<0.0001.

In total, 135 Tgm2-WT LT-HSCs, 131 Tgm2-KO LT-HSCs and their progenies were tracked from three independent movies. Tgm2-KO LT-HSCs represented a more than two fold higher apoptosis rate (**Figure 18A**) and at the same time showed a delay of 4 hours to exit quiescence and enter cell cycle (36.85 hours) compared to Tgm2-WT LT-HSCs (32.71 hours). However, no difference in cell cycle or apoptosis could be detected in the subsequent generations (**Figure 18B**).

On the other hand, 30 Tgm2-WT MPPs and Tgm2-KO MPPs and their progenies were tracked. The apoptosis rate between Tgm2-WT and Tgm2-KO MPPs were similar (**Figure 18A**). MPPs in general divided much faster than LT-HSCs, independent of the expression of Tgm2. However, no significant differences in entering into first cell cycle as well as subsequent generations could be observed between Tgm2-WT MPPs and Tgm2-KO MPPs (18.84 hours versus 20.80 hours, **Figure 18B**).

3.4.2. Tgm2 is not essential for *in vitro* proliferation

To investigate the *in vitro* differentiation of Tgm2-WT and Tgm2-KO cells, 200 FACS isolated LT-HSCs and 1000 MPPs were cultivated for 7 days. To further simulate the expression of Tgm2 and to determine whether an increased expression leads to alterations in cell proliferation and differentiation, Tgm2 was lentivirally overexpressed in sorted Tgm2-WT and Tgm2-KO LT-HSCs (200 cells) and MPPs (1000 cells). The transduced cells were distinguished by VENUS$^+$ expression. The cell counts and the differentiation status of cultivated cells were analyzed via FACS with several differentiation markers. The most immature cells after cultivation were depicted as CD117$^+$, CD16/32$^-$, CD48$^-$, and CD11a$^-$. The differentiation of the cells were defined by gaining the expression of CD48, CD11a, then CD16/32, and eventually losing CD117 expression.

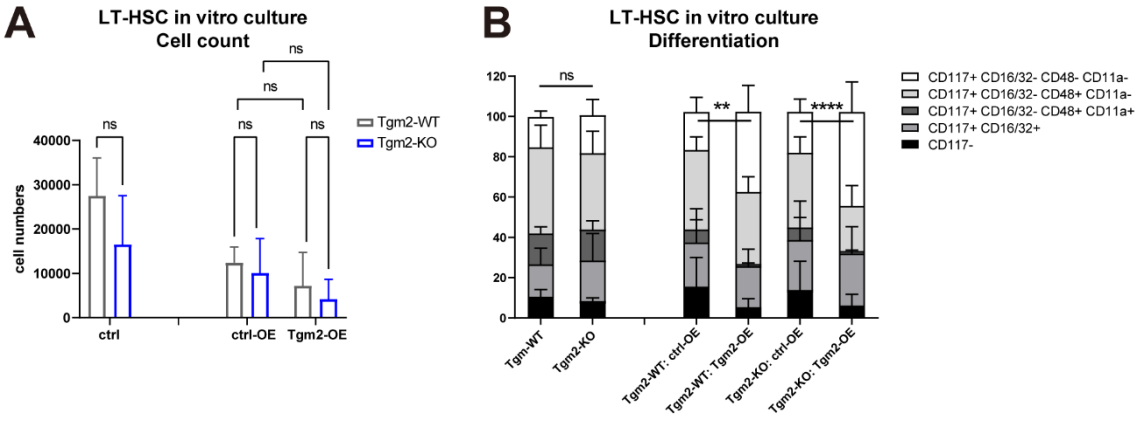

Figure 19 *In vitro* cell expansion and differentiation analysis of LT-HSCs.
(A) Cell expansion of Tgm2-WT and Tgm2-KO LT-HSCs, Tgm2-WT and Tgm2-KO LT-HSCs transduced with VENUS empty vector control, Tgm2-WT and Tgm2-KO LT-HSCs overexpressed with VENUS-murine-Tgm2 after 7 days cultivation in self-renewal-promoting minimal cytokine condition with SCF and TPO. **(B)** Quantification and statistical analyses of differentiation status of *in vitro* cultured LT-HSCs. Percentage is calculated from viable cells. *P value<0.05, **P value<0.01, ***P value<0.001 and ****P value<0.0001

Consistent with the observed higher apoptosis rate from the *in vitro* time-lapse images, Tgm2-KO LT-HSCs had less cells after 7 days *in vitro* culture. However, this was not rescued by overexpressing Tgm2 in Tgm2-KO LT-HSCs (**Figure 19A**). Both Tgm2-WT and Tgm2-KO LT-HSCs displayed similar differentiation pattern, with most cells were CD117$^+$ and around 20%

were still immature. Interestingly, overexpression of Tgm2 in Tgm2-WT or Tgm2-KO LT-HSCs resulted in a two fold increase of immature HSPCs (**Figure 19B**).

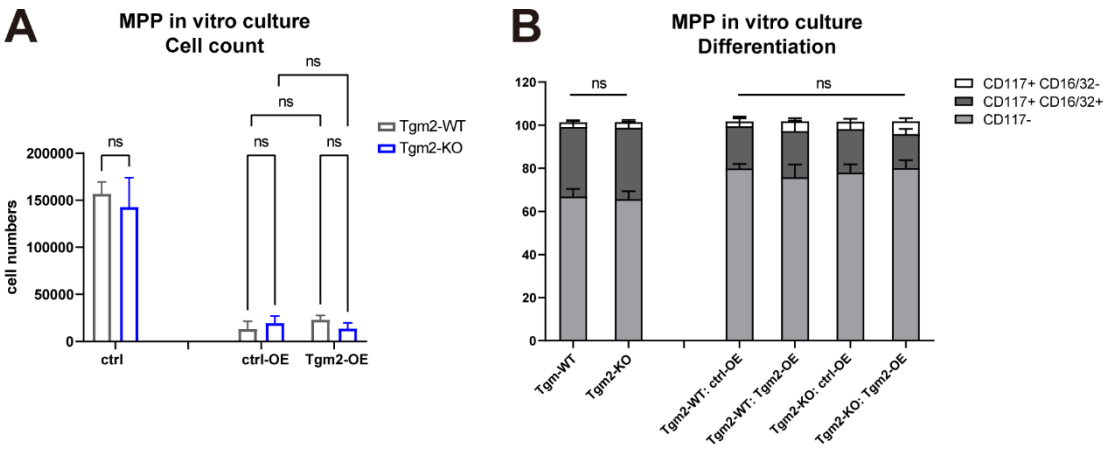

Figure 20 *In vitro* cell expansion and differentiation analysis of MPPs.
(A) Cell expansion of Tgm2-WT and Tgm2-KO MPPs, Tgm2-WT and Tgm2-KO MPPs transduced with VENUS empty vector control, Tgm2-WT and Tgm2-KO LT-HSCs overexpressed with VENUS-murine-Tgm2 after 7 days cultivation in self-renewal-promoting minimal cytokine condition with SCF, TPO, IL3 and IL6. **(B)** Quantification and statistical analyses of differentiation status of *in vitro* cultured MPPs. Percentage is calculated from viable cells.

On the contrary, Tgm2-WT and Tgm2-KO MPPs proliferated and expanded similarly upon *in vitro* culture (**Figure 20A**). Different from LT-HSCs, 7 days *in vitro* culture of MPPs ended up with more differentiated sub-populations ($CD117^-$). However, the differentiation pattern between Tgm2-WT and Tgm2-KO MPPs were not altered with or without the overexpression of Tgm2 (**Figure 20B**).

Hence, *in vitro* analysis of Tgm2-WT and Tgm2-KO cells suggested that Tgm2 was not effecting the *in vitro* proliferation of LT-HSCs and MPPs. However, Tgm2 expression might be essential for *in vitro* survival of LT-HSCs but not MPPs. LT-HSCs absent of Tgm2 were slower to enter cell cycle, but the subsequence cell division was immediately compensated. Tgm2 overexpressed LT-HSCs seemed to be maintained in a more undifferentiated stage, which needed further experimental evidence.

3.5. Transcriptomic analysis of LT-HSCs and MPPs from Tgm2-WT and Tgm2-KO mice

As the *in vitro* experiments did not illustrate prominent long-term functional alterations, it is important to assess potential alterations in gene expression profiles and whether compensatory genes with similar function were up-regulated to overcome the absence of Tgm2. Whole transcriptome profiles were obtained via RNA-sequencing of 500 freshly sorted LT-HSCs and MPPs from Tgm2-WT and Tgm2-KO mice.

3.5.1. Either LT-HSCs or MPPs from Tgm2-WT and Tgm2-KO mice harbor high similarity

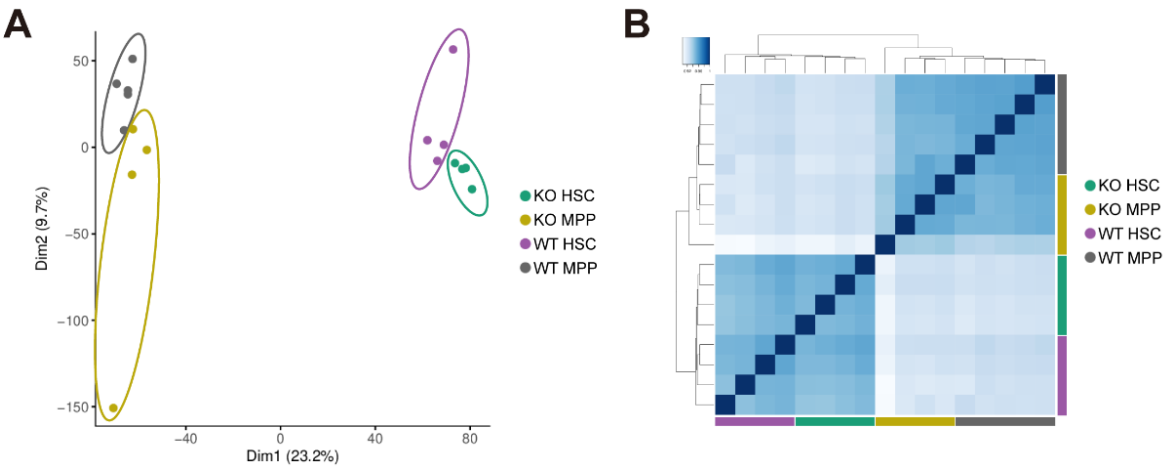

Figure 21 Variations of samples in bulk RNA sequencing.

(A) Principal component analysis (PCA) using FactoMineR based on DESeq normalized counts. The top two dimensions incorporating the largest amount of divergence is presented. X (Dim1) and Y (Dim2) axes are scaled to reflect variance (Dim1 = 23.2%; Dim2 = 9.7%). **(B)** Spearman correlation coefficient heatmap based on DESeq normalized counts. Darker blue indicates higher correlation; lighter blue indicates lower correlation.

The variation of the dataset is visualized through principal component analysis (PCA) (Ringnér 2008) as well as Spearman's rank correlation coefficient (Fieller et al. 1957). In PCA, a large number of variables are reduced into a smaller number of linearly transformed dimensions, providing an explanation for the variability in the dataset. Dimension (Dim) 1, or principal component (PC) 1, reflect the most variation within the data, whereas Dim2 describes the second most. The Spearman's rank correlation is a nonparametric measure using the rank values of the two variables. The more similar the expression profiles for all transcripts are between two samples, the higher the correlation coefficient will be. In **Figure 21**, clusters of LT-HSCs and MPPs were different based on Dim1 (23.2%) independent from Tgm2 expression, while the difference of Tgm2-WT and Tgm2-KO were based on Dim2 (9.7%). The Spearman's rank correlation heatmap indicated a definite grouping of replicates as well as a clear separation of LT-HSCs and MPPs. These analysis suggested that LT-HSCs or MPPs from Tgm2-WT and Tgm2-KO were very similar but still holding their distinct genetic profiling.

3.5.2. Absence of Tgm2 does not change the mRNA expression of stem cell signature genes

As the HSPC FACS staining for Tgm2-WT and Tgm2-KO mice did not show significant changes, mRNA expression of the genes encoded for FACS staining surface markers that distinguish LT-HSCs and MPPs were represented here as box plot (**Figure 22**).

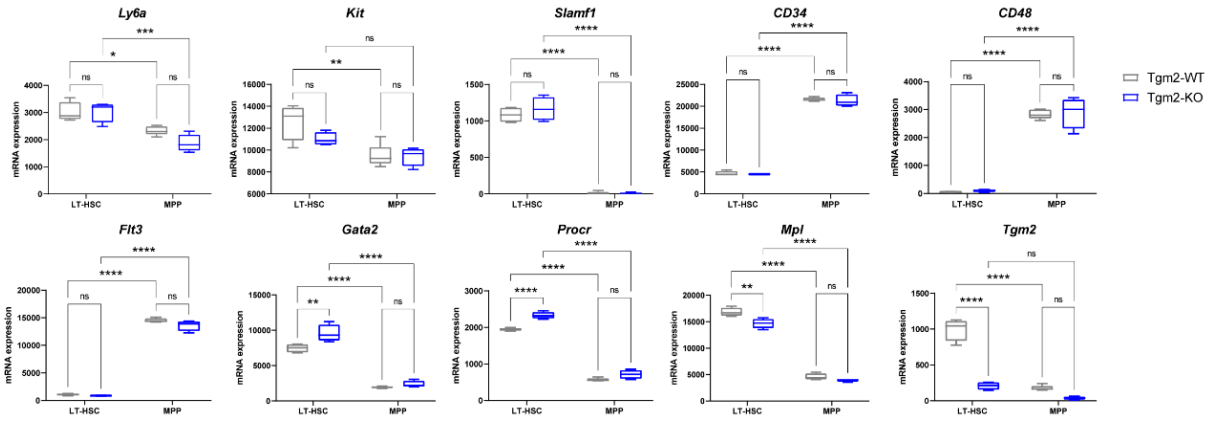

Figure 22 mRNA expression values for stem cell signature genes.

mRNA expression values normalized against library size for *Ly6a, Kit, Slamf1, CD34, CD48, Flt3, Gata2, Procr, Mpl* and *Tgm2* genes are shown for all samples. The mean ± SD is displayed. *P value<0.05, **P value<0.01, ***P value<0.001 and ****P value<0.0001.

Ly6a (coding for Sca1), *Kit* (coding for CD117/cKit), *Slamf1* (coding for CD150), *CD34*, *CD48*, *Flt3* (coding for CD135) were up/downregulated accordingly for LT-HSCs and MPPs but no differences between Tgm2-WT and Tgm2-KO LT-HSCs or MPPs. Some interesting LT-HSC signature genes were also presented. *Gata2*, predominantly expressed in stem cells and mast cells, has been reported to be involved in LT-HSC proliferation and survival (Tsai and Orkin 1997). *Procr*, coding for EPCR/CD201, has been reported to identify LT-HSCs (Kent et al. 2009). The gene expression of *Procr* was elevated in LT-HSCs upon Tgm2 knockout, but not in MPPs. On contrary, *Mpl* expression was diminished in Tgm2-KO LT-HSCs. *Mpl*, which encodes thrombopoietin (TPO) receptor and envolved in TPO/Mpl signaling, is not only supporting LT-HSC proliferation and self-renewal during regenerative processes (Fox et al. 2002), but also fostering HSC quiescence during steady-state hematopoiesis (Yoshihara et al. 2007; Qian et al. 2007). Interestingly, EPCR has been reported to support LT-HSC engraftment and expansion in Mpl knockout mice (Kohlscheen et al. 2019). Importantly, gene expression of Tgm2 showed that the generated conditional knockout mouse model was not only silencing Tgm2 at translational level as shown in **Figure 13**, but also at transcriptional level.

3.5.3. Gene expression of other Tgase family members did not vary significantly in Tgm2 deficient cells

Tgm2 is relatively more abundant and wider distributed than other members of the transglutaminase family. Thus, Tgm2 is actually involved in more physiological processes than other members. Many studies have suggested possible compensations by other Tgase family members for the absence of Tgm2, which might explain the fact that Tgm2 knockout mice do not result in lethal phenotype (Nurminskaya and Belkin 2012; Odii and Coussons 2014).

Therefore, whether an alteration of the mRNA expression of other Tgase family members upon Tgm2 knockout was visualized.

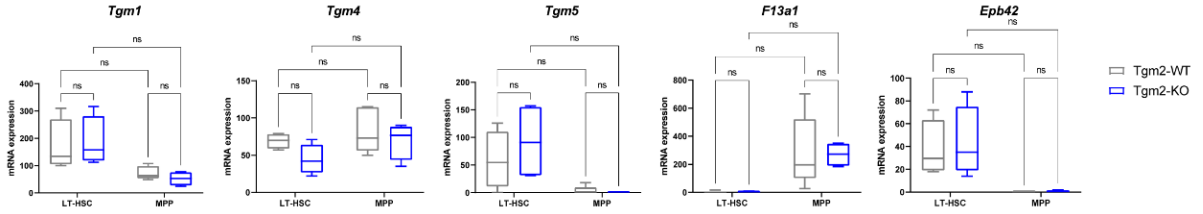

Figure 23 mRNA expression values for Tgase family members.

mRNA expression values normalized against library size for *Tgm1, Tgm4, Tgm5, F13a1* and *Epb42* genes are shown for all samples. The mean ± SD is displayed.

The relative gene expressions of *Tgm1, Tgm4, Tgm5, F13a1* (coding for FXIII-A) as well as *Epb42* (coding for Band 4.2) were presented in **Figure 23**. Besides *Tgm1*, the other family members represented a relatively low mRNA expression level in LT-HSCs and MPPs. Under the Tgm2 loss condition, the gene expression of these family members were not significantly altered to compensate the enzymatic function of Tgm2, at least in this short-term experimental setup with cells isolated from the BM 10 days after a successful generation of Tgm2 conditional knockout.

3.5.4. Tgm2-KO LT-HSCs and MPPs are transcriptionally more activated

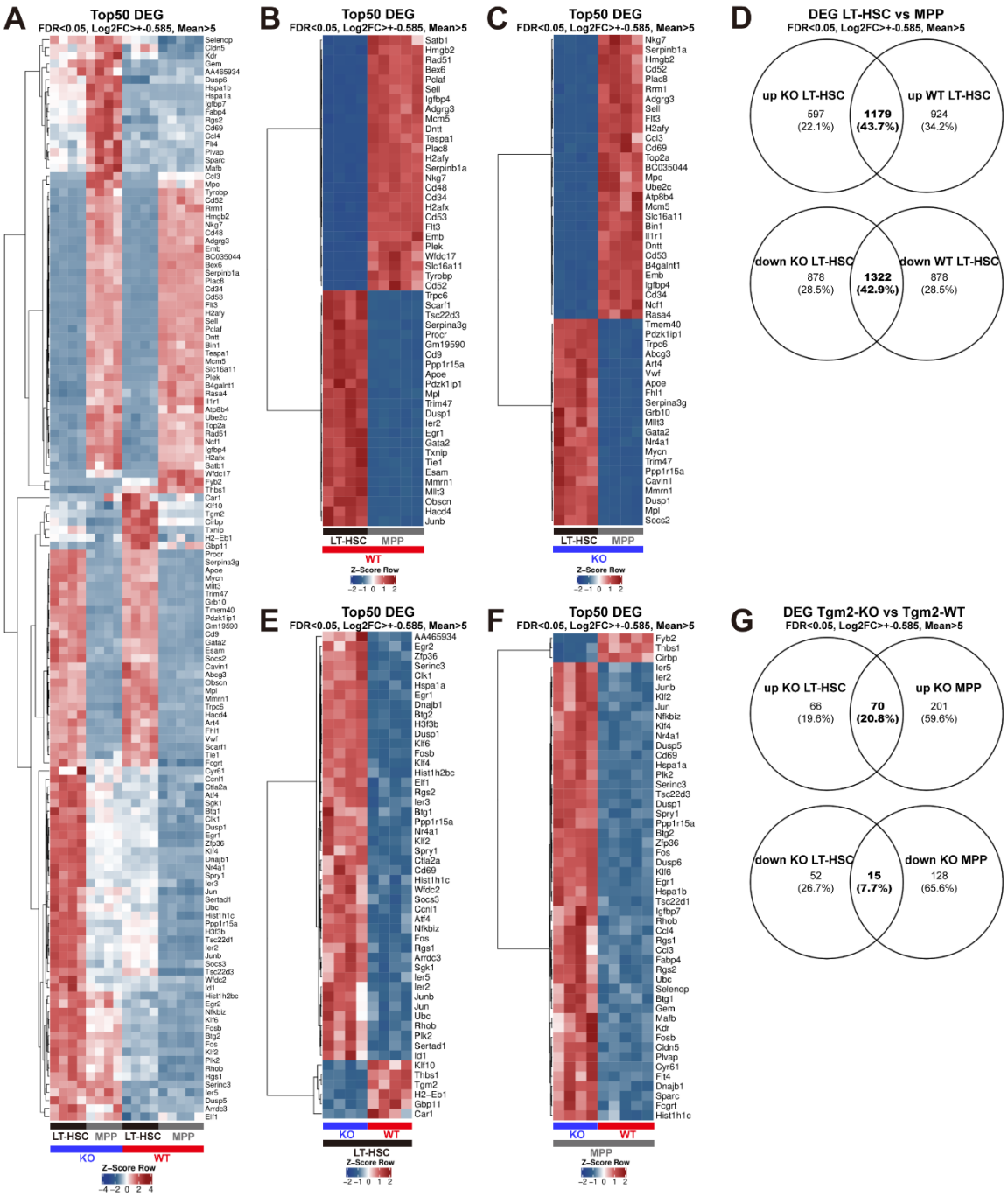

Figure 24 Differential gene expression profiles in different subsets.

(A) Combined heatmap of top50 most significantly differentially expressed DEGs (sorted by smallest padj). **(B)** Heatmap for selected top50 most significantly differentially expressed DEGs between Tgm2-WT LT-HSCs and MPPs (sorted by smallest padj). **(C)** Heatmap for selected top50 most significantly differentially expressed DEGs between Tgm2-KO LT-HSCs and MPPs (sorted by smallest padj). **(D)** Venn diagram displaying the number of up- or down-regulated DEGs in Tgm-KO LT-HSCs and Tgm2-WT LT-HSCs when comparing to their corresponding MPPs. **(E)** Heatmap for selected top50 most significantly differentially expressed DEGs between Tgm2-KO LT-HSCs and Tgm2-WT LT-HSCs (sorted by smallest padj). **(F)** Heatmap for selected top50 most significantly differentially expressed DEGs between Tgm2-KO MPPs and Tgm2-WT MPPs (sorted by smallest padj). **(G)** Venn diagram displaying the number of up- or down-regulated DEGs in Tgm-KO LT-HSCs and Tgm2-KO MPPs when comparing to their Tgm-WT counterparts. The commonly regulated genes are listed in **Appendix**

Table 16.

Red represent up-regulated and blue represent down-regulated DEGs.

Top 50 differential expression genes (DEGs) represented in heatmaps revealed a distinct profile for each of the four analyzed populations (**Figure 24**). Consistent with the PCA analysis (**Figure 21**), distinct gene clusters of LT-HSCs or MPPs were observed independent of Tgm2 expression (**Figure 24A**). Although the majority of DEGs between Tgm2-WT LT-HSCs versus MPPs and Tgm2-KO LT-HSCs versus MPPs were overlapping, there were specifically up and down regulated genes for WT LT-HSCs (924 up regulated and 878 down regulated DEGs) and KO LT-HSCs (597 up-regulated and 878 down regulated DEGs) (**Figure 24B, C, D**), indicating a transcriptional alteration of LT-HSCs and MPPs after knockout of Tgm2.

Previous studies have shown a high Tgm2 gene expression in LT-HSCs in comparison to MPPs (Forsberg et al. 2005; Forsberg et al. 2010; Qiu et al. 2014). Molecular changes in Tgm2 deficient LT-HSCs were different from those in Tgm2 deficient MPPs (**Figure 24A**), suggesting a different role of Tgm2 in distinct cell types. Compared to Tgm2-WT, there were obviously more upregulated genes in Tgm2-KO conditions for both LT-HSCs and MPPs compartments (**Figure 24E, F**). Using a 1.5 fold change (FC) and false discovery rate (FDR) p-value < 0.05 cut off, there were 136 DEGs being up-regulated and 67 DEGs being down-regulated in Tgm2-KO LT-HSCs compare to Tgm2-WT LT-HSCs. Similar observation was shown for the 414 DEGs between Tgm2-WT and Tgm2-KO MPPs, where 271 DEGs were up-regulated and 143 genes were down-regulated in Tgm2-KO MPPs (**Figure 24G**). This finding suggested that cells from Tgm2-KO mice were transcriptionally more activated.

70 out of 337 (20.8%) up-regulated DEGs were in common in Tgm2-KO LT-HSCs and MPPs, whereas only 15 out of 195 (7.7%) down-regulated ones were shared (**Figure 24G**). Importantly, among the 70 commonly up-regulated DEGs, genes involved in regulation of transcription from RNA polymerase II promoter in resonse to stress (*Atf3, Atf4, Egr1, Jun, Klf2, Ppp1r15a, Dnajb1*), positive regulation of cell death (*Apoe, Rhob, Atf3, Atf4, Btg1, Egr1, Fos, Nr4a1, Jun, Sik1, Ppp1r15a, Dusp1, Tsc22d1, Serinc3, Dusp6, Nfkbid*) as well as mitogen-activated protein kinase (MAPK) signaling pathways especially negativly regulate MAPK cascade (*Atf4, Fos, Nr4a1, Hspa8, Hspa1b, Jun, Dusp1, Dusp6, Hspa1a, Dusp5*) were found. On the other hand, genes involved in protein complex oligomerization (*Tgm2, Micu1, Mat2a*), regulation of translation and regulation of cellular amide metabolic process (*Cirbp, Ncl, Thbs1*) were shown to be commonly down-regulated (**Figure 25**).

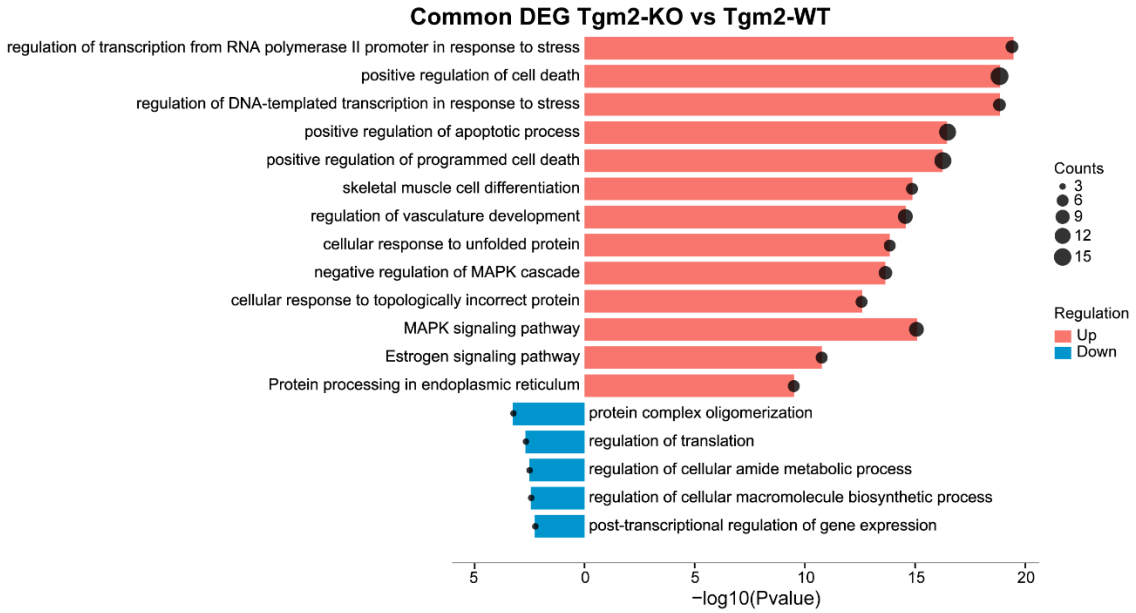

Figure 25 Bar graph of enriched pathway and process across the commonly regulated DEGs in Tgm2-KO LT-HSCs and Tgm2-KO MPPs versus their Tgm-WT counterparts.

Pathway and process enrichment analysis is carried out in Metascape with ontology sources GO Biological Processes and KEGG Pathway. All genes in the genome have been used as the enrichment background. Terms with a p-value < 0.01, a minimum count of 3, and an enrichment factor > 1.5 are collected and grouped into clusters based on their membership similarities. p-values are calculated based on the accumulative hypergeometric distribution, and q-values are calculated using the Benjamini-Hochberg procedure to account for multiple testings. The most significant terms are chosen and plotted via SRplot.

3.5.5. The absence of Tgm2 in LT-HSCs induces genes involve in apoptosis and MAPK signaling pathway

In order to characterize the alterations of biological processes and pathways in LT-HSCs after Tgm2 knockout, DEGs between Tgm-KO and Tgm2-WT LT-HSCs were provided for process and pathway enrichment analysis via Metascape with ontology sources: GO Biological Processes, KEGG Pathway, Reactome Gene Sets, and TRRUST. TRRUST (Transcriptional Regulatory Relationships Unraveled by Sentence-based Text mining) is a database of reference transcription factor (TF)–target regulatory interactions (Han et al. 2018).

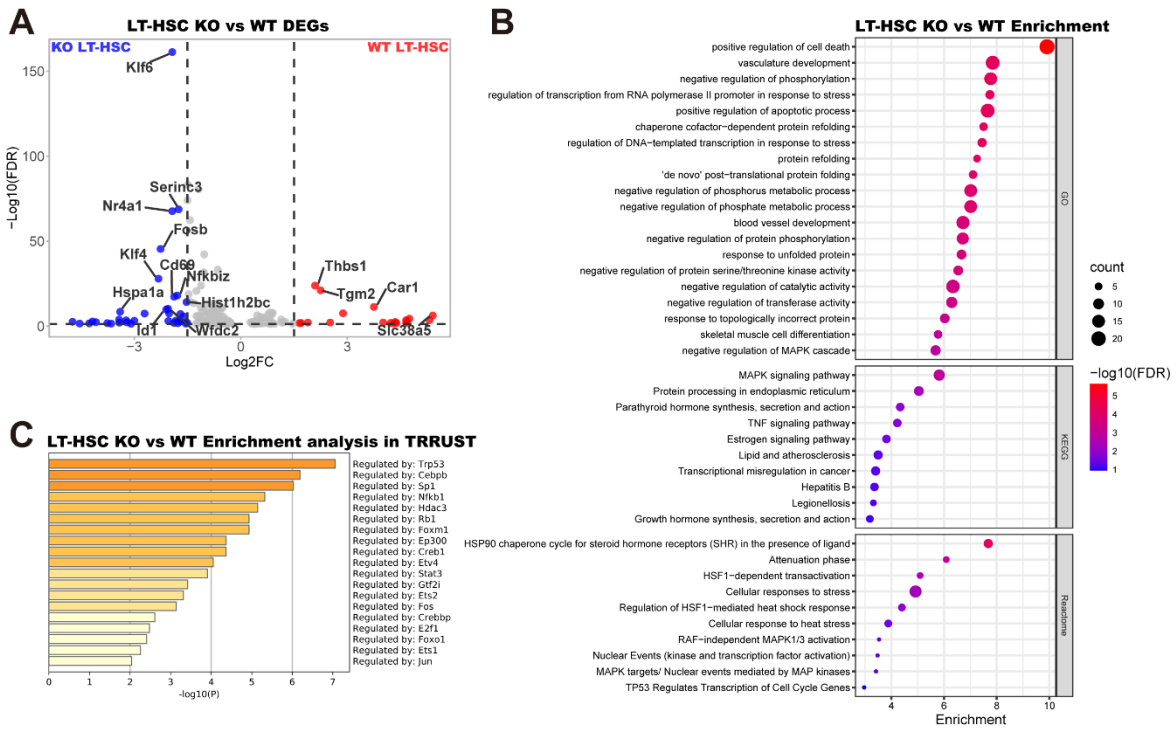

Figure 26 Gene expression profile of Tgm2-KO LT-HSCs.

(A) Volcano plots for DEGs in the Tgm2-KO LT-HSCs and Tgm2-WT LT-HSCs, with a horizontal dash line at the –Log10(FDR) = 1.3, and two vertical dash lines at Log2FC = ±1.5. **(B)** Enriched pathway and process in Tgm2-KO LT-HSCs. Pathway and process enrichment analysis is carried out in Metascape with ontology sources GO Biological Processes, KEGG Pathway, Reactome and TRRUST. The most statistically significant terms are chosen and plotted via SRplot. **(C)** Summary of enrichment analysis in TRRUST.

DEGs (**Appendix Table 14**) between Tgm2-KO and Tgm2-WT LT-HSCs were visualized as volcano plot (**Figure 26A**). Interestingly, under Tgm2 knockout condition, DNA-binding protein inhibitor *Id1*, promoting HSC proliferation and differentiation (Singh et al. 2018), and *CD69*, an activation marker for HSCs that being expressed in response to stimulation (Bujanover et al. 2018) were up-regulated. Another up-regulated gene, *Fosb*, which heterodimerize with Jun family proteins to form active AP1 (activator protein-1) transcription factors, have been implicated as positive modulators of apoptosis induced in hematopoietic progenitor cells of the myeloid lineage (Liebermann et al. 1998). Enrichment of Krüppel-like factors *Klf6* and *Klf4* was detected, which contribute to G1 cell cycle arrest and trigger apoptosis via inducing expression of cell cycle inhibitor $p21^{Cip1/Waf1}$ (Zhang et al. 2000; Andreoli et al. 2010). *Nr4a1*, also known as *Ngfib* or *Nur77*, is involved in cell cycle mediation, inflammation and apoptosis (Herring et al. 2019). Process and pathway enrichment analysis of the up-regulated DEGs (**Figure 26B**) revealed a significant induction of biological process enriched with genes involving in apoptosis (*Rhob, Atf3, Atf4, Btg1, Egr1, Nr4a1, Dnaja1, Jun, Sik1, Ppp1r15a, Ptgs2, Dusp1, Ptprf, Tsc22d1, Serinc3, Dusp6, Aifm2, Nfkbid*). MAPK signaling pathway was negatively regulated with an enrichment of genes inhibiting the MAPK cascade activation (*Apoe, Atf3, Dnaja1, Klf4, Dusp1, Rgs2, Spry1, Dusp6, Dusp5*). Moreover, many of these genes such as *Egr1, Klf2, and*

Klf4 transcriptions were control by transcription factor tumor suppressor p53 (*Trp53*) (**Figure 26C**).

3.5.6. The transcriptional effect of Tgm2 absent in MPPs differs from LT-HSCs

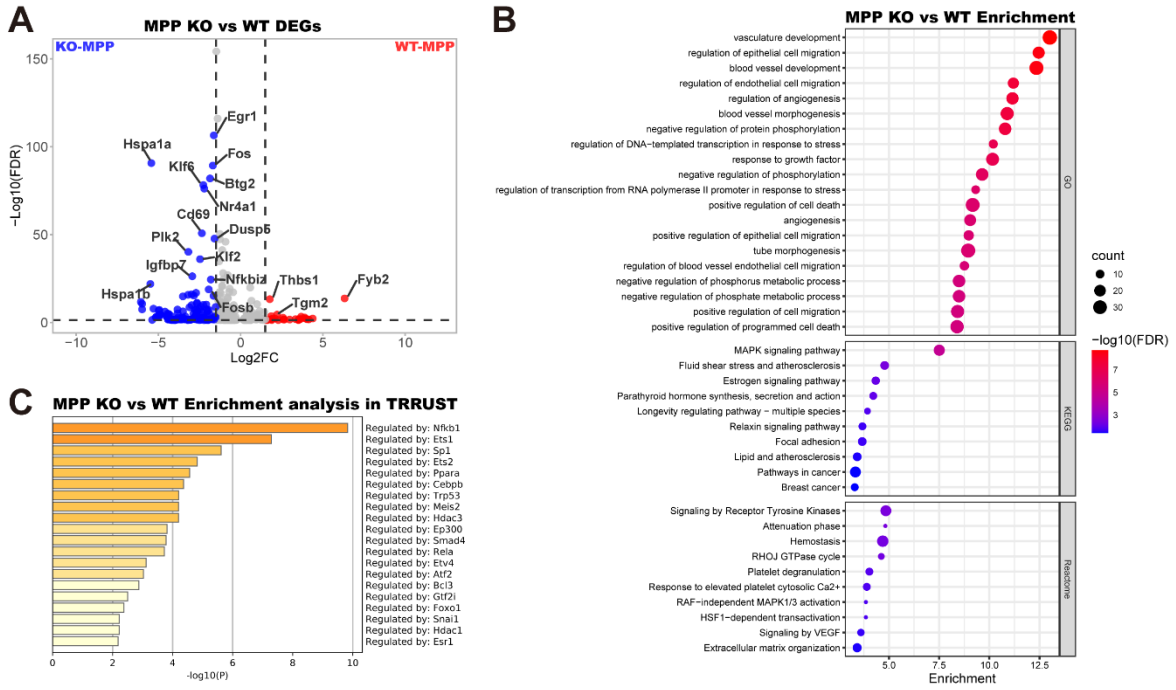

Figure 27 Gene expression profile of Tgm2-KO MPPs.

(A) Volcano plots for DEGs in the Tgm2-KO MPPs and Tgm2-WT MPPs, with a horizontal dash line at the –Log10(FDR) = 1.3, and two vertical dash lines at Log2FC = ±1.5. **(B)** Enriched pathway and process in Tgm2-KO MPPs. Pathway and process enrichment analysis is carried out in Metascape with ontology sources GO Biological Processes, KEGG Pathway, Reactome and TRRUST. The most statistically significant terms are chosen and plotted via SRplot. **(C)** Summary of enrichment analysis in TRRUST.

DEGs (**Appendix Table 15**) between Tgm2-KO and Tgm2-WT MPPs were visualized as volcano plot (**Figure 27A**). As with *Klf6*, *Klf2* also up-regulates *p21*$^{Cip1/Waf\ 1}$ (McConnell and Yang 2010) but at the same time regulates most of the NFκB-mediated activities (Jha and Das 2017). B-cell translocation gene *Btg2* is involved in regulating G2/M phase cell cycle arrest and apoptosis in monocytes (Kim et al. 2014b). Early growth response factor *Egr1* has been described with controversial role in regulating cell apoptosis in different cell types (Wang et al. 2021). Polo-like kinase *Plk2* is expressed in response to DNA-damage (Goroshchuk et al. 2019). With 70 commonly up-regulated genes, MPPs still exhibit a distinctive gene signature other than LT-HSCs. Besides positive regulation of cell death and MAPK signaling pathway, genes positively regulated vasculature development (*Rhob, Btg1, C5ar1, Cdh5, Dll1, Hspb1, Kdr, Klf4, Nos3, Tgfbr2, Pak4, Lrg1*) and cell migration (*Rhob, C5ar1, Cdh5, Egr1, Flt4, Hspb1, Igf1, Ccn1, Il6st, Jun, Kdr, Nos3, Pecam1, Lgmn, Ptger4, Sema3a, Plk2, Sparc, Tgfbr2, Plpp3, Cpne3, Amotl1, Dock8, Rhoj, Plvap, Fermt2, Dock1*) were among the up-regulated DEGs in Tgm2-KO MPPs (**Figure 27B**). Moreover, many of these genes such as *Cd38, Egr2, Myb,*

Ccl9, Nfkbiz transcriptions were controled by the transcription factor NFkB (*Nfkb1*) (**Figure 27C**).

In vitro analysis of cultivated LT-HSCs and MPPs showed high apoptosis rate and short-term cell cycle arrest only in Tgm2-KO LT-HSCs but not in Tgm2-KO MPPs (**Figure 18**). The distinct gene expression and pathway enrichment in Tgm2-KO MPPs might explain the differences of *in vitro* behavior of cultured Tgm2-KO LT-HSCs and MPPs.

3.6. Simultaneous proteo-genomic single cell sequencing analysis of LT-HSCs and LSKs from Tgm2-WT and Tgm2-KO mice

Single cell multi-omics technologies such as the BD Rhapsody platform has improved the resolution of heterogeneous cell types with simultaneous measurement of both gene and protein expression at single cell level. Monoclonal antibodies conjugated to poly-A tail oligos and a specific barcode sequence, so called BD AbSeqs, allow the detection of surface markers in compatibility with RNA sequencing platform (Stoeckius et al. 2017). In order to dissect transcriptional heterogeneity within the LT-HSCs and how it may change upon Tgm2 knockout under steady-state hematopoiesis, simultaneous quantification of mRNA and protein expression was performed using BD Rhapsody platform.

According to the designed workflow (**Figure 8**), FACS-isolated Tgm2-WT and Tgm2-KO LSKs and LT-HSCs were stained with Sample Tags and oligonucleotide- and fluorochrome-labeled antibodies. After loading on the Rhapsody system and library preprarations following the WTA amplification protocol with oligo-conjugated AbSeqs, approximately 21,359 mRNA targetes and 48 surface proteins were quantified . A sequencing profile with 14,899 captured single cells were generated. After recursive RSEC and DBEC, a 94.4% sequencing saturation of the mRNA library was achieved, with 37,751.45 mean reads per cell and 2,873 median genes per cell. Simultaniously, a 98.21% sequencing saturation with 17,104.34 mean reads per cell and 34 median targets per cell was obtained for the AbSeq library. A small proportion (0.05%) were assigned as multiplets and excluded from the SeqGeq analysis. A total of 12,868 Sample Tag determined single cells passed through the quality control, among which 4,527 WT LSK, 5,427 KO LSK, 1,574 WT LT-HSC and 1,340 KO LT-HSC were included.

3.6.1. Simultaneous proteo-genomic profiling separates LT-HSCs and progenitors

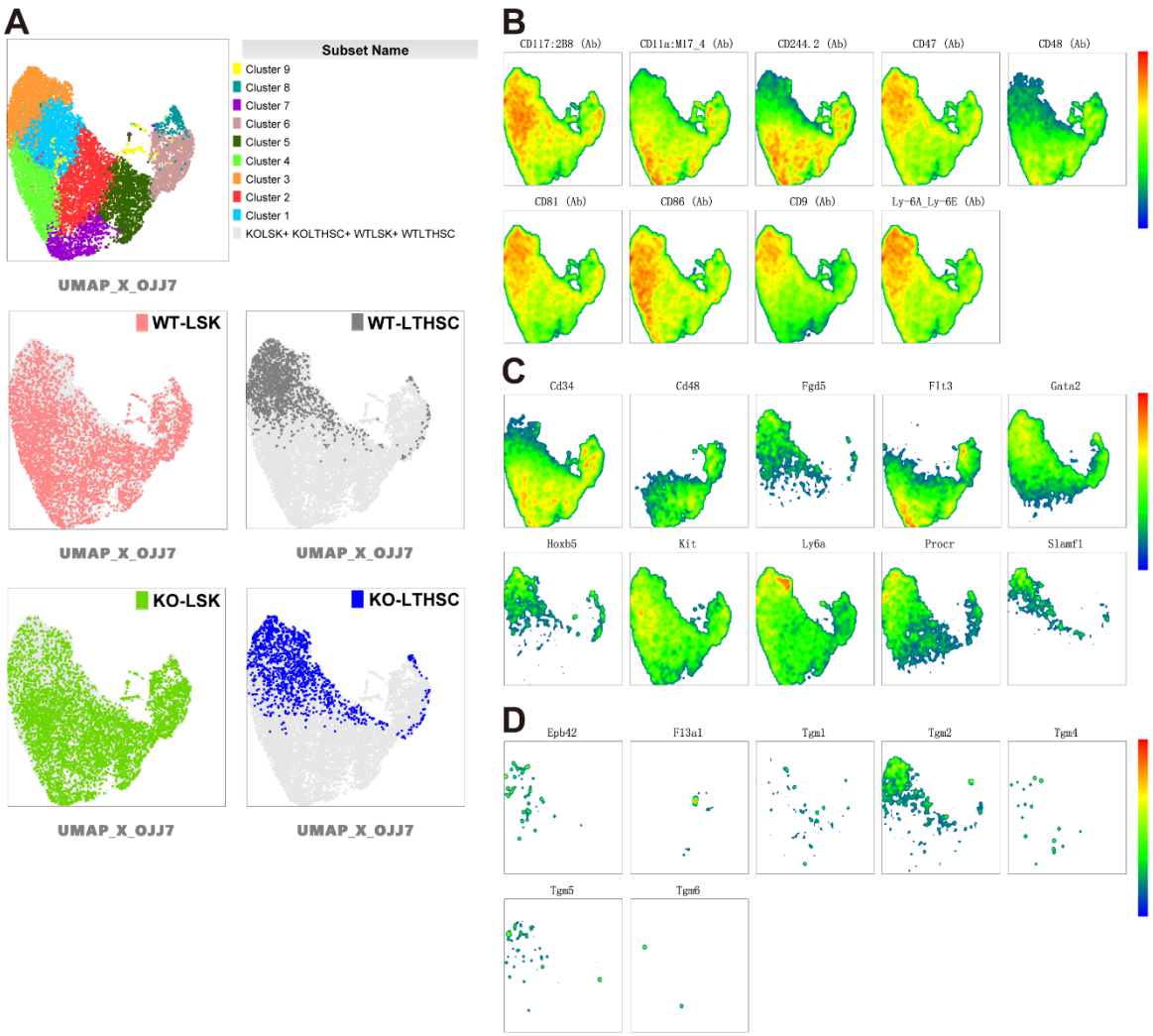

Figure 28 Seurat analysis of 12,868 captured single cells including Tgm2-WT and Tgm2-KO LSKs and LT-HSCs.

(A) UMAP plot depicting the clustering of all captured single cells. **(B)** Expression of CD117, CD11a, CD244. CD47, CD48, CD81, CD86, CD9 and Ly6A/Ly6E at protein level**. (C)** Expression of transcripts *CD34, CD48, Fgd5, Flt3, Gata2, Hoxb5, Kit, Ly6a, Procr* and *Slamf1*. **(D)** Expression of Tgase family member transcripts *Epb42, F13a1, Tgm1, Tgm2, Tgm4, Tgm5* and *Tgm6*.

With the defaut setting of the Seurat Plugin (V4.0.3) implemented by the SeqGeq software, linear dimensional reduction PCA was performed on 12,868 cells, which served as the base for subsequent graph-based clustering. Clusters were visualized by running non-linear dimensional reduction UMAP (Uniform Manifold Approximation and Projection). As shown in **Figure 28A**, 12,868 cells were separated into 9 different clusters, with LT-HSCs accumulating on the top area of the UMAP. Notably, both Tgm2-KO LSKs and LT-HSCs overlapped with Tgm2-WT cells, meaning none of the 9 clusters consisted cells from only Tgm2-KO cells. This observation again illustrated the high similarity of Tgm2-WT and Tgm2-KO cells. Several

interesting proteins that exhibited a gradient expression from LT-HSCs to later progenitors were visualized on the UMAP (**Figure 28B**). CD11a has been reported as a differentiation marker of HSCs (Fathman et al. 2014). CD244 has been described as a potent marker to exclude non-functional HSCs after *in vitro* culture (Koide et al. 2022). CD47 has been shown to be upregulated on circulating HSCs and can protect HSCs during inflammation-mediated mobilization (Jaiswal et al. 2009). CD81 has been proposed as a potential regulator that drives HSCs from proliferation back to quiescence (Lin et al. 2011). The expression of CD86 might be helpful to subdivide LT-HSCs into those with lymphopoietic or myeloid and erythroid potential (Shimazu et al. 2012). CD9 has been suggested as a positive marker to prospectivly isolate HSCs (Karlsson et al. 2013). CD117, CD48 and Ly-6A/Ly-6E are the markers applied in the fluorochrome-labeled antibody staining for LT-HSC isolation. In addition, a group of HSC marker genes were visualized (**Figure 28C**). Besides the genes that were introduced in the bulk transcriptomic analysis (**Figure 22**), gene *Fgd5* and *Hoxb5*, which have been described to be specifically highly expressed within the HSC compartment and adapted to generate reporter mouse strains (Gazit et al. 2014; Chen et al. 2016), were also included. All these protein and gene expressions confirmed that Cluster 3 represented the most immature LT-HSCs, Cluster 1 represented the activated/cycling or more differentiated LT-HSCs, and the remaining clusters represented progenitor cells. An accurate annotation of each cluster needed to be further investigated by analyzing the expression of other signature proteins and genes. A visualization of Tgase family members including *Tgm2* (**Figure 28D**) affirmed the specific high expression of *Tgm2* in immature LT-HSCs while only a low amount of mRNA expression of the other family members were quantified within LSK compartment.

3.6.2. Simultaneous proteo-genomic profiling reveals a heterogeneity of Tgm2 expression within bulk Tgm2-WT LT-HSCs

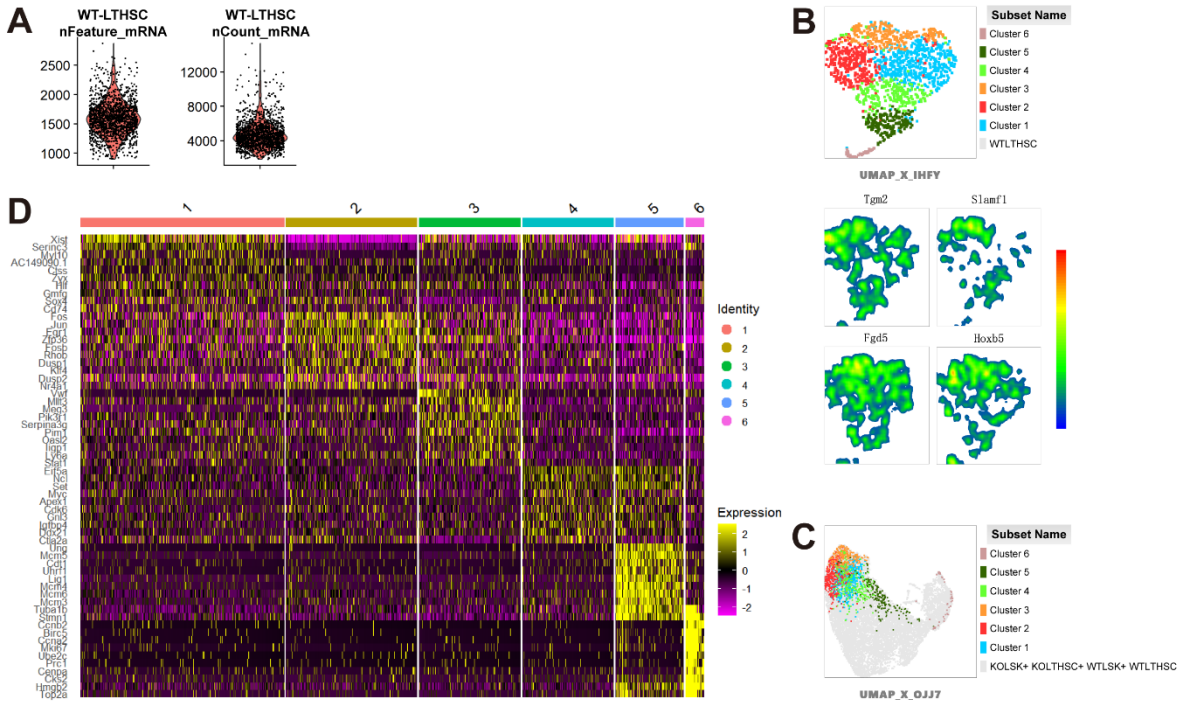

Figure 29 Seurat analysis of 1,574 captured Tgm2-WT LT-HSC single cells.
(A) Quality matrics of the analysis. nFeature_RNA: the number of unique genes detected per cell; nCount_RNA: the total number of molecules detected per cell. **(B)** UMAP plot depicting the clustering of Tgm2-WT LT-HSCs and the expression of transcripts *Tgm2, Slamf1, Fgd5* and *Hoxb5*. **(C)** Illustration of Tgm2-WT LT-HSC clusters projected on the UMAP of all captured single cells. **(D)** Heatmap depicting the top 10 signature genes in each identified Tgm2-WT LT-HSC cluster.

In order to access the expression pattern of Tgm2 expression among FACS sorted Tgm2-WT LT-HSCs, Seurat clustering was performed with the 1,574 WT LT-HSCs. Quality control was conducted and cells were filtered by the Seurat Plugin setting based on the number of unique genes detected in each cell (nFeature_RNA) and the total number of molecules detected within a cell (nCount_RNA) according to the fact that low-quality cells or empty droplets often have very few genes, whereas cell doublets or multiplets may exhibit an aberrantly high gene counts (**Figure 29A**). Tgm2-WT LT-HSCs were separated into 6 individual clusters with all cells from Cluster 3 and part of the cells from Cluster 2 harbored the highest *Tgm2* expression (**Figure 29B**). Interestingly, cells from Cluster 3 simutaniously exhibited highest *Slamf1*, *Fgd5* and *Hoxb5* expression, meaning cells from Cluster 3 should be the most dorment LT-HSCs while the other 5 clusters started to lose the *Tgm2* expression (**Figure 29B and C**). The top 10 marker genes for each cluster were used to generate the expression heatmap (**Figure 29D**). Of note, genes that have been reported as an early regulator of HSC erythroid and megakaryocytic differentiation such as Willebrand factor (*Vwf*) (Knapp and Eaves 2014) and *Mllt3* (Pina et al. 2008) were assigned as marker genes for Cluster 3. Besides, the long non-

coding RNA (lncRNA) maternally expressed gene 3 (*Meg3*), which has been shown to be highly expressed in mouse adult HSCs (Sommerkamp et al. 2019); proviral insertion in murine lymphomas 1 (*Pim1*), which has been shown to maintain HSC survival (An et al. 2013), as well as *Ly6a* were also among the marker genes of Cluster 3. Interestingly, Cluster 2, which started to lose the expression of *Tgm2*, showed an elevated expression of *Fos, Jun, Egr1, Fosb, Dusp1, Klf4, Dusp2* and *Nr4a1* that were also shown to be up-regulated in bulk transcriptomic analysis of Tgm2-KO LT-HSCs or MPPs (**Figure 26A and Figure 27A**). Moreover, Cluster 4 and Cluster 5 might represent the differentiated or cycling HSCs due to the increased expression of *Cdk6, Myc* (Wilson et al. 2004; Baena et al. 2007), and genes from the minichromosome maintenance protein complex (MCM) family. These data suggested a heterogeneous expression of Tgm2 in FACS isolated LT-HSC compartment. Tgm2 expression mainly accumulated within the most immature LT-HSCs that harbored erythroid and megakaryocytic cell fate.

3.6.3. Simultaneous proteo-genomic profiling suggests the activation of Tgm2-KO LT-HSCs

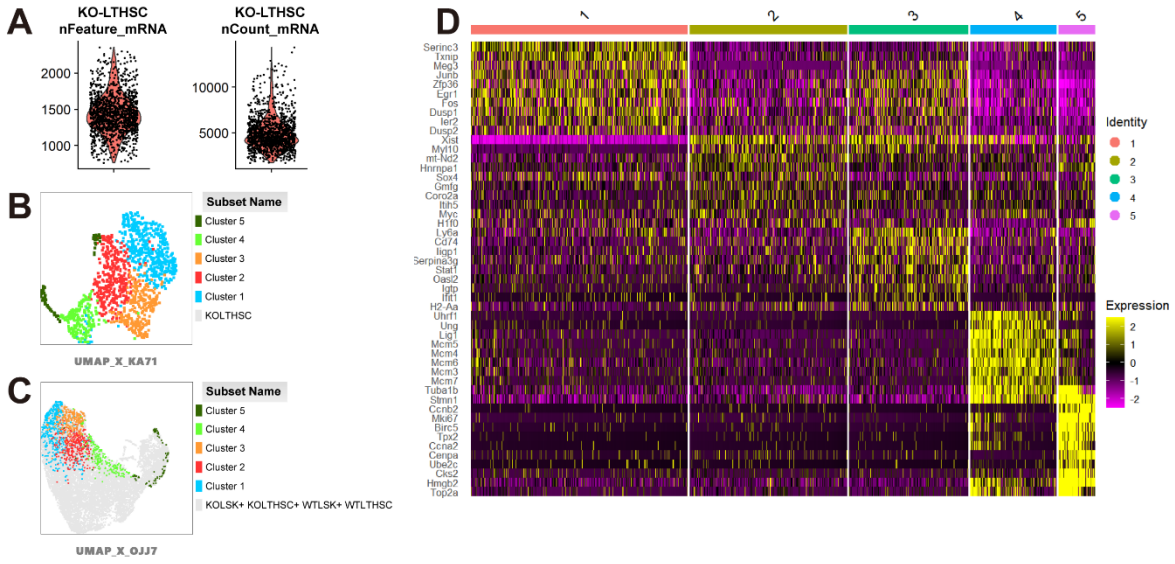

Figure 30 Seurat analysis of 1,340 captured Tgm2-KO LT-HSC single cells.

(A) Quality matrics of the analysis. nFeature_RNA: the number of unique genes detected per cell; nCount_RNA: the total number of molecules detected per cell. **(B)** UMAP plot depicting the clustering of Tgm2-KO LT-HSCs. **(C)** Illustration of Tgm2-KO LT-HSC clusters projected on the UMAP of all captured single cells. **(D)** Heatmap depicting the top 10 signature genes in each identified Tgm2-KO LT-HSC cluster.

Following the same strategy, 1,340 KO LT-HSCs were analyzed with Seurat clustering and resulted in 5 different clusters (**Figure 30B**). Different from WT LT-HSCs, the location of KO LT-HSCs were more spreaded towards the differentiated and cycling HSCs and progenitors from the UMAP projected with LSKs (**Figure 30C**). The top 10 marker genes for each cluster were used to generate the expression heatmap (**Figure 30D**). *Ly6a* expression hinted that the

cells from Cluster 3 might be the most primed LT-HSCs from Tgm2-KO mice. However, these cells already showed a higher expression of *CD74*, whose absence is essential for HSC survival, expansion and long-term self-renewal capacity (Becker-Herman et al. 2021), meaning cells from Cluster 3 started to lose their LT-HSC potential. Cluster 1, whose majority overlapped with the cells losing *Tgm2* expression within Tgm2-WT LT-HSCs, again displayed promoted expression of *Serinc3, Junb, Egr1, Fos, Dusp1* and *Dusp2* that were up-regulated in bulk transcriptomic analysis of Tgm2-KO LT-HSCs or MPPs (**Figure 26A and Figure 27A**). Importantly, elevated expression of these genes were also observed in Cluster 3, indicating the regulation were *Tgm2* dependent. However, the molecular mechanism behind the regulation required further experimental evidence.

3.7. Tgm2 conditional knockout LT-HSCs reveal slower recovery upon 5-FU treatment

As conditional knockout of Tgm2 was not showing significant alterations in steady state hematopoiesis, stress studies were performed. Upon stress hematopoiesis, HSCs are forced to exit quiescence and either self-renew or differentiate to mature hematopoietic cells. 5-fluorouracil (5-FU) is a cytotoxic chemotherapy medication for cancer treatment. Stem cells surviving after 5-FU treatment are believed to be more immature. 5-FU induced BM suppression activates HSCs *in vivo*, resulting in exit of quiescence and enter to cycle and proliferate (Harrison and Lerner 1991; Randall and Weissman 1997; Venezia et al. 2004).

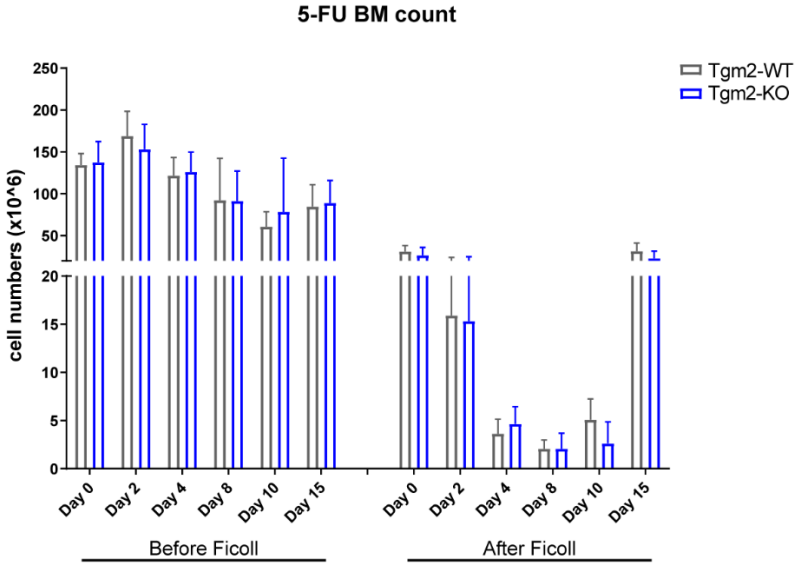

Figure 31 Kinetic changes of BM cell count upon 5-FU treatment.

Total bone marrow cell count (before ficoll) and BMMNCs enriched after gradient centrifugation (after ficoll) is presented.

Tgm2-WT and Tgm2-KO mice were treated with one dose of 5-FU injection on the 10th day after the last polyIC treatment. BM and spleen cells from 5-FU treated mice were analyzed

after 2, 4, 8, 10 and 15 days by FACS. In general, total BM cells were not affected upon 5-FU treatment, however, BMMNCs reduced dramatically 4 days after 5-FU treatment. Between Tgm2-WT and Tgm2-KO mice, both total BM cells and BMMNCs did not show any significant differences (**Figure 31**).

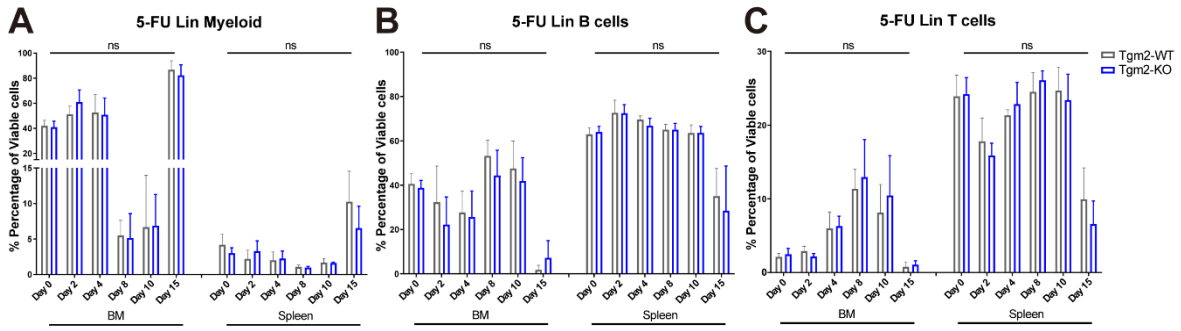

Figure 32 Kinetic changes of BM leukocytes distribution upon 5-FU treatment.
Percentage is calculated from total viable cells.

Myeloid, B cells and T cells were determined from total BM and spleen cells as described previously. BM cells consist of more myeloid cells than lymphocytes, whereas the opposite is the case in the spleen. In the BM, the percentage of myeloid cells dropped on day 8 and day 10, with an increased amount of lymphocytes especially T cell populations. A slight increase of myeloid cells and hence less B cells was observed on day 2 within Tgm2-KO mice in comparison to Tgm2-WT, although this difference was not statistically significant. In the spleen, the percentage of myeloid, B cells and T cells did not show differences between Tgm2-WT and Tgm2-KO over different time points (**Figure 32**).

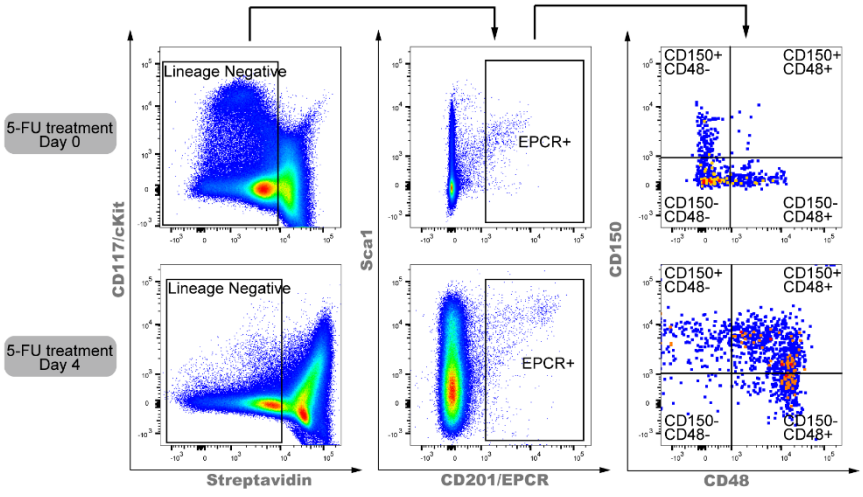

Figure 33 BM HSPC analysis with EPCR staining strategy.
FACS representation of EPCR, CD150 and CD48 expression within BM lineage negative cells from untreated mouse (day 0) and 5-FU treated mouse (day 4).

Stress hematopoiesis changes the phenotypes of LT-HSCs in the BM. It has been described that 5-FU treatment alters the expression of some surface markers such as Sca1, CD117/cKit

and CD34 for HSC identification. Therefore, endothelial protein C receptor (EPCR)-based fraction Lin^- $EPCR^+$ $CD150^+$ $CD48^-$ is used to identify HSCs in order to circumvent the change in HSC surface marker phenotype during the recovery from 5-FU induced BM suppression (Umemoto et al. 2018). EPCR contributes to the accurate identification of HSCs without relying on Sca1 or CD117/cKit expression (Kent et al. 2009; Umemoto et al. 2018). The most immature stem cell population is defined as $CD150^+$ $CD48^-$, and an activation of these cells gains CD48 expression. Cells losing CD150 expression are the progenitor cells, which can be further separated by CD48 expression due to their differentiation status (**Figure 33**).

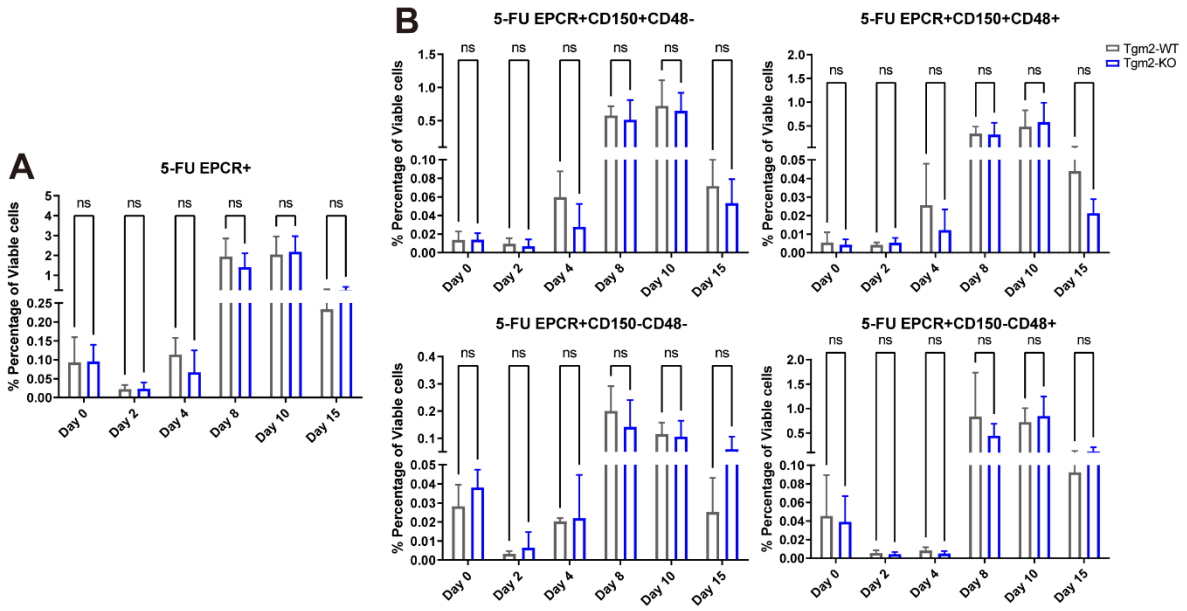

Figure 34 Kinetic changes of $EPCR^+$ and the subsequential $CD150^+$ $CD48^-$, $CD150^+$ $CD48^+$, $CD150^-$ $CD48^-$, $CD150^-$ $CD48^+$ fractions.

Percentage is calculated from total viable cells.

BMMNCs from Tgm2-WT and Tgm2-KO mice were analyzed with the above described strategy via FACS. As shown in **Figure 34**, a decrease of $EPCR^+$ cells was certainly observed on the 2nd day after 5-FU administration, but Tgm2-WT and Tgm2-KO mice were reacting similarly against the treatment. Within different immature stem and progenitor cell compartments, no significant differences were displayed between Tgm2-WT and Tgm2-KO mice. However, a very mild decline in Tgm2-KO mice was shown on day 4 for immature stem cells ($CD150^+$ $CD48^-$) and activated stem cells ($CD150^+$ $CD48^+$), suggesting Tgm2-KO stem cells might exhibit a delayed recovery under chemotherapeutic treatment.

3.8. Tgm2 conditional knockout LT-HSCs show full reconstitution potential upon transplantation

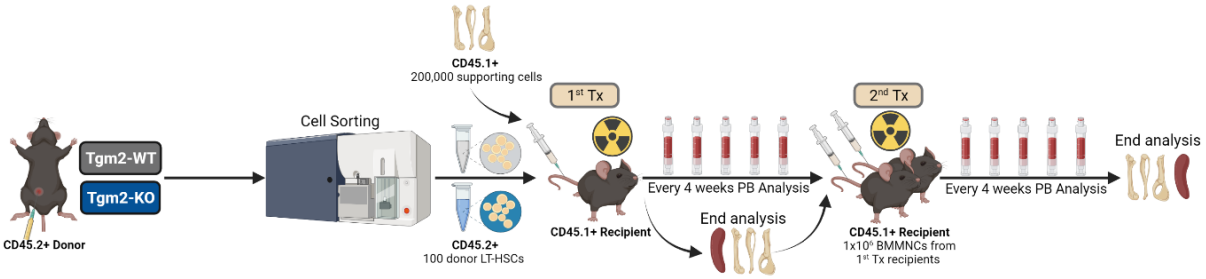

Figure 35 Schematic representation of serial transplantation experiment.

100 freshly sorted Tgm-WT or Tgm2-KO LT-HSCs are i.v injected in lethally irradiated B6.SJL mice as primary transplantation. 1x10^6 ficoll enriched BMMNC are i.v injected in lethally irradiated B6.SJL mice as secondary transplantation. PB analysis is performed every 4 weeks. BM and spleen are analyzed at the end of each transplantation round. Figure generated in BioRender.

LT-HSCs harbor the unique potential to provide long-term multi-lineage reconstitution of the hematopoietic system when serially transplanted into lethally irradiated recipients (Weissman and Shizuru 2008). To assess whether the long-term reconstitution potential of LT-HSCs were affected by the absence of Tgm2, 100 freshly FACS-sorted LT-HSCs from Tgm2-WT and Tgm2-KO together with 200,000 isolated competitor cells were transplanted into 8.5Gy lethally irradiated B6.SJL primary recipients. PB analysis was performed every 4 weeks for over 20 weeks. Afterwards, the BM and the spleen were collected and analyzed from the primary recipients. 1 x 10^6 BMMNCs from each primary recipient were serially transplanted into two lethally irradiated B6.SJL secondary recipients (to have replicates). PB analysis was again carried on for 20 weeks and the BM and the spleens were collected and analyzed at the end of the experiment (**Figure 35**).

3.8.1. PB analysis

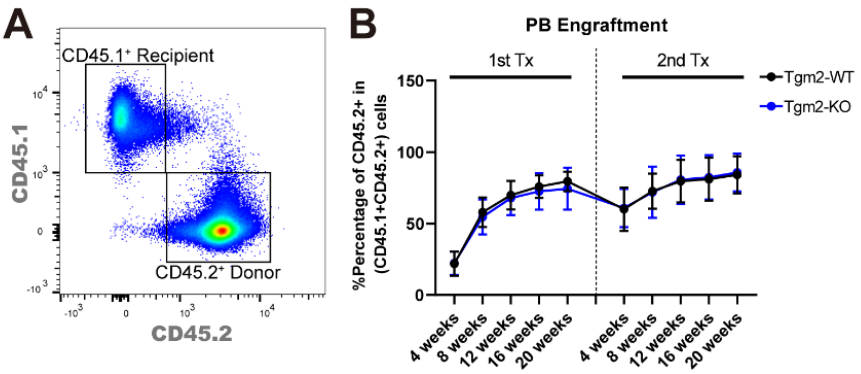

Figure 36 PB engraftment analysis.

(A) FACS representation of CD45.1 and CD45.2 staining. CD45.1 positive population represents the cells from recipient mice. CD45.2 positive population represents the cells from donor mice. **(B)** Engraftment kinetics in PB leukocytes during the two rounds of Tgm2-WT and Tgm2-KO transplantation.

To analyze the engraftment of transplanted cells, the markers CD45.1 and CD45.2 were used. CD45 is encoded by the *Ptprc* gene and is expressed on the surface of all hematopoietic cells except of erythrocytes and platelets (Komuro K. et al. 1974; Scheid M. P. and Triglia D. 1979). Different isoforms of CD45 have been identified in mice. In the C57BL/6 mouse line, the common form CD45.2 is encoded by the *Ptprc b* allele and expressed. In the B6.SJL mouse strain, another isoform CD45.1, encoded by another allelic variant *Ptprc a*, has been identified. In a competitive congenic BM transplantation assay, CD45.1 and CD45.2 enables the independent tracking and quantification of reconstituted donor cells (Jafri et al. 2017). Tgm2-WT and Tgm2-KO mice are C57BL/6 background, therefore CD45.2$^+$ cells were representing the donor cells from FACS measurement (**Figure 36A**). PB analysis was proceeded for 20 weeks for both primary and secondary transplantation. As shown in **Figure 36B**, the engraftment of Tgm2-WT and Tgm2-KO LT-HSCs did not show differences as both engrafted successfully over the whole experiment, indicating Tgm2 expression was not essential for the homing and engrafting of LT-HSCs. Furthermore, no difference was seen in the blood cell reconstitution or the self-renewal ability of LT-HSCs in the absence of Tgm2.

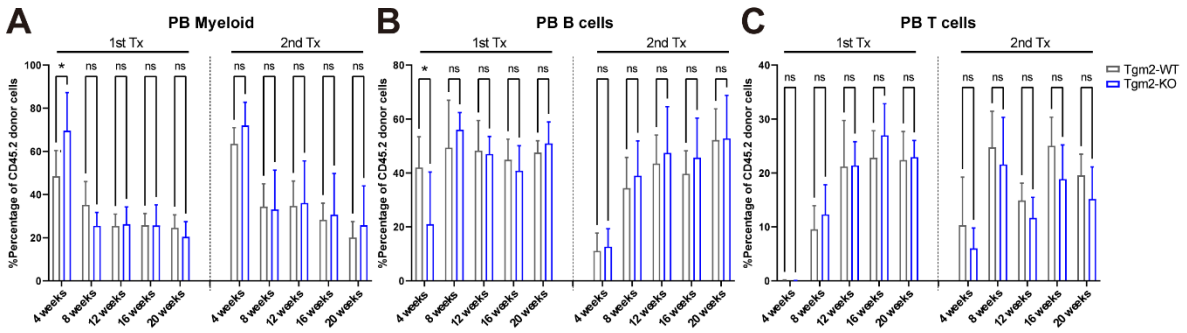

Figure 37 Long-term reconstitution in PB of Tgm2-WT and Tgm2-KO LT-HSCs.

Donor cell chimerism of leukocytes including myeloid cells **(A)**, B cells **(B)** and T cells **(C)** in PB from the recipients after primary and secondary transplantation. Percentage is calculated from CD45.2$^+$ donor cells. *P value<0.05.

LT-HSCs from both Tgm2-WT and Tgm2-KO mice harbored a multi-lineage reconstitution of reconstituting to all leukocytes including myeloid, B- and T-cells in the PB. Interestingly, LT-HSCs from Tgm2-KO mice reconstituted to more myeloid cells and less B cells in the first 4 weeks after primary transplantation, suggesting a fast response to myeloablation. This observation was short-term and was compensated afterwards (**Figure 37**). Thus, no lineage bias in any of the reconstituted blood populations were detected in later time point.

3.8.2. BM and spleen analysis

At the end of each round of transplantation, BM and spleen from the the sacrificed recipients were analyzed to investigate the engraftment, the reconstitution of different lineages as well as the distribution of BM stem and progenitor cells from donor population. Similar to the PB

analysis, the engraftment of LT-HSCs from Tgm2-WT and Tgm2-KO did not show any differences in the BM as well as the spleen (**Figure 38**)

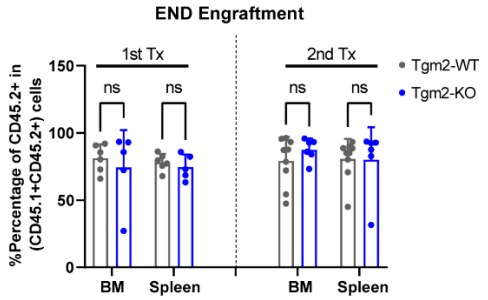

Figure 38 Engraftment in the BM and the spleen cells during the two rounds of Tgm2-WT and Tgm2-KO transplantation.

Percentage is calculated from CD45.2$^+$ donor cells.

All leukocyte lineages could also be detected in both BM and the spleen. In the BM, LT-HSCs from Tgm2-WT and Tgm2-KO mice reconstituted equally towards myeloid, B cells and T cells 20 weeks after primary and secondary transplantation (**Figure 39A**). In the spleen, these cells reconstituted also similarly after primary transplantation. However, analysis after the secondary transplantation revealed that LT-HSCs from Tgm2-KO mice reconstituted to more B cells and less T cells in comparison to LT-HSCs from Tgm2-WT mice (**Figure 39B**).

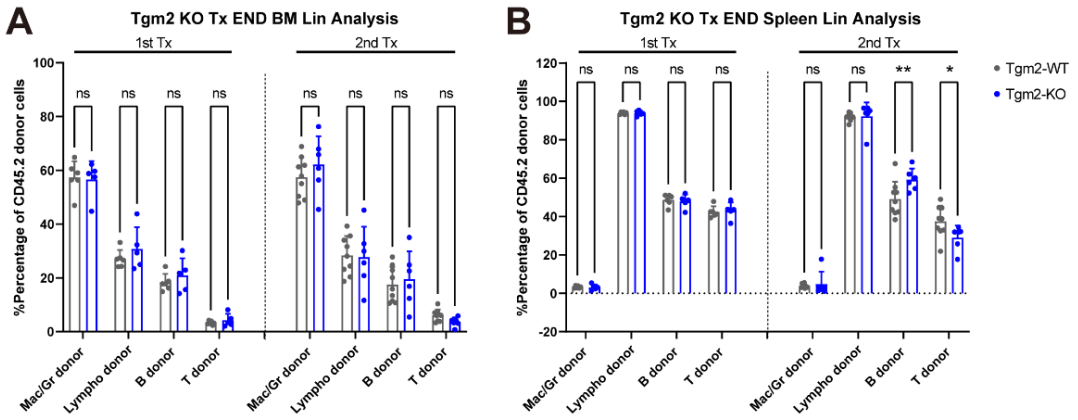

Figure 39 Long-term reconstitution in the BM and spleen of Tgm2-WT and Tgm2-KO LT-HSCs.

(A) BM leukocytes including myeloid cells, B cells and T cells in the BM from the recipients after primary and secondary transplantation. Percentage is calculated from CD45.2$^+$ donor cells. **(B)** Splenetic leukocytes including myeloid cells, B cells and T cells in the Spleen from the recipients after primary and secondary transplantation. Percentage is calculated from CD45.2$^+$ donor cells. *P value<0.05, **P value<0.01.

The differentiation of engrafted LT-HSCs was conducted by measuring the HSPC distribution of donor-derived cells. Around 2% of donor-derived LT-HSCs, 7% of donor-derived MPPs, 1% of donor-derived MEPs and 2% of donor derived GMPs were presented in the BM after primary and secondary transplantation, and yet no significant differences could be observed between Tgm2-WT and Tgm2-KO conditions (**Figure 40**).

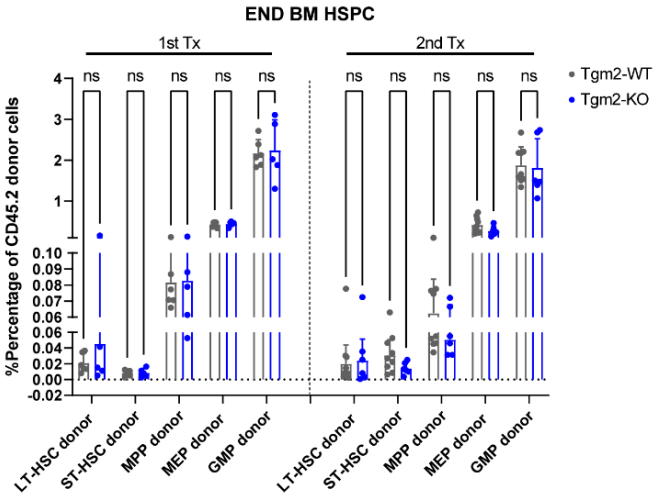

Figure 40 HSPCs derived from Tgm2-WT and Tgm2-KO donor LT-HSCs in BM.

BM LT-HSC, MPP, GMP, and MEP donor chimerism after primary and secondary transplantation of Tgm2-WT and Tgm2-KO LT-HSC-transplanted recipients. Percentage is calculated from $CD45.2^+$ donor cells.

Hence, the investigation of long-term multi-lineage reconstitution potential as well as stem and progenitor cell differentiation of LT-HSCs during serial transplantation were not Tgm2 dependent. However, transient elevated myeloid cells and reduced B cells found in the PB 4 weeks after Tgm2-KO LT-HSC primary transplantation suggested a short-term effect lineage reconstitution. To further explore the potential role of Tgm2 in the reconstitution potential of LT-HSC, a short-term competitive repopulation assay is necessary.

4. Discussion

4.1. Highly specific Tgm2 protein expression is associated with cell survival and stress response in LT-HSCs

In this study, highly specific expression of Tgm2 protein was detected in murine LT-HSCs by low input label-free mass spectrometric proteomics and WES protein analysis. This protein was almost absent with further decline towards oligopotent progenitors. In the conditional Tgm2 knockout mouse model generated with Mx1-Cre/*loxP* system, the distribution of mature blood cell lineages and immunophenotypically-defined HSPC populations within the BM were not changed under steady state hematopoiesis. Gene expression profiling and simultaneous single cell proteo-genomic profiling indicated that HSPCs and LT-HSCs from Tgm2-KO mice were transcriptionally more active. In Tgm2-KO LT-HSCs, 136 up-regulated genes demonstrated an enrichment of genes involved in apoptosis, as well as negative regulation of MAPK signaling pathway. These data pointed out the significant molecular changes in LT-HSCs after Tgm2 knockout.

In vitro continuous observation of prospectivly isolated LT-HSCs by time-lapse microscopy-based cell tracking revealed a delayed entry into cell cycle with a two fold increased apoptosis rate after knocking out Tgm2, indicating Tgm2 expression could be essential for survival of LT-HSCs. These features were not observed in Tgm2-deleted MPPs, suggesting Tgm2 playing a specific function at the level of LT-HSCs. Although, competitive BM serial transplantation displayed an equal overall engraftment and multi-lineage reconstitution of LT-HSCs from Tgm2-WT and Tgm2-KO mice, LT-HSCs from Tgm2-KO mice reconstituted to more myeloid cells and fewer B cells in the first 4 weeks after primary transplantation. Moreover, the administration of 5-FU revealed a trend towards delayed recovery of LT-HSCs lacking Tgm2. These findings suggested a potential involvement of Tgm2 in accurate stress response of LT-HSCs.

4.2. Tgm2 plays an anti-apoptotic role in LT-HSCs

Opposing roles of Tgm2 with regard to cell death and survival has been described and remained under investigation (Fésüs and Szondy 2005; Piacentini et al. 2011; Tatsukawa et al. 2016). Studies over the last three decades demonstrated Tgm2 as pro- and anti-apoptotic.Traditionally, it is believed that the pro-apoptotic activity of Tgm2 is based on its calcium-dependent crosslinking function (Fok and Mehta 2007). Conversely, the anti-apoptotic activity is generally independent from its transamidation and enzymatic cross-linking activities. Indeed, this pro-survival signal is principally mediated by adhesive capabilities of Tgm2 and

integrins to fibronectin, which could result in the activation of cell survival and antiapoptotic signalling pathways, and extracellular matrix stabilization (Mehta et al. 2006). Therefore, the pro- and anti-apoptotic effects of Tgm2 are dependent on the protein cellular localization and on the activation of different pathways. The cytosolic Tgm2 is pro-apoptotic, whereas nuclear and extracellular Tgm2 acts anti-apoptotic (Milakovic et al. 2004; Chhabra et al. 2009). On contrary, the previous study from our laboratory has revealed the transamidation activity of Tgm2 is critical for pro-survival function and its ablation led to the induction of Caspase-3 driven apoptosis in colorectal carcinoma cells (Malkomes et al. 2021).

In the presented results, Tgm2 ablation led to an induction of *Klf4* and *Klf6* genes that contribute to G1 cell cycle arrest and trigger apoptosis (**Figure 26**), correlated with the observation of increased apoptosis level and a temporary cell cycle arrest of *in vitro* cultured LT-HSCs (**Figure 18**), pointing out a potential anti-apoptotic role of Tgm2 in LT-HSCs. Besides, many cell activation genes such as *CD69* and *Id1* are up-regulated upon Tgm2 knockout, which might involve in balancing cell death and maintaining the cell proliferation process to sustain the number of LT-HSCs. p53-targeted genes involved in both apoptotic (e.g. *Atf3, Egr1, Dusp1*) and cell cycle arrest (e.g. *Klf4*) were significantly induced in LT-HSCs after knockout of Tgm2. Differentially up-regulated genes in Tgm2-KO LT-HSCs that are control by transcription factor *Trp53* resulted as the top hit in the TRRUST analysis (**Figure 26**).

p53 is primarily expressed in LT-HSCs (Forsberg et al. 2005). p53-deficiant HSCs exhibit higher proliferation rate and poor repopulation capacity (TeKippe et al. 2003; Liu et al. 2009). Data from different studies have indicated that p53 plays a cytoprotective role in HSCs by preventing their entry into the cell-cycle and maintaining their quiescence (Liu et al. 2009; Pant et al. 2012; Yamashita et al. 2016). Study from our laboratory has reported a direct interation of Tgm2 and p53 in colorectal carcinoma cells, resulting in an inactivation of p53-mediated tumor suppression. Tgm2 knockdown colorectal carcinoma cells show induced cell death and up-regulated p53 signaling (Malkomes et al. 2021). Coincidentally, higher cell apoptosis rate and up-reglated p53-mediated transcription were observed in LT-HSCs in the presented study. These evidences pointed out the possible exhibition of Tgm2 and p53 interaction in LT-HSCs. Experiments such as proximity ligation assay and immunoprecipitation with LT-HSCs need to be established since assays with low cell number always remain as a challenge.

Loss of Tgm2 did not cause obvious effect in cell death or proliferation in MPPs, meaning different functions of Tgm2 may exist in the BM. In order to further investigate the mechanism behind, it is essential to study the localization and enzymatic function of Tgm2 in these cell types respectively.

4.3. Tgm2 regulates functional response to hematopoietic stress via MAPK signaling pathways

Under homeostasis condition, HSCs are mainly quiescent and rarely enter the cell cycle to self-renew or differentiate. Under conditions of hematopoietic stress including BM transplantation, infection and inflammation, chemotherapeutic treatment, and aging, quiescent HSCs are pushed into cell cycle to increase the production of mature myeloid cells. Sustained ROS level is resulted under stress conditions that promotes DNA damage and differentiation, which ends up with HSC exhaustion and hematopoietic failure (Singh et al. 2020). BM transplantation promotes HSC replication that leads to functional decline and HSCs exhaust during serial transplantation. 5-FU treatment, which is toxic to cycling cells, promotes quiescent HSC proliferation and DNA damage (Schoedel et al. 2016). A very mild decline of immature stem cells ($CD150^+$ $CD48^-$) and activated stem cells ($CD150^+$ $CD48^+$) in Tgm2-KO mice were observed on day 4 upon 5-FU administration, suggesting Tgm2-KO stem cells might exhibit a delayed recovery upon chemotherapeutic treatment (**Figure 34**). Further, BM transplantation showed LT-HSCs from Tgm2-KO mice reconstituted to more myeloid cells in the first 4 weeks after primary transplantation, suggesting a transient myeloid-bias might exist in Tgm2-KO LT-HSCs (**Figure 37**). The observation from this study indeed represented an accurate stress response phenotype in cells lacking Tgm2. High expression of Tgm2 might be essential in regulating stress response in LT-HSCs, meaning lacking Tgm2 might cause the cells being more sensitive towards stress. All these phenotype appeared only transient and disappeared after a certain period of time, suggesting potential genes or proteins were expressed in order to rescue the LT-HSCs against stress. However, the mechanism behind needs further investigation.

Another driver of HSC proliferation is inflammation initiated by bacterial and viral infections and tissue injury. PolyIC is a synthetic analog of double stranded RNA, which is detected by toll-like receptor 3 (TLR-3) that leads to a potent immune response characterized by the production of inflammatory cytokines such as IL-1β, IL-6, TNFα as well as interferons. PolyIC has been suggested to trigger HSC cycling as well as aging (Gidáli et al. 1981; Essers et al. 2009; Cabezas-Wallscheid et al. 2017). Therefore, the conditional knockout model using the Mx1-Cre system can be potentially associated with undesired side effects caused by the polyIC administration. Although polyIC induced rapid and transient changes in cellular phenotypes could be resolved by day 8, the interpretation of experimental results might still be affected in short-term studies. In this study, both Mx1-$Cre^-$$Tgm2^{loxP/loxP}$ and Mx1-$Cre^+$$Tgm2^{loxP/loxP}$ mice were both treated to rule out the effect caused solely by polyIC, suggesting the transient effect which has been observed with Tgm2-KO LT-HSCs obtained 10 days after the last polyIC

administration were caused either by the loss of Tgm2 or the combined effect of polyIC treatmet and Tgm2 ablation.

Gene expression profiling from this study revealed a significant induction of genes involved in negativly regulating MAPK signaling after Tgm2 knockout (**Figure 25**). The MAPKs are a family of serine/threonine kinases that play an essential role in various cellular functions, including proliferation, differentiation, migration, and apoptosis (Dong et al. 2002; Wada and Penninger 2004; Yue and López 2020). Three major groups of MAPKs have been characterized in mammals, including ERKs, JNKs, and p38/MAPKs. MAPK signaling has been demonstrated to play a key role in the maintenance of HSC quiescence. ERKs and p38/MAPKs signaling has been shown to negatively regulates HSC self-renewal and homeostasis (Ito et al. 2006; Jang and Sharkis 2007; Saulnier et al. 2012). Activation of ERK MAPK signaling pathway has been reported to promote proliferation of cord blood-derived $Lin^{-}CD34^{+}CD133^{+}$ cells as well as myeloid commitment of HSCs (Oostendorp et al. 2008). On the other hand, activated HSCs under stress condition are always bound with elevated level of ROS, which induce phosphorylation and activation of p38/MAPKs signaling pathway. Inhibition of p38/MAPKs protects HSCs from losing self-renewal capacity and exhaustion. In the present study, a group of genes coding for dual-specificity MAPK phosphatases (MKPs or DUSPs) such as Dusp1, Dusp5, Dusp6 have been switched on under loss of Tgm2 condition (**Appendix Table 14**). DUSPs are the largest group of protein phosphatases dedicated to the specific regulation of MAPK activity (Caunt and Keyse 2013). Dusp1, for instance, is a nuclear phosphatase that can bind and dephosphorylate all three classes of MAPKs. Dusp5 and Dusp6 can bind specifically to the ERK1 and ERK2 MAPKs and dephosphorylate and inactivate ERK/MAPK signaling pathway. Up-regulation of these genes negatively regulate MAPK pathway and protect the cells from exhaustion.

4.4. Compensation for the loss of Tgm2

Two mouse knockout models for Tgm2 were developed simultaneously by different groups to evaluate its *in vivo* function (Nanda et al. 2001; Laurenzi and Melino 2001) with no obvious developmental phenotype has been observed in either of them. It has been discussed by different scientists that a common biological phenomenon of backup compensation might exist, which occurs when functionally overlapping proteins compensate for the loss of each other. For example, in Tgm2 null chondrocytes, the compensatory activation of FXIIIa has been observed, resulting in an unchanged level of total transamidase activity (Nurminskaya and Kaartinen 2006). An induction of Tgm1 and FXIIIa expression in liver and kidney from Tgm2 knockout mice have been also described, while no compensation for the loss of Tgm2 in

skeleton muscle could be observed (Deasey et al. 2013). The compensation mechanism can be described as transcriptional or functional compensation. The presented data here showed the transcriptional level of *Tgm1, Tgm4, Tgm5, F13a1* as well as *Epb42* were not altered to compensate the loss of Tgm2, at least with LT-HSCs and MPPs isolated from the BM 10 days after a successful generation of Tgm2 conditional knockout (**Figure 23** and **Figure 28D**). As Tgm2 plays a role in various biological process and acts as a multi-functional protein, whether Tgm2 is acting as transamidase, GTPase or other non-enzymatic functions in LT-HSCs remains unclear. It is important to identify the localization and enzymatic function, e.g. transglutaminase activity, of Tgm2 within LT-HSCs and MPPs. This could delineate a possibility of expression of other genes compensating the deficient Tgm2 function.

4.5. Tgm2 can be served as a potential intracellular marker for murine LT-HSCs

Genes such as *Fgd5, α-catulin and Hoxb5*, which specifically highly expressed within the HSC compartment, have been adapted to generate genetically engineered fluorescent protein reporter mouse strains (Gazit et al. 2014; Acar et al. 2015; Chen et al. 2016). Both the published gene expression data as well as the presented results here have confirmed that Tgm2 is transcriptionally and translationally exclusively expressed in LT-HSCs within the immature BM HSPCs. Single cell proteo-genomic profiling revealed the heterogeneity of Tgm2 expression within LT-HSCs (**Figure 29**). Although the correlation between Tgm2 expression heterogeneity and LT-HSC functional heterogeneity needs to be further verified, this specific expression of Tgm2 might help us to identify LT-HSCs in the murine BM, without using an extensive combination of different surface markers. A Tgm2 reporter mouse model might provide the possibility of simple identification and isolation of LT-HSCs expressing fluorescent reporters under the endogenous Tgm2 locus control.

Traditionally, reporter mice are generated with the knock-in strategy using mouse embryonic stem (ES) cells. Knock-in mouse ES cells first undergoes homologous recombination mediated gene targeting, which typically has a low success frequency. Then these knock-in ES cells are injected into wildtype mouse preimplantation embryos to establish chimeric founders. Only when the knock-in ES cells contributed to the germline of the chimeric founders, knock-in mouse lines can be established. However, it is known that this technology requires the screening of a very high number of ES cell clones, following by the subsequent time consuming chimera generation and breeding (Gu 2020; Thomas and Capecchi 1987). Recently, the CRISPR/Cas9 system have completely changed the landscape in gene editing and improved the efficiency of reporter mice generation (Hsu et al., 2014). A technology called Easi-CRISPR

has been more recently developed, in which a long single-stranded DNA is used as donor templates instead of double-stranded plasmid DNA. By microinjection of ribonucleoprotein complexes of Cas9 protein bound with a complexed crRNA and tracrRNA guide alongside a long ssDNA template encoding the desired knock-in sequence flanked by around 100 base homology arms, Easi-CRISPR has been used to accomplish knock-in of fragments varying from 800 base pairs to 1.4 kilobase pairs with efficiencies ranging from 25-67%. However, at present, long single-stranded DNA template synthesis remains a primary limitation of Easi-CRISPR, with insertion of fragments greater than 1-2 kilobases remaining a challenge (Quadros et al. 2017; Gu 2020).

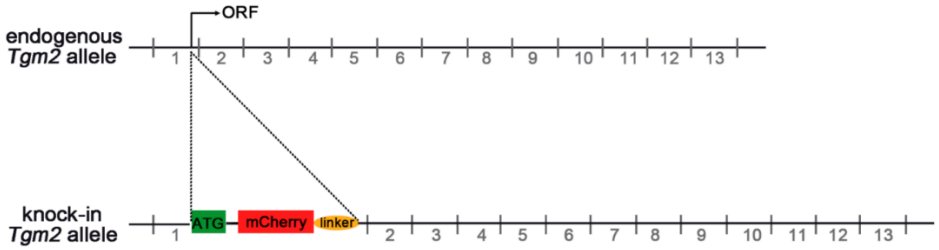

Figure 41 Targeting strategy to generate a mCherry-linker-Tgm2 knock-in mouse reporter line.

In order to investigate the endogenous expression of Tgm2 in different mouse cell types, the open reading frame (ORF) of around 1 kilobases fragment including the red fluorescent protein "mCherry" is designed to knock into the endogenous start codon of Tgm2, resulting in a fusion protein of mCherry-Tgm2 without changing the ORF in the endogenous sequence of the Tgm2 (**Figure 41**). These mCherry-Tgm2 reporter mice are currently under generation in cooperation with Dr. Phillip Grote from the Transgenic Core Facility in Georg-Speyer-Haus (Frankfurt am Main, Germany). Three different guide RNAs (gRNAs) were designed and used for the microinjection. Five ES cell clones with C57BL/6J background were successfully obtained. Further steps are still ongoing. A successful generation of a Tgm2 reporter mouse line not only can simplify the identification and isolation of hematopoietic LT-HSCs *in vivo*, but can also be used for live imaging of embryos and tissues, as well as lineage tracing and pathways analysis of LT-HSCs under various conditions.

5. References

Acar, Melih; Kocherlakota, Kiranmai S.; Murphy, Malea M.; Peyer, James G.; Oguro, Hideyuki; Inra, Christopher N. et al. (2015): Deep imaging of bone marrow shows non-dividing stem cells are mainly perisinusoidal. In *Nature* 526 (7571), pp. 126–130. DOI: 10.1038/nature15250.

Adolfsson, Jörgen; Borge, Ole Johan; Bryder, David; Theilgaard-Mönch, Kim; Åstrand-Grundström, Ingbritt; Sitnicka, Ewa et al. (2001): Upregulation of Flt3 Expression within the Bone Marrow Lin−Sca1+c-kit+ Stem Cell Compartment Is Accompanied by Loss of Self-Renewal Capacity. In *Immunity* 15 (4), pp. 659–669. DOI: 10.1016/S1074-7613(01)00220-5.

Adolfsson, Jörgen; Månsson, Robert; Buza-Vidas, Natalija; Hultquist, Anne; Liuba, Karina; Jensen, Christina T. et al. (2005): Identification of Flt3+ lympho-myeloid stem cells lacking erythro-megakaryocytic potential a revised road map for adult blood lineage commitment. In *Cell* 121 (2), pp. 295–306. DOI: 10.1016/j.cell.2005.02.013.

Agnihotri, Navneet; Mehta, Kapil (2017): Transglutaminase-2. Evolution from pedestrian protein to a promising therapeutic target. In *Amino acids* 49 (3), pp. 425–439. DOI: 10.1007/s00726-016-2320-2.

Akashi, K.; Traver, D.; Miyamoto, T.; Weissman, I. L. (2000): A clonogenic common myeloid progenitor that gives rise to all myeloid lineages. In *Nature* 404 (6774), pp. 193–197. DOI: 10.1038/35004599.

An, Ningfei; Lin, Ying-Wei; Mahajan, Sandeep; Kellner, Joshua N.; Wang, Yong; Li, Zihai et al. (2013): Pim1 serine/threonine kinase regulates the number and functions of murine hematopoietic stem cells. In *Stem cells (Dayton, Ohio)* 31 (6), pp. 1202–1212. DOI: 10.1002/stem.1369.

Andreoli, Verónica; Gehrau, Ricardo C.; Bocco, Jose Luis (2010): Biology of Krüppel-like factor 6 transcriptional regulator in cell life and death. In *IUBMB life* 62 (12), pp. 896–905. DOI: 10.1002/iub.396.

Andrews S. (2010): FastQC: a quality control tool for high throughput sequence data. Available online at http://www.bioinformatics.babraham.ac.uk/projects/fastqc.

Antonyak, M. A.; Singh, U. S.; Lee, D. A.; Boehm, J. E.; Combs, C.; Zgola, M. M. et al. (2001): Effects of tissue transglutaminase on retinoic acid-induced cellular differentiation and protection against apoptosis. In *The Journal of biological chemistry* 276 (36), pp. 33582–33587. DOI: 10.1074/jbc.M105318200.

Baena, Esther; Ortiz, Maitane; Martínez-A, Carlos; Alborán, Ignacio Moreno de (2007): c-Myc is essential for hematopoietic stem cell differentiation and regulates Lin(-)Sca-1(+)c-Kit(-) cell generation through p21. In *Experimental hematology* 35 (9), pp. 1333–1343. DOI: 10.1016/j.exphem.2007.05.015.

Becker-Herman, Shirly; Rozenberg, Milena; Hillel-Karniel, Carmit; Gil-Yarom, Naama; Kramer, Mattias P.; Barak, Avital et al. (2021): CD74 is a regulator of hematopoietic stem cell maintenance. In *PLoS biology* 19 (3), e3001121. DOI: 10.1371/journal.pbio.3001121.

Begg, Gillian E.; Carrington, Lyle; Stokes, Philippa H.; Matthews, Jacqueline M.; Wouters, Merridee A.; Husain, Ahsan et al. (2006): Mechanism of allosteric regulation of transglutaminase 2 by GTP. In *Proceedings of the National Academy of Sciences* 103 (52), pp. 19683–19688. DOI: 10.1073/pnas.0609283103.

Böiers, Charlotta; Carrelha, Joana; Lutteropp, Michael; Luc, Sidinh; Green, Joanna C. A.; Azzoni, Emanuele et al. (2013): Lymphomyeloid contribution of an immune-restricted progenitor emerging prior to definitive hematopoietic stem cells. In *Cell stem cell* 13 (5), pp. 535–548. DOI: 10.1016/j.stem.2013.08.012.

Bowie, Michelle B.; Kent, David G.; Dykstra, Brad; McKnight, Kristen D.; McCaffrey, Lindsay; Hoodless, Pamela A.; Eaves, Connie J. (2007): Identification of a new intrinsically timed developmental checkpoint that reprograms key

hematopoietic stem cell properties. In *Proceedings of the National Academy of Sciences* 104 (14), pp. 5878–5882. DOI: 10.1073/pnas.0700460104.

Bujanover, Nir; Goldstein, Oron; Greenshpan, Yariv; Turgeman, Hodaya; Klainberger, Amit; Scharff, Ye'ela; Gazit, Roi (2018): Identification of immune-activated hematopoietic stem cells. In *Leukemia* 32 (9), pp. 2016–2020. DOI: 10.1038/s41375-018-0220-z.

Cabezas-Wallscheid, Nina; Buettner, Florian; Sommerkamp, Pia; Klimmeck, Daniel; Ladel, Luisa; Thalheimer, Frederic B. et al. (2017): Vitamin A-Retinoic Acid Signaling Regulates Hematopoietic Stem Cell Dormancy. In *Cell* 169 (5), 807-823.e19. DOI: 10.1016/j.cell.2017.04.018.

Cabezas-Wallscheid, Nina; Klimmeck, Daniel; Hansson, Jenny; Lipka, Daniel B.; Reyes, Alejandro; Wang, Qi et al. (2014): Identification of regulatory networks in HSCs and their immediate progeny via integrated proteome, transcriptome, and DNA methylome analysis. In *Cell stem cell* 15 (4), pp. 507–522. DOI: 10.1016/j.stem.2014.07.005.

Cao, L.; Shao, M.; Schilder, J.; Guise, T.; Mohammad, K. S.; Matei, D. (2012): Tissue transglutaminase links TGF-β, epithelial to mesenchymal transition and a stem cell phenotype in ovarian cancer. In *Oncogene* 31 (20), pp. 2521–2534. DOI: 10.1038/onc.2011.429.

Caunt, Christopher J.; Keyse, Stephen M. (2013): Dual-specificity MAP kinase phosphatases (MKPs): shaping the outcome of MAP kinase signalling. In *The FEBS journal* 280 (2), pp. 489–504. DOI: 10.1111/j.1742-4658.2012.08716.x.

Cellura, D.; Pickard, K.; Quaratino, S.; Parker, H.; Strefford, J. C.; Thomas, G. J. et al. (2015): miR-19-Mediated Inhibition of Transglutaminase-2 Leads to Enhanced Invasion and Metastasis in Colorectal Cancer. In *Molecular cancer research : MCR* 13 (7), pp. 1095–1105. DOI: 10.1158/1541-7786.MCR-14-0466.

Challen, Grant A.; Boles, Nathan C.; Chambers, Stuart M.; Goodell, Margaret A. (2010): Distinct hematopoietic stem cell subtypes are differentially regulated by TGF-beta1. In *Cell stem cell* 6 (3), pp. 265–278. DOI: 10.1016/j.stem.2010.02.002.

Challen, Grant A.; Pietras, Eric M.; Wallscheid, Nina Cabezas; Signer, Robert A. J. (2021): Simplified murine multipotent progenitor isolation scheme: Establishing a consensus approach for multipotent progenitor identification. In *Experimental hematology*. DOI: 10.1016/j.exphem.2021.09.007.

Chen, James Y.; Miyanishi, Masanori; Wang, Sean K.; Yamazaki, Satoshi; Sinha, Rahul; Kao, Kevin S. et al. (2016): Hoxb5 marks long-term haematopoietic stem cells and reveals a homogenous perivascular niche. In *Nature* 530 (7589), pp. 223–227. DOI: 10.1038/nature16943.

Chhabra, Arnav; Verma, Amit; Mehta, Kapil (2009): Tissue transglutaminase promotes or suppresses tumors depending on cell context. In *Anticancer research* 29 (6), pp. 1909–1919.

Cho, Sung-Yup; Lee, Jin-Haeng; Bae, Han-Dong; Jeong, Eui Man; Jang, Gi-Yong; Kim, Chai-Wan et al. (2010): Transglutaminase 2 inhibits apoptosis induced by calcium- overload through down-regulation of Bax. In *Experimental & molecular medicine* 42 (9), pp. 639–650. DOI: 10.3858/emm.2010.42.9.063.

Dahlin, Joakim S.; Hamey, Fiona K.; Pijuan-Sala, Blanca; Shepherd, Mairi; Lau, Winnie W. Y.; Nestorowa, Sonia et al. (2018): A single-cell hematopoietic landscape resolves 8 lineage trajectories and defects in Kit mutant mice. In *Blood* 131 (21), e1-e11. DOI: 10.1182/blood-2017-12-821413.

D'Amato, Mauro; Iannicola, Carlo; Monteriù, Giorgia; Piacentini, Mauro (1999): Mapping and sequencing of the murine 'tissue' Transglutaminase (Tgm2) gene. Absence of mutations in MRLlpr/lpr mice. In *Cell death and differentiation* 6 (3), pp. 216–217. DOI: 10.1038/sj.cdd.4400494.

Datta, Sunando; Antonyak, Marc A.; Cerione, Richard A. (2007): GTP-binding-defective forms of tissue transglutaminase trigger cell death. In *Biochemistry* 46 (51), pp. 14819–14829. DOI: 10.1021/bi701422h.

Deasey, Stephanie; Shanmugasundaram, Shobana; Nurminskaya, Maria (2013): Tissue-specific responses to loss of transglutaminase 2. In *Amino acids* 44 (1), pp. 179–187. DOI: 10.1007/s00726-011-1183-9.

Dong, Chen; Davis, Roger J.; Flavell, Richard A. (2002): MAP kinases in the immune response. In *Annual review of immunology* 20, pp. 55–72. DOI: 10.1146/annurev.immunol.20.091301.131133.

Doulatov, Sergei; Notta, Faiyaz; Laurenti, Elisa; Dick, John E. (2012): Hematopoiesis: a human perspective. In *Cell stem cell* 10 (2), pp. 120–136. DOI: 10.1016/j.stem.2012.01.006.

Dull, T.; Zufferey, R.; Kelly, M.; Mandel, R. J.; Nguyen, M.; Trono, D.; Naldini, L. (1998): A third-generation lentivirus vector with a conditional packaging system. In *Journal of virology* 72 (11), pp. 8463–8471. DOI: 10.1128/JVI.72.11.8463-8471.1998.

Dykstra, Brad; Kent, David; Bowie, Michelle; McCaffrey, Lindsay; Hamilton, Melisa; Lyons, Kristin et al. (2007): Long-term propagation of distinct hematopoietic differentiation programs in vivo. In *Cell stem cell* 1 (2), pp. 218–229. DOI: 10.1016/j.stem.2007.05.015.

Eckert, Richard L. (2019): Transglutaminase 2 takes center stage as a cancer cell survival factor and therapy target. In *Molecular carcinogenesis* 58 (6), pp. 837–853. DOI: 10.1002/mc.22986.

Essers, Marieke A. G.; Offner, Sandra; Blanco-Bose, William E.; Waibler, Zoe; Kalinke, Ulrich; Duchosal, Michel A.; Trumpp, Andreas (2009): IFNalpha activates dormant haematopoietic stem cells in vivo. In *Nature* 458 (7240), pp. 904–908. DOI: 10.1038/nature07815.

Falasca, Laura; Farrace, Maria Grazia; Rinaldi, Alessandra; Tuosto, Loretta; Melino, Gennard; Piacentini, Mauro (2008): Transglutaminase type II is involved in the pathogenesis of endotoxic shock. In *Journal of immunology (Baltimore, Md. : 1950)* 180 (4), pp. 2616–2624. DOI: 10.4049/jimmunol.180.4.2616.

Fathman, John W.; Fernhoff, Nathaniel B.; Seita, Jun; Chao, Connie; Scarfone, Vanessa M.; Weissman, Irving L.; Inlay, Matthew A. (2014): Upregulation of CD11A on hematopoietic stem cells denotes the loss of long-term reconstitution potential. In *Stem cell reports* 3 (5), pp. 707–715. DOI: 10.1016/j.stemcr.2014.09.007.

Fésüs, László; Szondy, Zsuzsa (2005): Transglutaminase 2 in the balance of cell death and survival. In *FEBS Lett* 579 (15), pp. 3297–3302. DOI: 10.1016/j.febslet.2005.03.063.

Fieller, E. C.; Hartley, H. O.; Pearson, E. S. (1957): Tests for Rank Correlation Coefficients. I. In *Biometrika* 44 (3/4), p. 470. DOI: 10.2307/2332878.

Fisher, Matthew L.; Adhikary, Gautam; Xu, Wen; Kerr, Candace; Keillor, Jeffrey W.; Eckert, Richard L. (2015): Type II transglutaminase stimulates epidermal cancer stem cell epithelial-mesenchymal transition. In *Oncotarget* 6 (24), pp. 20525–20539. DOI: 10.18632/oncotarget.3890.

Fok, Jansina Y.; Mehta, Kapil (2007): Tissue transglutaminase induces the release of apoptosis inducing factor and results in apoptotic death of pancreatic cancer cells. In *Apoptosis : an international journal on programmed cell death* 12 (8), pp. 1455–1463. DOI: 10.1007/s10495-007-0079-3.

FORD, C. E.; HAMERTON, J. L.; BARNES, D. W.; LOUTIT, J. F. (1956): Cytological identification of radiation-chimaeras. In *Nature* 177 (4506), pp. 452–454. DOI: 10.1038/177452a0.

Forsberg, E. Camilla; Passegué, Emmanuelle; Prohaska, Susan S.; Wagers, Amy J.; Koeva, Martina; Stuart, Joshua M.; Weissman, Irving L. (2010): Molecular signatures of quiescent, mobilized and leukemia-initiating hematopoietic stem cells. In *PloS one* 5 (1), e8785. DOI: 10.1371/journal.pone.0008785.

Forsberg, E. Camilla; Prohaska, Susan S.; Katzman, Sol; Heffner, Garrett C.; Stuart, Josh M.; Weissman, Irving L. (2005): Differential expression of novel potential regulators in hematopoietic stem cells. In *PLoS genetics* 1 (3), e28. DOI: 10.1371/journal.pgen.0010028.

Fox, Norma; Priestley, Greg; Papayannopoulou, Thalia; Kaushansky, Kenneth (2002): Thrombopoietin expands hematopoietic stem cells after transplantation. In *The Journal of clinical investigation* 110 (3), pp. 389–394. DOI: 10.1172/JCI15430.

Fraij, B. M.; Birckbichler, P. J.; Patterson, M. K.; Lee, K. N.; Gonzales, R. A. (1992): A retinoic acid-inducible mRNA from human erythroleukemia cells encodes a novel tissue transglutaminase homologue. In *The Journal of biological chemistry* 267 (31), pp. 22616–22623.

Fraij, Bassam M.; Gonzales, Robert A. (1996): A third human tissue transglutaminase homologue as a result of alternative gene transcripts. In *Biochimica et Biophysica Acta (BBA) - Gene Structure and Expression* 1306 (1), pp. 63–74. DOI: 10.1016/0167-4781(95)00219-7.

Frisdal, Eric; Lesnik, Philippe; Olivier, Maryline; Robillard, Paul; Chapman, M. John; Huby, Thierry et al. (2011): Interleukin-6 protects human macrophages from cellular cholesterol accumulation and attenuates the proinflammatory response. In *The Journal of biological chemistry* 286 (35), pp. 30926–30936. DOI: 10.1074/jbc.M111.264325.

Gazit, Roi; Mandal, Pankaj K.; Ebina, Wataru; Ben-Zvi, Ayal; Nombela-Arrieta, César; Silberstein, Leslie E.; Rossi, Derrick J. (2014): Fgd5 identifies hematopoietic stem cells in the murine bone marrow. In *Journal of Experimental Medicine* 211 (7), pp. 1315–1331. DOI: 10.1084/jem.20130428.

Gentile, V.; Saydak, M.; Chiocca, E. A.; Akande, O.; Birckbichler, P. J.; Lee, K. N. et al. (1991): Isolation and characterization of cDNA clones to mouse macrophage and human endothelial cell tissue transglutaminases. In *The Journal of biological chemistry* 266 (1), pp. 478–483.

Gidáli, J.; Fehér, I.; Tálas, M. (1981): Proliferation inhibition of murine pluripotent haemopoietic stem cells by interferon or poly I:C. In *Cell and tissue kinetics* 14 (1), pp. 1–7. DOI: 10.1111/j.1365-2184.1981.tb00505.x.

Goedhart, Joachim; Luijsterburg, Martijn S. (2020): VolcaNoseR is a web app for creating, exploring, labeling and sharing volcano plots. In *Scientific reports* 10 (1), p. 20560. DOI: 10.1038/s41598-020-76603-3.

Goodell, M. A.; Brose, K.; Paradis, G.; Conner, A. S.; Mulligan, R. C. (1996): Isolation and functional properties of murine hematopoietic stem cells that are replicating in vivo. In *Journal of Experimental Medicine* 183 (4), pp. 1797–1806. DOI: 10.1084/jem.183.4.1797.

Goroshchuk, Oksana; Kolosenko, Iryna; Vidarsdottir, Linda; Azimi, Alireza; Palm-Apergi, Caroline (2019): Polo-like kinases and acute leukemia. In *Oncogene* 38 (1), pp. 1–16. DOI: 10.1038/s41388-018-0443-5.

Gu, Bin (2020): Light up the embryos: knock-in reporter generation for mouse developmental biology. In *Animal reproduction* 17 (3), e20200055. DOI: 10.1590/1984-3143-AR2020-0055.

Gundemir, Soner; Colak, Gozde; Tucholski, Janusz; Johnson, Gail V. W. (2012): Transglutaminase 2. A molecular Swiss army knife. In *Biochimica et biophysica acta* 1823 (2), pp. 406–419. DOI: 10.1016/j.bbamcr.2011.09.012.

H. S. Micklem and John F. Lontit (1966): Tissue Grafting and Radiation. New York: New York Academy of Sciences Press.

Haas, Simon; Hansson, Jenny; Klimmeck, Daniel; Loeffler, Dirk; Velten, Lars; Uckelmann, Hannah et al. (2015): Inflammation-Induced Emergency Megakaryopoiesis Driven by Hematopoietic Stem Cell-like Megakaryocyte Progenitors. In *Cell stem cell* 17 (4), pp. 422–434. DOI: 10.1016/j.stem.2015.07.007.

Han, Byeong-Gu; Cho, Jea-Won; Cho, Young Doo; Jeong, Kyung-Chae; Kim, Soo-Youl; Lee, Byung Il (2010): Crystal structure of human transglutaminase 2 in complex with adenosine triphosphate. In *International journal of biological macromolecules* 47 (2), pp. 190–195. DOI: 10.1016/j.ijbiomac.2010.04.023.

Han, Heonjong; Cho, Jae-Won; Lee, Sangyoung; Yun, Ayoung; Kim, Hyojin; Bae, Dasom et al. (2018): TRRUST v2: an expanded reference database of human and mouse transcriptional regulatory interactions. In *Nucleic acids research* 46 (D1), D380-D386. DOI: 10.1093/nar/gkx1013.

Harrison, D. E.; Lerner, C. P. (1991): Most primitive hematopoietic stem cells are stimulated to cycle rapidly after treatment with 5-fluorouracil. In *Blood* 78 (5), pp. 1237–1240.

Hasegawa, Go; Suwa, Motoi; Ichikawa, Yasuo; Ohtsuka, Tetsuro; Kumagai, Satoru; Kikuchi, Masashi et al. (2003): A novel function of tissue-type transglutaminase: protein disulphide isomerase. In *The Biochemical journal* 373 (Pt 3), pp. 793–803. DOI: 10.1042/BJ20021084.

Herring, Jacob A.; Elison, Weston S.; Tessem, Jeffery S. (2019): Function of Nr4a Orphan Nuclear Receptors in Proliferation, Apoptosis and Fuel Utilization Across Tissues. In *Cells* 8 (11). DOI: 10.3390/cells8111373.

Hodrea, Judit; Demény, Máté A.; Majai, Gyöngyike; Sarang, Zsolt; Korponay-Szabó, Ilma Rita; Fésüs, László (2010): Transglutaminase 2 is expressed and active on the surface of human monocyte-derived dendritic cells and macrophages. In *Immunology letters* 130 (1-2), pp. 74–81. DOI: 10.1016/j.imlet.2009.12.010.

Iismaa, Siiri E.; Mearns, Bryony M.; Lorand, Laszlo; Graham, Robert M. (2009): Transglutaminases and disease. Lessons from genetically engineered mouse models and inherited disorders. In *Physiological reviews* 89 (3), pp. 991–1023. DOI: 10.1152/physrev.00044.2008.

Ito, Keisuke; Hirao, Atsushi; Arai, Fumio; Takubo, Keiyo; Matsuoka, Sahoko; Miyamoto, Kana et al. (2006): Reactive oxygen species act through p38 MAPK to limit the lifespan of hematopoietic stem cells. In *Nat Med* 12 (4), pp. 446–451. DOI: 10.1038/nm1388.

Jafri, Salema; Moore, Stephen D.; Morrell, Nicholas W.; Ormiston, Mark L. (2017): A sex-specific reconstitution bias in the competitive CD45.1/CD45.2 congenic bone marrow transplant model. In *Scientific reports* 7 (1), p. 3495. DOI: 10.1038/s41598-017-03784-9.

Jaiswal, Siddhartha; Jamieson, Catriona H. M.; Pang, Wendy W.; Park, Christopher Y.; Chao, Mark P.; Majeti, Ravindra et al. (2009): CD47 is upregulated on circulating hematopoietic stem cells and leukemia cells to avoid phagocytosis. In *Cell* 138 (2), pp. 271–285. DOI: 10.1016/j.cell.2009.05.046.

Jambrovics, Károly; Uray, Iván P.; Keressztesy, Zsolt; Keillor, Jeffrey W.; Fésüs, László; Balajthy, Zoltán (2018): Transglutaminase 2 programs differentiating acute promyelocytic leukemia cells in all-trans retinoic acid treatment to inflammatory stage through NF-kB activation. In *Haematologica*. DOI: 10.3324/haematol.2018.192823.

Jang, G-Y; Jeon, J-H; Cho, S-Y; Shin, D-M; Kim, C-W; Jeong, E. M. et al. (2010): Transglutaminase 2 suppresses apoptosis by modulating caspase 3 and NF-kappaB activity in hypoxic tumor cells. In *Oncogene* 29 (3), pp. 356–367. DOI: 10.1038/onc.2009.342.

Jang, Yoon-Young; Sharkis, Saul J. (2007): A low level of reactive oxygen species selects for primitive hematopoietic stem cells that may reside in the low-oxygenic niche. In *Blood* 110 (8), pp. 3056–3063. DOI: 10.1182/blood-2007-05-087759.

Jha, Prerana; Das, Hiranmoy (2017): KLF2 in Regulation of NF-κB-Mediated Immune Cell Function and Inflammation. In *International journal of molecular sciences* 18 (11). DOI: 10.3390/ijms18112383.

Jin, Xi; Stamnaes, Jorunn; Klöck, Cornelius; DiRaimondo, Thomas R.; Sollid, Ludvig M.; Khosla, Chaitan (2011): Activation of extracellular transglutaminase 2 by thioredoxin. In *The Journal of biological chemistry* 286 (43), pp. 37866–37873. DOI: 10.1074/jbc.M111.287490.

Johnson, Kristen; Hashimoto, Sanshiro; Lotz, Martin; Pritzker, Kenneth; Terkeltaub, Robert (2001): Interleukin-1 Induces Pro-Mineralizing Activity of Cartilage Tissue Transglutaminase and Factor XIIIa. In *The American Journal of Pathology* 159 (1), pp. 149–163. DOI: 10.1016/S0002-9440(10)61682-3.

Junkunlo, Kingkamon; Söderhäll, Kenneth; Söderhäll, Irene (2018): Transglutaminase inhibition stimulates hematopoiesis and reduces aggressive behavior of crayfish, Pacifastacus leniusculus. In *The Journal of biological chemistry*. DOI: 10.1074/jbc.RA118.005489.

Junkunlo, Kingkamon; Söderhäll, Kenneth; Söderhäll, Irene; Noonin, Chadanat (2016): Reactive Oxygen Species Affect Transglutaminase Activity and Regulate Hematopoiesis in a Crustacean. In *The Journal of biological chemistry* 291 (34), pp. 17593–17601. DOI: 10.1074/jbc.M116.741348.

Karlsson, Göran; Rörby, Emma; Pina, Cristina; Soneji, Shamit; Reckzeh, Kristian; Miharada, Kenichi et al. (2013): The tetraspanin CD9 affords high-purity capture of all murine hematopoietic stem cells. In *Cell reports* 4 (4), pp. 642–648. DOI: 10.1016/j.celrep.2013.07.020.

Kemp, Richard; Ireland, Heather; Clayton, Elizabeth; Houghton, Carol; Howard, Louise; Winton, Douglas J. (2004): Elimination of background recombination: somatic induction of Cre by combined transcriptional regulation and hormone binding affinity. In *Nucleic acids research* 32 (11), e92. DOI: 10.1093/nar/gnh090.

Kent, David G.; Copley, Michael R.; Benz, Claudia; Wöhrer, Stefan; Dykstra, Brad J.; Ma, Elaine et al. (2009): Prospective isolation and molecular characterization of hematopoietic stem cells with durable self-renewal potential. In *Blood* 113 (25), pp. 6342–6350. DOI: 10.1182/blood-2008-12-192054.

Kiel, Mark J.; Yilmaz, Omer H.; Iwashita, Toshihide; Yilmaz, Osman H.; Terhorst, Cox; Morrison, Sean J. (2005): SLAM family receptors distinguish hematopoietic stem and progenitor cells and reveal endothelial niches for stem cells. In *Cell* 121 (7), pp. 1109–1121. DOI: 10.1016/j.cell.2005.05.026.

Kim, Hyeonhui; Kim, Minki; Im, Sun-Kyoung; Fang, Sungsoon (2018): Mouse Cre-LoxP system: general principles to determine tissue-specific roles of target genes. In *Laboratory animal research* 34 (4), pp. 147–159. DOI: 10.5625/lar.2018.34.4.147.

Kim, Jin-Hee; Jeong, Eui Man; Jeong, Young-Joo; Lee, Wang Jae; Kang, Jae Seung; Kim, In-Gyu; Hwang, Young-il (2012): Transglutaminase 2 modulates antigen-specific antibody response by suppressing Blimp-1 and AID expression of B cells in mice. In *Immunology letters* 147 (1-2), pp. 18–28. DOI: 10.1016/j.imlet.2012.05.003.

Kim, Jin-Hee; Jeong, Eui Man; Jeong, Young-Joo; Lee, Wang Jae; Kang, Jae Seung; Kim, In-Gyu; Hwang, Young-il (2014a): Transglutaminase 2 on the surface of dendritic cells is proposed to be involved in dendritic cell-T cell interaction. In *Cellular immunology* 289 (1-2), pp. 55–62. DOI: 10.1016/j.cellimm.2014.03.008.

Kim, M.; Cooper, D. D.; Hayes, S. F.; Spangrude, G. J. (1998): Rhodamine-123 staining in hematopoietic stem cells of young mice indicates mitochondrial activation rather than dye efflux. In *Blood* 91 (11), pp. 4106–4117.

Kim, Yuna; Ryu, Jewon; Ryu, Min Sook; Lim, Sunny; Han, Ki Ok; Lim, In Kyoung; Han, Ki Hoon (2014b): C-reactive protein induces G2/M phase cell cycle arrest and apoptosis in monocytes through the upregulation of B-cell translocation gene 2 expression. In *FEBS Lett* 588 (4), pp. 625–631. DOI: 10.1016/j.febslet.2014.01.008.

Knapp, David Jhf; Eaves, Connie J. (2014): Control of the hematopoietic stem cell state. In *Cell research* 24 (1), pp. 3–4. DOI: 10.1038/cr.2013.139.

Kohlscheen, Saskia; Schenk, Franziska; Rommel, Marcel G. E.; Cullmann, Katharina; Modlich, Ute (2019): Endothelial protein C receptor supports hematopoietic stem cell engraftment and expansion in Mpl-deficient mice. In *Blood* 133 (13), pp. 1465–1478. DOI: 10.1182/blood-2018-03-837344.

Koide, Shuhei; Sigurdsson, Valgardur; Radulovic, Visnja; Saito, Kiyoka; Zheng, Zhiqian; Lang, Stefan et al. (2022): CD244 expression represents functional decline of murine hematopoietic stem cells after in vitro culture. In *iScience* 25 (1), p. 103603. DOI: 10.1016/j.isci.2021.103603.

Komuro K.; ItakuraK.; Boyse E. A.; John M. (1974): Ly-5: A new T-lymphocyte antigen system. In *Immunogenetics* (1), pp. 452–456.

Kondo, Motonari; Weissman, Irving L.; Akashi, Koichi (1997): Identification of Clonogenic Common Lymphoid Progenitors in Mouse Bone Marrow. In *Cell* 91 (5), pp. 661–672. DOI: 10.1016/S0092-8674(00)80453-5.

Kühn, R.; Schwenk, F.; Aguet, M.; Rajewsky, K. (1995): Inducible gene targeting in mice. In *Science* 269 (5229), pp. 1427–1429. DOI: 10.1126/science.7660125.

Kumar, Anupam; Gao, Hui; Xu, Jia; Reuben, James; Yu, Dihua; Mehta, Kapil (2011): Evidence that aberrant expression of tissue transglutaminase promotes stem cell characteristics in mammary epithelial cells. In *PloS one* 6 (6), e20701. DOI: 10.1371/journal.pone.0020701.

Kuncio, G. S.; Tsyganskaya, M.; Zhu, J.; Liu, S. L.; Nagy, L.; Thomazy, V. et al. (1998): TNF-alpha modulates expression of the tissue transglutaminase gene in liver cells. In *The American journal of physiology* 274 (2), G240-5. DOI: 10.1152/ajpgi.1998.274.2.G240.

Lai, T. S.; Bielawska, A.; Peoples, K. A.; Hannun, Y. A.; Greenberg, C. S. (1997): Sphingosylphosphocholine reduces the calcium ion requirement for activating tissue transglutaminase. In *The Journal of biological chemistry* 272 (26), pp. 16295–16300. DOI: 10.1074/jbc.272.26.16295.

Lai, T. S.; Hausladen, A.; Slaughter, T. F.; Eu, J. P.; Stamler, J. S.; Greenberg, C. S. (2001): Calcium regulates S-nitrosylation, denitrosylation, and activity of tissue transglutaminase. In *Biochemistry* 40 (16), pp. 4904–4910. DOI: 10.1021/bi002321t.

Lai, Thung S.; Davies, Christopher; Greenberg, Charles S. (2010): Human tissue transglutaminase is inhibited by pharmacologic and chemical acetylation. In *Protein science : a publication of the Protein Society* 19 (2), pp. 229–235. DOI: 10.1002/pro.301.

Lai, Thung-S; Greenberg, Charles S. (2013): TGM2 and implications for human disease: role of alternative splicing. In *Frontiers in bioscience (Landmark edition)* 18 (2), pp. 504–519. DOI: 10.2741/4117.

Lai, Thung-S; Liu, Yusha; Li, Weidong; Greenberg, Charles S. (2007): Identification of two GTP-independent alternatively spliced forms of tissue transglutaminase in human leukocytes, vascular smooth muscle, and endothelial cells. In *FASEB journal : official publication of the Federation of American Societies for Experimental Biology* 21 (14), pp. 4131–4143. DOI: 10.1096/fj.06-7598com.

Laurenzi, V. de; Melino, G. (2001): Gene disruption of tissue transglutaminase. In *Molecular and cellular biology* 21 (1), pp. 148–155. DOI: 10.1128/MCB.21.1.148-155.2001.

Li, Ling; Bhatia, Ravi (2011): Stem cell quiescence. In *Clinical cancer research : an official journal of the American Association for Cancer Research* 17 (15), pp. 4936–4941. DOI: 10.1158/1078-0432.CCR-10-1499.

Liebermann, D. A.; Gregory, B.; Hoffman, B. (1998): AP-1 (Fos/Jun) transcription factors in hematopoietic differentiation and apoptosis. In *International journal of oncology* 12 (3), pp. 685–700. DOI: 10.3892/ijo.12.3.685.

Lin, Kuanyin K.; Rossi, Lara; Boles, Nathan C.; Hall, Brian E.; George, Thaddeus C.; Goodell, Margaret A. (2011): CD81 is essential for the re-entry of hematopoietic stem cells to quiescence following stress-induced proliferation via deactivation of the Akt pathway. In *PLoS biology* 9 (9), e1001148. DOI: 10.1371/journal.pbio.1001148.

Lin, Xionghui; Söderhäll, Kenneth; Söderhäll, Irene (2008): Transglutaminase activity in the hematopoietic tissue of a crustacean, Pacifastacus leniusculus, importance in hemocyte homeostasis. In *BMC immunology* 9, p. 58. DOI: 10.1186/1471-2172-9-58.

Liu, Shenping; Cerione, Richard A.; Clardy, Jon (2002): Structural basis for the guanine nucleotide-binding activity of tissue transglutaminase and its regulation of transamidation activity. In *Proceedings of the National Academy of Sciences* 99 (5), pp. 2743–2747. DOI: 10.1073/pnas.042454899.

Liu, Yan; Elf, Shannon E.; Miyata, Yasuhiko; Sashida, Goro; Liu, Yuhui; Huang, Gang et al. (2009): p53 regulates hematopoietic stem cell quiescence. In *Cell stem cell* 4 (1), pp. 37–48. DOI: 10.1016/j.stem.2008.11.006.

Luciani, Alessandro; Villella, Valeria Rachela; Vasaturo, Angela; Giardino, Ida; Raia, Valeria; Pettoello-Mantovani, Massimo et al. (2009): SUMOylation of tissue transglutaminase as link between oxidative stress and inflammation. In *Journal of immunology (Baltimore, Md. : 1950)* 183 (4), pp. 2775–2784. DOI: 10.4049/jimmunol.0900993.

Malkomes, Patrizia; Lunger, Ilaria; Oppermann, Elsie; Abou-El-Ardat, Khalil; Oellerich, Thomas; Günther, Stefan et al. (2021): Transglutaminase 2 promotes tumorigenicity of colon cancer cells by inactivation of the tumor suppressor p53. In *Oncogene* 40 (25), pp. 4352–4367. DOI: 10.1038/s41388-021-01847-w.

Malorni, W.; Farrace, M. G.; Matarrese, P.; Tinari, A.; Ciarlo, L.; Mousavi-Shafaei, P. et al. (2009): The adenine nucleotide translocator 1 acts as a type 2 transglutaminase substrate: implications for mitochondrial-dependent apoptosis. In *Cell death and differentiation* 16 (11), pp. 1480–1492. DOI: 10.1038/cdd.2009.100.

McConnell, Beth B.; Yang, Vincent W. (2010): Mammalian Krüppel-like factors in health and diseases. In *Physiological reviews* 90 (4), pp. 1337–1381. DOI: 10.1152/physrev.00058.2009.

MCCULLOCH, E. A.; TILL, J. E. (1960): The radiation sensitivity of normal mouse bone marrow cells, determined by quantitative marrow transplantation into irradiated mice. In *Radiation research* 13, pp. 115–125.

McGrath, Kathleen E.; Frame, Jenna M.; Fegan, Katherine H.; Bowen, James R.; Conway, Simon J.; Catherman, Seana C. et al. (2015): Distinct Sources of Hematopoietic Progenitors Emerge before HSCs and Provide Functional Blood Cells in the Mammalian Embryo. In *Cell reports* 11 (12), pp. 1892–1904. DOI: 10.1016/j.celrep.2015.05.036.

Medvinsky, Alexander; Dzierzak, Elaine (1996): Definitive Hematopoiesis Is Autonomously Initiated by the AGM Region. In *Cell* 86 (6), pp. 897–906. DOI: 10.1016/S0092-8674(00)80165-8.

Mehta, Kapil (2005): Mammalian transglutaminases: a family portrait. In *Progress in experimental tumor research* 38, pp. 1–18. DOI: 10.1159/000084229.

Mehta, Kapil; Fok, Jansina Y.; Mangala, Lingegowda S. (2006): Tissue transglutaminase: from biological glue to cell survival cues. In *Frontiers in bioscience : a journal and virtual library* 11, pp. 173–185. DOI: 10.2741/1789.

Mian, S.; El Alaoui, S.; Lawry, J.; Gentile, V.; Davies, P.J.A.; Griffin, M. (1995): The importance of the GTP-binding protein tissue transglutaminase in the regulation of cell cycle progression. In *FEBS Lett* 370 (1-2), pp. 27–31. DOI: 10.1016/0014-5793(95)00782-5.

Michael Love, Simon Anders, Wolfgang Huber (2017): DESeq2: Bioconductor.

Milakovic, Tamara; Tucholski, Janusz; McCoy, Eric; Johnson, Gail V. W. (2004): Intracellular localization and activity state of tissue transglutaminase differentially impacts cell death. In *The Journal of biological chemistry* 279 (10), pp. 8715–8722. DOI: 10.1074/jbc.M308479200.

Mishra, Suresh; Melino, Gerry; Murphy, Liam J. (2007): Transglutaminase 2 kinase activity facilitates protein kinase A-induced phosphorylation of retinoblastoma protein. In *The Journal of biological chemistry* 282 (25), pp. 18108–18115. DOI: 10.1074/jbc.M607413200.

Mishra, Suresh; Murphy, Liam J. (2004): Tissue transglutaminase has intrinsic kinase activity: identification of transglutaminase 2 as an insulin-like growth factor-binding protein-3 kinase. In *The Journal of biological chemistry* 279 (23), pp. 23863–23868. DOI: 10.1074/jbc.M311919200.

Mishra, Suresh; Murphy, Liam J. (2006): The p53 oncoprotein is a substrate for tissue transglutaminase kinase activity. In *Biochemical and biophysical research communications* 339 (2), pp. 726–730. DOI: 10.1016/j.bbrc.2005.11.071.

Mishra, Suresh; Saleh, Ali; Espino, Paula S.; Davie, James R.; Murphy, Liam J. (2006): Phosphorylation of histones by tissue transglutaminase. In *The Journal of biological chemistry* 281 (9), pp. 5532–5538. DOI: 10.1074/jbc.M506864200.

Morita, Yohei; Ema, Hideo; Nakauchi, Hiromitsu (2010): Heterogeneity and hierarchy within the most primitive hematopoietic stem cell compartment. In *Journal of Experimental Medicine* 207 (6), pp. 1173–1182. DOI: 10.1084/jem.20091318.

Morrison, Sean J.; Weissman, Irving L. (1994): The long-term repopulating subset of hematopoietic stem cells is deterministic and isolatable by phenotype. In *Immunity* 1 (8), pp. 661–673. DOI: 10.1016/1074-7613(94)90037-X.

Muller-Sieburg, Christa E.; Cho, Rebecca H.; Karlsson, Lars; Huang, Jing-F; Sieburg, Hans B. (2004): Myeloid-biased hematopoietic stem cells have extensive self-renewal capacity but generate diminished lymphoid progeny with impaired IL-7 responsiveness. In *Blood* 103 (11), pp. 4111–4118. DOI: 10.1182/blood-2003-10-3448.

Muller-Sieburg, Christa E.; Whitlock, Cheryl A.; Weissman, Irving L. (1986): Isolation of two early B lymphocyte progenitors from mouse marrow: A committed Pre-Pre-B cell and a clonogenic Thy-1lo hematopoietic stem cell. In *Cell* 44 (4), pp. 653–662. DOI: 10.1016/0092-8674(86)90274-6.

Müller-Sieburg, Christa E.; Cho, Rebecca H.; Thoman, Marilyn; Adkins, Becky; Sieburg, Hans B. (2002): Deterministic regulation of hematopoietic stem cell self-renewal and differentiation. In *Blood* 100 (4), pp. 1302–1309.

Murthy, S. N. P.; Iismaa, S.; Begg, G.; Freymann, D. M.; Graham, R. M.; Lorand, L. (2002): Conserved tryptophan in the core domain of transglutaminase is essential for catalytic activity. In *Proceedings of the National Academy of Sciences of the United States of America* 99 (5), pp. 2738–2742. DOI: 10.1073/pnas.052715799.

Nadalutti, C.; Viiri, K. M.; Kaukinen, K.; Mäki, M.; Lindfors, K. (2011): Extracellular transglutaminase 2 has a role in cell adhesion, whereas intracellular transglutaminase 2 is involved in regulation of endothelial cell proliferation and apoptosis. In *Cell proliferation* 44 (1), pp. 49–58. DOI: 10.1111/j.1365-2184.2010.00716.x.

Nakorn, Thanyaphong Na; Miyamoto, Toshihiro; Weissman, Irving L. (2003): Characterization of mouse clonogenic megakaryocyte progenitors. In *Proceedings of the National Academy of Sciences* 100 (1), pp. 205–210. DOI: 10.1073/pnas.262655099.

Nanda, N.; Iismaa, S. E.; Owens, W. A.; Husain, A.; Mackay, F.; Graham, R. M. (2001): Targeted inactivation of Gh/tissue transglutaminase II. In *The Journal of biological chemistry* 276 (23), pp. 20673–20678. DOI: 10.1074/jbc.M010846200.

Ng, Ashley P.; Alexander, Warren S. (2017): Haematopoietic stem cells: past, present and future. In *Cell death discovery* 3, p. 17002. DOI: 10.1038/cddiscovery.2017.2.

Nurminskaya, Maria; Kaartinen, Mari T. (2006): Transglutaminases in mineralized tissues. In *Frontiers in bioscience : a journal and virtual library* 11, pp. 1591–1606. DOI: 10.2741/1907.

Nurminskaya, Maria V.; Belkin, Alexey M. (2012): Cellular functions of tissue transglutaminase. In *International review of cell and molecular biology* 294, pp. 1–97. DOI: 10.1016/B978-0-12-394305-7.00001-X.

Odii, Benedict Onyekachi; Coussons, Peter (2014): Biological functionalities of transglutaminase 2 and the possibility of its compensation by other members of the transglutaminase family. In *TheScientificWorldJournal* 2014, p. 714561. DOI: 10.1155/2014/714561.

Oliverio, S.; Beltran, J. S. O.; Occhigrossi, L.; Bordoni, V.; Agrati, C.; D'Eletto, M. et al. (2020): Transglutaminase Type 2 is Involved in the Hematopoietic Stem Cells Homeostasis. In *Biochemistry. Biokhimiia* 85 (10), pp. 1159–1168. DOI: 10.1134/S0006297920100041.

Oostendorp, Robert A. J.; Gilfillan, Siv; Parmar, Amanda; Schiemann, Matthias; Marz, Stefanie; Niemeyer, Markus et al. (2008): Oncostatin M-mediated regulation of KIT-ligand-induced extracellular signal-regulated kinase signaling maintains hematopoietic repopulating activity of Lin-CD34+CD133+ cord blood cells. In *Stem cells (Dayton, Ohio)* 26 (8), pp. 2164–2172. DOI: 10.1634/stemcells.2007-1049.

Osawa, M.; Hanada, K.; Hamada, H.; Nakauchi, H. (1996): Long-term lymphohematopoietic reconstitution by a single CD34-low/negative hematopoietic stem cell. In *Science* 273 (5272), pp. 242–245. DOI: 10.1126/science.273.5272.242.

Pant, Vinod; Quintás-Cardama, Alfonso; Lozano, Guillermina (2012): The p53 pathway in hematopoiesis: lessons from mouse models, implications for humans. In *Blood* 120 (26), pp. 5118–5127. DOI: 10.1182/blood-2012-05-356014.

Park, Kang-Seo; Kim, Dae-Seok; Jeong, Kyung-Chae; Kim, Soo-Youl (2009): Increase in transglutaminase 2 expression is associated with NF-kappaB activation in breast cancer tissues. In *Frontiers in bioscience (Landmark edition)* 14 (5), pp. 1945–1951. DOI: 10.2741/3354.

Piacentini, Mauro; D'Eletto, Manuela; Falasca, Laura; Farrace, Maria Grazia; Rodolfo, Carlo (2011): Transglutaminase 2 at the crossroads between cell death and survival. In *Advances in enzymology and related areas of molecular biology* 78, pp. 197–246. DOI: 10.1002/9781118105771.ch5.

Pierce, Andrew; Whetton, Anthony D.; Meyer, Stefan; Ravandi-Kashani, Farhad; Borthakur, Gautam; Coombes, Kevin R. et al. (2013): Transglutaminase 2 expression in acute myeloid leukemia. Association with adhesion molecule expression and leukemic blast motility. In *Proteomics* 13 (14), pp. 2216–2224. DOI: 10.1002/pmic.201200471.

Pietras, Eric M.; Reynaud, Damien; Kang, Yoon-A; Carlin, Daniel; Calero-Nieto, Fernando J.; Leavitt, Andrew D. et al. (2015): Functionally Distinct Subsets of Lineage-Biased Multipotent Progenitors Control Blood Production in Normal and Regenerative Conditions. In *Cell stem cell* 17 (1), pp. 35–46. DOI: 10.1016/j.stem.2015.05.003.

Pina, Cristina; May, Gillian; Soneji, Shamit; Hong, Dengli; Enver, Tariq (2008): MLLT3 regulates early human erythroid and megakaryocytic cell fate. In *Cell stem cell* 2 (3), pp. 264–273. DOI: 10.1016/j.stem.2008.01.013.

Pinkas, Daniel M.; Strop, Pavel; Brunger, Axel T.; Khosla, Chaitan (2007): Transglutaminase 2 undergoes a large conformational change upon activation. In *PLoS biology* 5 (12), e327. DOI: 10.1371/journal.pbio.0050327.

Qian, Hong; Buza-Vidas, Natalija; Hyland, Craig D.; Jensen, Christina T.; Antonchuk, Jennifer; Månsson, Robert et al. (2007): Critical role of thrombopoietin in maintaining adult quiescent hematopoietic stem cells. In *Cell stem cell* 1 (6), pp. 671–684. DOI: 10.1016/j.stem.2007.10.008.

Qiu, Jiajing; Papatsenko, Dmitri; Niu, Xiaohong; Schaniel, Christoph; Moore, Kateri (2014): Divisional history and hematopoietic stem cell function during homeostasis. In *Stem cell reports* 2 (4), pp. 473–490. DOI: 10.1016/j.stemcr.2014.01.016.

Quadros, Rolen M.; Miura, Hiromi; Harms, Donald W.; Akatsuka, Hisako; Sato, Takehito; Aida, Tomomi et al. (2017): Easi-CRISPR: a robust method for one-step generation of mice carrying conditional and insertion alleles using long ssDNA donors and CRISPR ribonucleoproteins. In *Genome biology* 18 (1), p. 92. DOI: 10.1186/s13059-017-1220-4.

Randall, T. D.; Weissman, I. L. (1997): Phenotypic and functional changes induced at the clonal level in hematopoietic stem cells after 5-fluorouracil treatment. In *Blood* 89 (10), pp. 3596–3606.

Rieger, Michael A.; Hoppe, Philipp S.; Smejkal, Benjamin M.; Eitelhuber, Andrea C.; Schroeder, Timm (2009): Hematopoietic cytokines can instruct lineage choice. In *Science* 325 (5937), pp. 217–218. DOI: 10.1126/science.1171461.

Rieger, Michael A.; Schroeder, Timm (2012): Hematopoiesis. In *Cold Spring Harbor Perspectives in Biology* 4 (12), a008250-a008250. DOI: 10.1101/cshperspect.a008250.

Ringnér, Markus (2008): What is principal component analysis? In *Nature biotechnology* 26 (3), pp. 303–304. DOI: 10.1038/nbt0308-303.

Ritter, S. J.; Davies, P. J. (1998): Identification of a transforming growth factor-beta1/bone morphogenetic protein 4 (TGF-beta1/BMP4) response element within the mouse tissue transglutaminase gene promoter. In *The Journal of biological chemistry* 273 (21), pp. 12798–12806. DOI: 10.1074/jbc.273.21.12798.

Rodriguez-Fraticelli, Alejo E.; Wolock, Samuel L.; Weinreb, Caleb S.; Panero, Riccardo; Patel, Sachin H.; Jankovic, Maja et al. (2018): Clonal analysis of lineage fate in native haematopoiesis. In *Nature* 553 (7687), pp. 212–216. DOI: 10.1038/nature25168.

Rybtsov, Stanislav; Sobiesiak, Malgorzata; Taoudi, Samir; Souilhol, Céline; Senserrich, Jordi; Liakhovitskaia, Anna et al. (2011): Hierarchical organization and early hematopoietic specification of the developing HSC lineage in the AGM region. In *Journal of Experimental Medicine* 208 (6), pp. 1305–1315. DOI: 10.1084/jem.20102419.

Sarkar, Nirmal K.; Clarke, Donald D.; Waelsch, Heinrich (1957): An enzymically catalyzed incorporation of amines into proteins. In *Biochimica et biophysica acta* 25, pp. 451–452. DOI: 10.1016/0006-3002(57)90512-7.

Saulnier, Nathalie; Guihard, Soizic; Holy, Xavier; Decembre, Elodie; Jurdic, Pierre; Clay, Denis et al. (2012): ERK1 regulates the hematopoietic stem cell niches. In *PloS one* 7 (1), e30788. DOI: 10.1371/journal.pone.0030788.

Schambach, A.; Bohne, J.; Baum, C.; Hermann, F. G.; Egerer, L.; Laer, D. von; Giroglou, T. (2006): Woodchuck hepatitis virus post-transcriptional regulatory element deleted from X protein and promoter sequences enhances retroviral vector titer and expression. In *Gene therapy* 13 (7), pp. 641–645. DOI: 10.1038/sj.gt.3302698.

Scheid M. P.; Triglia D. (1979): Further description of theLy-5 system. In *Immunogenetics* (9), pp. 423–433.

Schoedel, Kristina B.; Morcos, Mina N. F.; Zerjatke, Thomas; Roeder, Ingo; Grinenko, Tatyana; Voehringer, David et al. (2016): The bulk of the hematopoietic stem cell population is dispensable for murine steady-state and stress hematopoiesis. In *Blood* 128 (19), pp. 2285–2296. DOI: 10.1182/blood-2016-03-706010.

Seita, Jun; Sahoo, Debashis; Rossi, Derrick J.; Bhattacharya, Deepta; Serwold, Thomas; Inlay, Matthew A. et al. (2012): Gene Expression Commons: an open platform for absolute gene expression profiling. In *PloS one* 7 (7), e40321. DOI: 10.1371/journal.pone.0040321.

Shimazu, Tomoyuki; Iida, Ryuji; Zhang, Qingzhao; Welner, Robert S.; Medina, Kay L.; Alberola-Lla, José; Kincade, Paul W. (2012): CD86 is expressed on murine hematopoietic stem cells and denotes lymphopoietic potential. In *Blood* 119 (21), pp. 4889–4897. DOI: 10.1182/blood-2011-10-388736.

Shweke, Nasim; Boulos, Nada; Jouanneau, Chantal; Vandermeersch, Sophie; Melino, Gerry; Dussaule, Jean-Claude et al. (2008): Tissue transglutaminase contributes to interstitial renal fibrosis by favoring accumulation of

fibrillar collagen through TGF-beta activation and cell infiltration. In *The American Journal of Pathology* 173 (3), pp. 631–642. DOI: 10.2353/ajpath.2008.080025.

Sieburg, Hans B.; Cho, Rebecca H.; Dykstra, Brad; Uchida, Naoyuki; Eaves, Connie J.; Muller-Sieburg, Christa E. (2006): The hematopoietic stem compartment consists of a limited number of discrete stem cell subsets. In *Blood* 107 (6), pp. 2311–2316. DOI: 10.1182/blood-2005-07-2970.

Singh, Satyendra K.; Singh, Shweta; Gadomski, Stephen; Sun, Lei; Pfannenstein, Alexander; Magidson, Valentin et al. (2018): Id1 Ablation Protects Hematopoietic Stem Cells from Stress-Induced Exhaustion and Aging. In *Cell stem cell* 23 (2), 252-265.e8. DOI: 10.1016/j.stem.2018.06.001.

Singh, Shweta; Jakubison, Brad; Keller, Jonathan R. (2020): Protection of hematopoietic stem cells from stress-induced exhaustion and aging. In *Current opinion in hematology* 27 (4), pp. 225–231. DOI: 10.1097/MOH.0000000000000586.

Small, K.; Feng, J. F.; Lorenz, J.; Donnelly, E. T.; Yu, A.; Im, M. J. et al. (1999): Cardiac specific overexpression of transglutaminase II (G(h)) results in a unique hypertrophy phenotype independent of phospholipase C activation. In *The Journal of biological chemistry* 274 (30), pp. 21291–21296. DOI: 10.1074/jbc.274.30.21291.

Sommerkamp, Pia; Renders, Simon; Ladel, Luisa; Hotz-Wagenblatt, Agnes; Schönberger, Katharina; Zeisberger, Petra et al. (2019): The long non-coding RNA Meg3 is dispensable for hematopoietic stem cells. In *Scientific reports* 9 (1), p. 2110. DOI: 10.1038/s41598-019-38605-8.

Sommerkamp, Pia; Romero-Mulero, Mari Carmen; Narr, Andreas; Ladel, Luisa; Hustin, Lucie; Schönberger, Katharina et al. (2021): Mouse multipotent progenitor 5 cells are located at the interphase between hematopoietic stem and progenitor cells. In *Blood* 137 (23), pp. 3218–3224. DOI: 10.1182/blood.2020007876.

Song, Heesang; Chang, Woochul; Lim, Soyeon; Seo, Hye-Sun; Shim, Chi Young; Park, Sungha et al. (2007): Tissue transglutaminase is essential for integrin-mediated survival of bone marrow-derived mesenchymal stem cells. In *Stem cells (Dayton, Ohio)* 25 (6), pp. 1431–1438. DOI: 10.1634/stemcells.2006-0467.

Spangrude, G. J.; Heimfeld, S.; Weissman, I. L. (1988a): Purification and characterization of mouse hematopoietic stem cells. In *Science* 241 (4861), pp. 58–62. DOI: 10.1126/science.2898810.

Spangrude, G. J.; Muller-Sieburg, C. E.; Heimfeld, S.; Weissman, I. L. (1988b): Two rare populations of mouse Thy-1lo bone marrow cells repopulate the thymus. In *Journal of Experimental Medicine* 167 (5), pp. 1671–1683. DOI: 10.1084/jem.167.5.1671.

Stamnaes, Jorunn; Pinkas, Daniel M.; Fleckenstein, Burkhard; Khosla, Chaitan; Sollid, Ludvig M. (2010): Redox regulation of transglutaminase 2 activity. In *The Journal of biological chemistry* 285 (33), pp. 25402–25409. DOI: 10.1074/jbc.M109.097162.

Stoeckius, Marlon; Hafemeister, Christoph; Stephenson, William; Houck-Loomis, Brian; Chattopadhyay, Pratip K.; Swerdlow, Harold et al. (2017): Simultaneous epitope and transcriptome measurement in single cells. In *Nat Methods* 14 (9), pp. 865–868. DOI: 10.1038/nmeth.4380.

Tatsukawa, H.; Furutani, Y.; Hitomi, K.; Kojima, S. (2016): Transglutaminase 2 has opposing roles in the regulation of cellular functions as well as cell growth and death. In *Cell death & disease* 7 (6), e2244. DOI: 10.1038/cddis.2016.150.

Tatsukawa, Hideki; Fukaya, Yayoi; Frampton, Gordon; Martinez-Fuentes, Antonio; Suzuki, Kenji; Kuo, Ting-Fang et al. (2009): Role of transglutaminase 2 in liver injury via cross-linking and silencing of transcription factor Sp1. In *Gastroenterology* 136 (5), 1783-95.e10. DOI: 10.1053/j.gastro.2009.01.007.

Tatsukawa, Hideki; Hitomi, Kiyotaka (2021): Role of Transglutaminase 2 in Cell Death, Survival, and Fibrosis. In *Cells* 10 (7). DOI: 10.3390/cells10071842.

TeKippe, Michael; Harrison, David E.; Chen, Jichun (2003): Expansion of hematopoietic stem cell phenotype and activity in Trp53-null mice. In *Experimental hematology* 31 (6), pp. 521–527. DOI: 10.1016/s0301-472x(03)00072-9.

Thalheimer, Frederic B.; Wingert, Susanne; Giacomo, Pangrazio de; Haetscher, Nadine; Rehage, Maike; Brill, Boris et al. (2014): Cytokine-regulated GADD45G induces differentiation and lineage selection in hematopoietic stem cells. In *Stem cell reports* 3 (1), pp. 34–43. DOI: 10.1016/j.stemcr.2014.05.010.

Thomas, Kirk R.; Capecchi, Mario R. (1987): Site-directed mutagenesis by gene targeting in mouse embryo-derived stem cells. In *Cell* 51 (3), pp. 503–512. DOI: 10.1016/0092-8674(87)90646-5.

Tong, Louis; Png, Evelyn; Aihua, Hou; Yong, Siew Sian; Yeo, Hui Ling; Riau, Andri et al. (2013): Molecular mechanism of transglutaminase-2 in corneal epithelial migration and adhesion. In *Biochimica et biophysica acta* 1833 (6), pp. 1304–1315. DOI: 10.1016/j.bbamcr.2013.02.030.

Truett, G. E.; Heeger, P.; Mynatt, R. L.; Truett, A. A.; Walker, J. A.; Warman, M. L. (2000): Preparation of PCR-quality mouse genomic DNA with hot sodium hydroxide and tris (HotSHOT). In *BioTechniques* 29 (1), 52, 54. DOI: 10.2144/00291bm09.

Tsai, F. Y.; Orkin, S. H. (1997): Transcription factor GATA-2 is required for proliferation/survival of early hematopoietic cells and mast cell formation, but not for erythroid and myeloid terminal differentiation. In *Blood* 89 (10), pp. 3636–3643.

Tucholski, Janusz; Johnson, Gail V. W. (2002): Tissue transglutaminase differentially modulates apoptosis in a stimuli-dependent manner. In *Journal of neurochemistry* 81 (4), pp. 780–791. DOI: 10.1046/j.1471-4159.2002.00859.x.

Tucholski, Janusz; Roth, Kevin A.; Johnson, Gail V. W. (2006): Tissue transglutaminase overexpression in the brain potentiates calcium-induced hippocampal damage. In *Journal of neurochemistry* 97 (2), pp. 582–594. DOI: 10.1111/j.1471-4159.2006.03780.x.

Tyanova, Stefka; Temu, Tikira; Sinitcyn, Pavel; Carlson, Arthur; Hein, Marco Y.; Geiger, Tamar et al. (2016): The Perseus computational platform for comprehensive analysis of (prote)omics data. In *Nature methods* 13 (9), pp. 731–740. DOI: 10.1038/nmeth.3901.

Uchida, N.; Weissman, I. L. (1992): Searching for hematopoietic stem cells: evidence that Thy-1.1lo Lin- Sca-1+ cells are the only stem cells in C57BL/Ka-Thy-1.1 bone marrow. In *Journal of Experimental Medicine* 175 (1), pp. 175–184. DOI: 10.1084/jem.175.1.175.

Uchida, Naoyuki; Dykstra, Brad; Lyons, Kristin J.; Leung, Frank Y. K.; Eaves, Connie J. (2003): Different in vivo repopulating activities of purified hematopoietic stem cells before and after being stimulated to divide in vitro with the same kinetics. In *Experimental hematology* 31 (12), pp. 1338–1347. DOI: 10.1016/j.exphem.2003.09.001.

Umemoto, Terumasa; Hashimoto, Michihiro; Matsumura, Takayoshi; Nakamura-Ishizu, Ayako; Suda, Toshio (2018): Ca2+-mitochondria axis drives cell division in hematopoietic stem cells. In *The Journal of experimental medicine* 215 (8), pp. 2097–2113. DOI: 10.1084/jem.20180421.

Venezia, Teresa A.; Merchant, Akil A.; Ramos, Carlos A.; Whitehouse, Nathan L.; Young, Andrew S.; Shaw, Chad A.; Goodell, Margaret A. (2004): Molecular signatures of proliferation and quiescence in hematopoietic stem cells. In *PLoS biology* 2 (10), e301. DOI: 10.1371/journal.pbio.0020301.

Verma, Amit; Guha, Sushovan; Wang, Huamin; Fok, Jansina Y.; Koul, Dimpy; Abbruzzese, James; Mehta, Kapil (2008): Tissue transglutaminase regulates focal adhesion kinase/AKT activation by modulating PTEN expression in pancreatic cancer cells. In *Clinical cancer research : an official journal of the American Association for Cancer Research* 14 (7), pp. 1997–2005. DOI: 10.1158/1078-0432.CCR-07-1533.

Verma, Amit; Mehta, Kapil (2007): Tissue transglutaminase-mediated chemoresistance in cancer cells. In *Drug resistance updates : reviews and commentaries in antimicrobial and anticancer chemotherapy* 10 (4-5), pp. 144–151. DOI: 10.1016/j.drup.2007.06.002.

Wada, Teiji; Penninger, Josef M. (2004): Mitogen-activated protein kinases in apoptosis regulation. In *Oncogene* 23 (16), pp. 2838–2849. DOI: 10.1038/sj.onc.1207556.

Wang, Bin; Guo, Hanfei; Yu, Hongquan; Chen, Yong; Xu, Haiyang; Zhao, Gang (2021): The Role of the Transcription Factor EGR1 in Cancer. In *Frontiers in oncology* 11, p. 642547. DOI: 10.3389/fonc.2021.642547.

Weissman, Irving L.; Shizuru, Judith A. (2008): The origins of the identification and isolation of hematopoietic stem cells, and their capability to induce donor-specific transplantation tolerance and treat autoimmune diseases. In *Blood* 112 (9), pp. 3543–3553. DOI: 10.1182/blood-2008-08-078220.

Wilson, Anne; Laurenti, Elisa; Oser, Gabriela; van der Wath, Richard C.; Blanco-Bose, William; Jaworski, Maike et al. (2008): Hematopoietic stem cells reversibly switch from dormancy to self-renewal during homeostasis and repair. In *Cell* 135 (6), pp. 1118–1129. DOI: 10.1016/j.cell.2008.10.048.

Wilson, Anne; Murphy, Mark J.; Oskarsson, Thordur; Kaloulis, Konstantinos; Bettess, Michael D.; Oser, Gabriela M. et al. (2004): c-Myc controls the balance between hematopoietic stem cell self-renewal and differentiation. In *Genes & development* 18 (22), pp. 2747–2763. DOI: 10.1101/gad.313104.

Wu, A. M.; TILL, J. E.; Siminovitch, L.; MCCULLOCH, E. A. (1968): Cytological evidence for a relationship between normal hemotopoietic colony-forming cells and cells of the lymphoid system. In *Journal of Experimental Medicine* 127 (3), pp. 455–464. DOI: 10.1084/jem.127.3.455.

Yamamoto, Ryo; Morita, Yohei; Ooehara, Jun; Hamanaka, Sanae; Onodera, Masafumi; Rudolph, Karl Lenhard et al. (2013): Clonal analysis unveils self-renewing lineage-restricted progenitors generated directly from hematopoietic stem cells. In *Cell* 154 (5), pp. 1112–1126. DOI: 10.1016/j.cell.2013.08.007.

Yamashita, Masayuki; Nitta, Eriko; Suda, Toshio (2016): Regulation of hematopoietic stem cell integrity through p53 and its related factors. In *Annals of the New York Academy of Sciences* 1370 (1), pp. 45–54. DOI: 10.1111/nyas.12986.

Yee, Jiing-Kuan; Friedmann, Theodore; Burns, Jane C. (1994): Chapter 5 Generation of High-Titer Pseudotyped Retroviral Vectors with Very Broad Host Range. In Michael G. Roth (Ed.): Protein expression in animal cells, vol. 43. San Diego, London: Academic Press (Methods in cell biology 0091-679X v.43), pp. 99–112.

Yoshihara, Hiroki; Arai, Fumio; Hosokawa, Kentaro; Hagiwara, Tetsuya; Takubo, Keiyo; Nakamura, Yuka et al. (2007): Thrombopoietin/MPL signaling regulates hematopoietic stem cell quiescence and interaction with the osteoblastic niche. In *Cell stem cell* 1 (6), pp. 685–697. DOI: 10.1016/j.stem.2007.10.020.

Yu, Weijia; Schmachtel, Tessa; Fawaz, Malak; Rieger, Michael A. (2022): Isolation of murine bone marrow hematopoietic stem and progenitor cell populations via flow cytometry. In : Elsevier (Methods in Cell Biology).

Yue, Jicheng; López, José M. (2020): Understanding MAPK Signaling Pathways in Apoptosis. In *International journal of molecular sciences* 21 (7). DOI: 10.3390/ijms21072346.

References

Zhang, W.; Geiman, D. E.; Shields, J. M.; Dang, D. T.; Mahatan, C. S.; Kaestner, K. H. et al. (2000): The gut-enriched Kruppel-like factor (Kruppel-like factor 4) mediates the transactivating effect of p53 on the p21WAF1/Cip1 promoter. In *The Journal of biological chemistry* 275 (24), pp. 18391–18398. DOI: 10.1074/jbc.C000062200.

Zhou, Yingyao; Zhou, Bin; Pache, Lars; Chang, Max; Khodabakhshi, Alireza Hadj; Tanaseichuk, Olga et al. (2019): Metascape provides a biologist-oriented resource for the analysis of systems-level datasets. In *Nature communications* 10 (1), p. 1523. DOI: 10.1038/s41467-019-09234-6.

6. Appendix

6.1. Vector maps

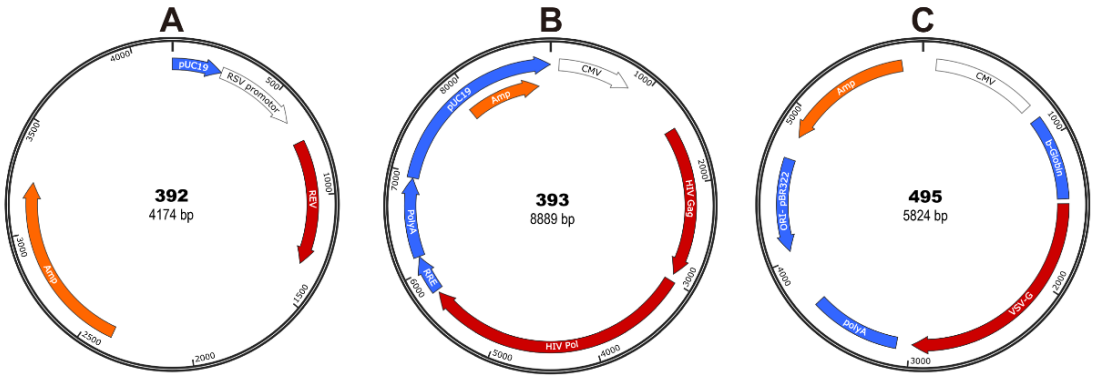

Figure 42 Packaging plasmids for lentiviral production

(A) Expression plasmid pRSV.HIV-REV for lentiviral reverse transcriptase (REV) of HIV-1. **(B)** Expression plasmid pMDLg.HIVGag-Pol.pRRE for structural genes (gag/pol) of HIV-1 for lentiviral particle assembly. **(C)** Expression plasmid pMD2.G.VSV-G for VSV-G (env) for pseudo typing of lentiviral particles.

RSV: Rous sarcoma virus promoter; CMV: cytomegalo virus promoter; Amp: ampicillin resistance gene; HIV: human immunodeficiency virus; RRE: Rev response element; VSV-G: glycoprotein G of VSV.

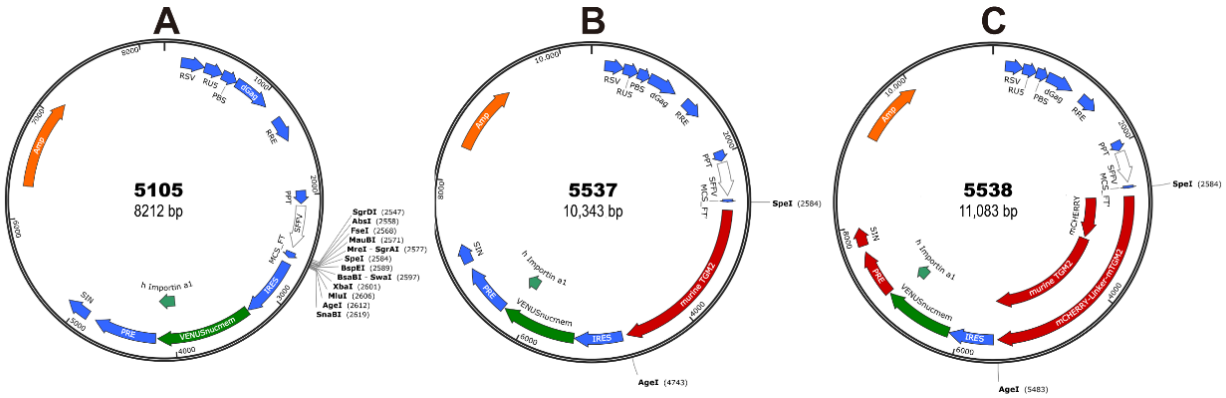

Figure 43 Lentiviral expression plasmids.

(A) VENUS lentiviral control expression vector used for control transduction and as basis for other lentiviral expression vectors. **(B)** VENUS lentiviral expressing vector for murine Tgm2 expression. **(C)** VENUS lentiviral expressing vector for mCherry-linker-murine Tgm2 expression.

RSV:Rous sarcoma virus enhancer; PBS: Primer binding site ; Gag: Group specific antigen; UTR: Untranslated region; RRE: Rev response element; PPT: Polypurine tract; SFFV: Spleen focus-forming virus, Promoter; MCS: Multiple cloning site; IRES: Internal ribosome binding site; VENUS: green fluorescent protein; PRE: posttranscriptional regulatory element; SIN: Self inactivating UTR; Amp: ampicillin resistance gene.

6.2. Differential expressed genes lists

Table 14 mRNA expression data of DEGs between Tgm2-KO LT-HSCs versus Tgm2-WT LT-HSCs

Ensembl gene	baseMean	baseMean HSC-KO	baseMean HSC-WT	log2FoldChange HSC-KO/HSC-WT	pvalue	padj
Slc38a5	21	0	41	-5,41	0,00	0,00
Rhd	28	0	55	-5,32	0,00	0,00
Gypa	13	0	26	-4,75	0,00	0,00
Upk1b	12	0	25	-4,68	0,00	0,00
Syce1	12	0	24	-4,66	0,00	0,00
Prss50	12	0	24	-4,66	0,00	0,01
Spta1	10	0	20	-4,39	0,00	0,01
Cmya5	16	1	31	-4,35	0,00	0,00
Capn11	9	0	19	-4,31	0,00	0,02
Kcnj5	9	0	18	-4,22	0,00	0,01
Il17rb	8	0	15	-4,01	0,00	0,01
Car1	290	39	541	-3,75	0,00	0,00
Gbp11	124	29	220	-2,88	0,00	0,00
Klf1	68	20	117	-2,52	0,00	0,01
Tgm2	552	191	913	-2,25	0,00	0,00
Thbs1	518	196	839	-2,09	0,00	0,00
Pfn2	41	17	66	-1,89	0,00	0,01
Olfml3	38	17	58	-1,70	0,00	0,01
Slc13a2	68	32	104	-1,65	0,00	0,01
Creb5	104	55	154	-1,46	0,00	0,04
Hist2h4	179	106	253	-1,25	0,00	0,00
Aldh1b1	193	117	269	-1,19	0,00	0,01
Hist2h2be	241	148	333	-1,16	0,00	0,01
Micu1	632	394	869	-1,14	0,00	0,00
Elp6	197	134	260	-0,95	0,00	0,04
H2-Eb1	691	483	899	-0,90	0,00	0,00
Myl10	1961	1380	2542	-0,88	0,00	0,00
Zswim1	372	264	480	-0,86	0,00	0,01
Dok3	246	176	317	-0,85	0,00	0,04
Nfatc2	608	437	778	-0,83	0,00	0,00
Klf10	2429	1754	3104	-0,82	0,00	0,00
1700023H06Rik	282	204	359	-0,81	0,00	0,04
Usp9x	596	435	756	-0,79	0,00	0,00
9030619P08Rik	626	457	794	-0,79	0,00	0,00
Rasa4	530	389	670	-0,78	0,00	0,00
Cirbp	2690	1985	3395	-0,77	0,00	0,00
Chpf2	980	732	1229	-0,75	0,00	0,01
Fasn	1732	1320	2144	-0,70	0,00	0,00
Hist1h1e	928	712	1143	-0,68	0,00	0,00
Cndp2	794	618	970	-0,65	0,00	0,02
Abcc1	1311	1023	1599	-0,64	0,00	0,01

Slc35b1	425	333	517	-0,63	0,00	0,01
Cd74	2681	2105	3257	-0,63	0,00	0,00
Tk2	904	713	1096	-0,62	0,00	0,01
Ell	758	608	908	-0,58	0,00	0,01
Tns1	773	620	926	-0,58	0,00	0,00
Txnip	9946	7997	11896	-0,57	0,00	0,00
Mkl1	846	683	1008	-0,56	0,00	0,03
Nol6	1326	1075	1578	-0,55	0,00	0,02
Tut1	971	793	1150	-0,53	0,00	0,00
Pcp4l1	1468	1209	1726	-0,51	0,00	0,00
Nhp2	1703	1424	1983	-0,48	0,00	0,00
Slc39a11	1740	1461	2019	-0,47	0,00	0,03
Cux1	3913	3292	4535	-0,46	0,00	0,00
Mat2a	5092	4289	5895	-0,46	0,00	0,00
Ipo4	1536	1296	1777	-0,46	0,00	0,00
Flii	2387	2014	2760	-0,45	0,00	0,01
Fam212a	2118	1806	2429	-0,43	0,00	0,00
Tapbpl	1037	887	1187	-0,42	0,00	0,03
Vars	6620	5667	7573	-0,42	0,00	0,03
Tap2	2149	1843	2456	-0,41	0,00	0,00
Ddx58	1088	939	1238	-0,40	0,00	0,05
Surf4	3719	3236	4201	-0,38	0,00	0,03
Srebf2	6095	5383	6806	-0,34	0,00	0,01
Mmrn1	6206	5522	6890	-0,32	0,00	0,04
Ncl	10400	9271	11529	-0,31	0,00	0,00
Bin2	7434	6744	8123	-0,27	0,00	0,01
Gimap6	8383	9195	7571	0,28	0,00	0,01
Myb	4308	4749	3867	0,30	0,00	0,01
Zcchc6	2080	2314	1845	0,33	0,00	0,01
Ddx5	10521	11739	9303	0,34	0,00	0,00
Eif4a2	3524	3938	3110	0,34	0,00	0,01
Mycn	5102	5718	4486	0,35	0,00	0,03
Vim	3474	3896	3052	0,35	0,00	0,01
Gata2	7811	8785	6836	0,36	0,00	0,05
Apoe	12037	13612	10462	0,38	0,00	0,01
Tsc22d3	7410	8384	6436	0,38	0,00	0,00
D8Ertd738e	1546	1757	1335	0,40	0,00	0,00
Uhrf2	1491	1695	1286	0,40	0,00	0,05
Dnaja1	2365	2721	2009	0,44	0,00	0,00
Eif1	5545	6400	4690	0,45	0,00	0,00
S100a10	2360	2735	1985	0,46	0,00	0,00
Gm8995	1965	2282	1649	0,47	0,00	0,01
Ddah2	1182	1384	980	0,50	0,00	0,00
Gpr171	7180	8420	5940	0,50	0,00	0,00
Kti12	750	880	619	0,51	0,00	0,02
S1pr1	1031	1213	848	0,52	0,00	0,03

Tsc22d1	19560	23049	16072	0,52	0,00	0,00
Taf7	1097	1297	896	0,53	0,00	0,04
Hspa8	12783	15140	10426	0,54	0,00	0,00
Ptp4a1	697	829	564	0,56	0,00	0,01
Mgst1	739	882	597	0,56	0,00	0,04
Parp6	597	712	482	0,56	0,00	0,02
Tgoln1	2396	2864	1927	0,57	0,00	0,00
Swt1	736	883	589	0,58	0,00	0,04
Fcho2	1262	1516	1009	0,59	0,00	0,00
Topors	1927	2317	1538	0,59	0,00	0,01
Elf1	4520	5434	3607	0,59	0,00	0,00
Zfp942	437	526	348	0,60	0,00	0,04
Ptger4	814	984	644	0,61	0,00	0,05
Dnajb9	1656	2007	1305	0,62	0,00	0,00
Marcksl1	1753	2129	1376	0,63	0,00	0,00
Clk1	3170	3852	2489	0,63	0,00	0,00
Gm37352	721	877	566	0,63	0,00	0,00
Gem	1120	1362	877	0,63	0,00	0,01
Hspa5	17210	20984	13437	0,64	0,00	0,00
Hoxa9	1900	2318	1482	0,64	0,00	0,00
H3f3b	38006	46409	29602	0,65	0,00	0,00
Cdk11b	1788	2185	1391	0,65	0,00	0,00
Ccnl1	2807	3431	2182	0,65	0,00	0,00
Sertad3	580	710	449	0,66	0,00	0,00
Pkig	548	671	425	0,66	0,00	0,01
Dnajb4	776	951	600	0,66	0,00	0,03
Cfap20	1230	1512	948	0,67	0,00	0,00
Socs2	858	1057	658	0,68	0,00	0,00
Ctla2a	5824	7191	4458	0,69	0,00	0,00
Ier3	1721	2129	1313	0,70	0,00	0,00
Snord78	396	490	301	0,70	0,00	0,01
Ccl4	2665	3302	2028	0,70	0,00	0,01
Slc4a2	354	440	267	0,72	0,00	0,02
Tmem39a	405	507	304	0,73	0,00	0,01
Csrnp1	1068	1338	799	0,74	0,00	0,01
Dusp6	2366	2972	1761	0,75	0,00	0,00
Aifm2	285	359	212	0,76	0,00	0,04
Fbxo30	613	771	455	0,76	0,00	0,01
Atf4	2543	3199	1888	0,76	0,00	0,00
Jun	79184	99659	58709	0,76	0,00	0,00
C030037D09Rik	459	579	338	0,77	0,00	0,01
Junb	27376	34762	19990	0,80	0,00	0,00
Ier2	40872	51954	29790	0,80	0,00	0,00
Rpl22l1	1340	1704	976	0,80	0,00	0,00
Nfkbid	723	923	522	0,82	0,00	0,00
Rgs1	9928	12691	7165	0,82	0,00	0,00

Hist1h1c	4861	6221	3502	0,83	0,00	0,00
Dynll1	1378	1769	986	0,84	0,00	0,00
Pdgfd	351	452	250	0,86	0,00	0,01
Ubc	10543	13613	7473	0,87	0,00	0,00
Tuba1a	481	623	339	0,88	0,00	0,00
Ier5	1126	1468	784	0,90	0,00	0,00
Socs3	1147	1497	797	0,91	0,00	0,00
Cuedc1	376	492	260	0,92	0,00	0,03
Amigo2	582	765	399	0,94	0,00	0,00
Dyrk3	911	1201	621	0,95	0,00	0,00
Btg1	2586	3431	1741	0,98	0,00	0,00
Rhob	3106	4151	2061	1,01	0,00	0,00
Egr1	43550	58486	28615	1,03	0,00	0,00
Ppp1r15a	22538	30321	14754	1,04	0,00	0,00
Gm23212	190	256	124	1,04	0,00	0,00
Cdkn1a	384	521	247	1,07	0,00	0,00
Sgk1	771	1051	490	1,10	0,00	0,00
Jade3	268	366	170	1,10	0,00	0,02
Zfp36	29885	40902	18868	1,12	0,00	0,00
Sertad1	1156	1586	726	1,13	0,00	0,00
Zfp36l1	256	353	158	1,15	0,00	0,00
Dusp1	54398	75592	33203	1,19	0,00	0,00
Tiparp	893	1241	544	1,19	0,00	0,00
Sik1	616	859	373	1,20	0,00	0,00
Gm26532	118	165	71	1,21	0,00	0,01
Tob1	472	664	279	1,25	0,00	0,00
Rgs2	2732	3849	1616	1,25	0,00	0,00
Arhgef10l	112	158	66	1,26	0,00	0,03
Arrdc3	1749	2500	998	1,32	0,00	0,00
Plk2	1354	1973	734	1,43	0,00	0,00
Fos	89431	130532	48330	1,43	0,00	0,00
Spry1	1166	1716	617	1,47	0,00	0,00
Dnajb1	6375	9394	3355	1,49	0,00	0,00
Btg2	11197	16557	5836	1,50	0,00	0,00
Lrp5	78	116	40	1,51	0,00	0,01
Hist1h2bc	810	1204	416	1,53	0,00	0,00
Plvap	287	428	145	1,55	0,00	0,03
Nr4a2	240	362	119	1,60	0,00	0,00
AA465934	216	331	101	1,70	0,00	0,00
Egr3	97	149	45	1,71	0,00	0,00
Ttc26	135	207	62	1,73	0,00	0,00
Serinc3	19217	29603	8830	1,75	0,00	0,00
Igfbp7	101	157	45	1,77	0,00	0,02
Nfkbiz	1493	2315	671	1,79	0,00	0,00
Sparc	229	358	100	1,83	0,00	0,00
Lrg1	341	536	145	1,88	0,00	0,01

Cd69	753	1186	321	1,88	0,00	0,00
Nr4a1	5960	9442	2478	1,93	0,00	0,00
Klf6	15426	24443	6409	1,93	0,00	0,00
Egr2	240	385	94	2,02	0,00	0,00
Dusp5	1524	2455	594	2,04	0,00	0,00
Wfdc2	198	320	76	2,05	0,00	0,00
Id1	282	458	106	2,10	0,00	0,00
Fosb	1182	1956	408	2,26	0,00	0,00
Klf4	617	1028	205	2,32	0,00	0,00
Klf2	7357	12762	1952	2,71	0,00	0,00
Ptgs2	108	193	23	3,00	0,00	0,00
Gm37718	32	58	6	3,09	0,00	0,04
Atf3	453	818	88	3,21	0,00	0,01
Raph1	43	78	7	3,23	0,00	0,00
Hspa1a	114	209	19	3,40	0,00	0,00
Ptprf	33	62	5	3,42	0,00	0,01
Adamts5	69	128	11	3,43	0,00	0,00
CT009757.6	22	42	2	3,65	0,00	0,03
Stox2	8	16	0	3,76	0,00	0,02
Tmod2	16	32	1	4,08	0,00	0,00
Hspa1b	257	488	26	4,18	0,00	0,00
Cfd	9	18	0	4,27	0,00	0,02
Tmem26	17	33	0	4,54	0,00	0,03
Fbxo40	13	26	0	4,74	0,00	0,00

Table 15 mRNA expression data of DEGs between Tgm2-KO MPPs versus Tgm2-WT MPPs

Ensembl gene	baseMean	baseMean MPP-KO	baseMean MPP-WT	log2FoldChange MPP-KO/MPP-WT	pvalue	padj
Fyb2	83	1	149	-6.32	0.00	0.00
Clec7a	15	0	26	-4.38	0.00	0.01
Arhgap24	9	0	17	-4.14	0.00	0.02
Gm5086	9	0	15	-4.04	0.00	0.01
Cacna1b	8	0	14	-3.95	0.00	0.01
Ly6k	25	2	44	-3.89	0.00	0.00
Ccr5	20	2	34	-3.68	0.00	0.00
Entpd3	30	3	52	-3.63	0.00	0.01
Gm45138	6	0	11	-3.55	0.00	0.01
Slc1a3	6	0	10	-3.52	0.00	0.03
Ddx43	9	0	15	-3.51	0.00	0.04
Wnk4	14	1	24	-3.34	0.00	0.01
Kbtbd12	25	4	41	-2.98	0.00	0.02
Slc13a2	53	13	85	-2.65	0.00	0.02
Gm5148	16	3	25	-2.60	0.00	0.02
Gbp11	89	23	142	-2.58	0.00	0.00
Porcn	42	13	65	-2.29	0.00	0.04

Tgm2	126	41	193	-2.21	0.00	0.00
S100a9	143	50	217	-2.08	0.00	0.01
Glrp1	34	13	51	-1.90	0.00	0.01
Amz1	43	17	64	-1.89	0.00	0.04
Gbp4	172	69	254	-1.86	0.00	0.00
Creb5	58	23	87	-1.86	0.00	0.01
Thbs1	835	356	1219	-1.77	0.00	0.00
8430419K02Rik	58	26	83	-1.64	0.00	0.04
Gm9958	53	25	76	-1.56	0.00	0.04
AL603745.2	43	21	60	-1.50	0.00	0.02
Gbp6	150	76	209	-1.45	0.00	0.00
Cyp2r1	103	54	143	-1.38	0.00	0.04
AA467197	102	56	138	-1.30	0.00	0.01
Rab34	70	39	94	-1.26	0.00	0.01
Gdf3	257	146	346	-1.24	0.00	0.03
Zfp532	151	86	203	-1.23	0.00	0.02
Slc29a2	227	131	303	-1.20	0.00	0.01
Wfdc17	2861	1709	3782	-1.15	0.00	0.00
Trpc6	452	282	587	-1.06	0.00	0.00
Slc25a33	187	118	242	-1.03	0.00	0.01
Bpifc	408	260	527	-1.01	0.00	0.00
Myl10	1869	1202	2403	-1.00	0.00	0.00
Pgr	263	171	337	-0.98	0.00	0.00
BC002059	173	113	221	-0.96	0.00	0.02
Smim10l2a	166	110	211	-0.93	0.00	0.02
Pecr	527	354	666	-0.91	0.00	0.00
Gjb3	226	153	284	-0.89	0.00	0.00
Trmt6	953	652	1194	-0.87	0.00	0.00
Spint1	213	146	266	-0.86	0.00	0.02
Gm43305	248	171	310	-0.85	0.00	0.00
9030619P08Rik	1647	1206	1999	-0.73	0.00	0.00
Sepsecs	494	362	600	-0.73	0.00	0.02
Taf4b	450	330	546	-0.73	0.00	0.00
Slc35f2	639	473	772	-0.70	0.00	0.02
Cirbp	2208	1670	2638	-0.66	0.00	0.00
Mettl22	417	315	498	-0.66	0.00	0.01
Hnrnpa0	505	386	601	-0.64	0.00	0.03
Tmem250-ps	1603	1226	1905	-0.64	0.00	0.02
Txnrd3	716	550	850	-0.63	0.00	0.01
Inafm2	909	698	1077	-0.63	0.00	0.00
Zfp512b	602	467	709	-0.60	0.00	0.05
Col16a1	602	468	709	-0.60	0.00	0.04
Rtp4	1355	1057	1594	-0.59	0.00	0.00
Mat2a	7630	5993	8940	-0.58	0.00	0.00
Fpgs	809	635	948	-0.58	0.00	0.01
Tnip3	1008	805	1170	-0.54	0.00	0.02

Pigt	1157	925	1343	-0.54	0.00	0.01
Abhd14b	232	185	269	-0.54	0.00	0.04
Zfand4	471	377	546	-0.53	0.00	0.05
Nme1	1831	1466	2122	-0.53	0.00	0.00
Golt1b	1454	1167	1683	-0.53	0.00	0.02
Muc13	4763	3827	5512	-0.53	0.00	0.00
Inip	1746	1409	2015	-0.52	0.00	0.01
Dfna5	978	792	1127	-0.51	0.00	0.03
Aacs	1286	1045	1478	-0.50	0.00	0.01
Uspl1	1123	919	1287	-0.49	0.00	0.00
Pcp4l1	1960	1609	2240	-0.48	0.00	0.00
mt-Rnr1	4774	3929	5450	-0.47	0.00	0.04
St6galnac4	2010	1659	2290	-0.46	0.00	0.00
Fam212a	1607	1333	1826	-0.45	0.00	0.00
Hmgb3	1235	1025	1403	-0.45	0.00	0.00
Ifitm1	6832	5680	7753	-0.45	0.00	0.03
Rhbdd2	1088	905	1234	-0.45	0.00	0.01
Micu1	903	751	1024	-0.45	0.00	0.04
Pomk	732	610	829	-0.44	0.00	0.01
Mettl21a	544	455	615	-0.44	0.00	0.04
Klf10	2021	1691	2285	-0.43	0.00	0.04
Ptrh2	1069	895	1209	-0.43	0.00	0.04
Rbm3	2737	2294	3092	-0.43	0.00	0.00
Gar1	801	672	904	-0.43	0.00	0.01
S100a6	411	345	464	-0.43	0.00	0.03
Ntpcr	1023	861	1152	-0.42	0.00	0.02
Akip1	825	697	927	-0.41	0.00	0.04
Bcap29	2263	1914	2543	-0.41	0.00	0.01
Uchl3	1055	892	1185	-0.41	0.00	0.04
Lax1	1315	1115	1475	-0.40	0.00	0.01
Slc25a5	12075	10241	13542	-0.40	0.00	0.01
Vamp8	4044	3431	4534	-0.40	0.00	0.04
Dtd1	1511	1284	1693	-0.40	0.00	0.03
Hnrnpr	2396	2038	2682	-0.40	0.00	0.01
Parl	1879	1606	2098	-0.38	0.00	0.01
Ldha	14480	12389	16153	-0.38	0.00	0.00
Tsr2	650	556	725	-0.38	0.00	0.03
Nhp2	3011	2577	3358	-0.38	0.00	0.04
Fbl	1477	1266	1646	-0.38	0.00	0.00
Arl2bp	1630	1400	1813	-0.37	0.00	0.04
Dtd2	633	544	704	-0.37	0.00	0.03
Msto1	1006	868	1116	-0.36	0.00	0.04
Ccnh	1953	1688	2166	-0.36	0.00	0.02
Smyd2	884	765	980	-0.36	0.00	0.05
Ncl	16497	14280	18271	-0.36	0.00	0.00
Mtap	2072	1797	2292	-0.35	0.00	0.01

Med1	1651	1432	1826	-0.35	0.00	0.05
Bex6	909	791	1004	-0.34	0.00	0.03
Ube2k	1347	1172	1486	-0.34	0.00	0.04
Mfsd1	1830	1593	2019	-0.34	0.00	0.01
1110004F10Rik	3215	2800	3546	-0.34	0.00	0.01
Dkc1	4280	3748	4705	-0.33	0.00	0.02
Nop58	3409	2997	3738	-0.32	0.00	0.02
Cct8	9335	8207	10238	-0.32	0.00	0.02
Ash2l	2185	1923	2395	-0.32	0.00	0.05
Metap2	3834	3387	4192	-0.31	0.00	0.01
Stt3a	6397	5662	6985	-0.30	0.00	0.01
Nfu1	1433	1272	1562	-0.30	0.00	0.03
Sdha	8317	7385	9063	-0.30	0.00	0.00
Fxyd5	6738	5986	7341	-0.29	0.00	0.04
Sumo3	4270	3793	4651	-0.29	0.00	0.01
Slc25a1	2452	2179	2670	-0.29	0.00	0.01
Imp4	1989	1772	2163	-0.29	0.00	0.05
Srpk1	3430	3059	3728	-0.29	0.00	0.04
Mars	2325	2075	2525	-0.28	0.00	0.05
Psma7	5947	5316	6451	-0.28	0.00	0.03
Nop56	6673	5968	7236	-0.28	0.00	0.02
Gosr2	3126	2809	3380	-0.27	0.00	0.03
Eprs	4737	4257	5121	-0.27	0.00	0.01
Rtcb	4264	3834	4608	-0.27	0.00	0.02
Parvg	5380	4842	5811	-0.26	0.00	0.05
Sf3a3	2997	2703	3232	-0.26	0.00	0.02
Gtpbp4	2483	2242	2676	-0.25	0.00	0.04
Cnbp	30982	28014	33356	-0.25	0.00	0.01
Eif5a	25465	23058	27390	-0.25	0.00	0.04
Cfl1	13889	12584	14933	-0.25	0.00	0.02
Rpa2	3439	3128	3687	-0.24	0.00	0.04
Cdca7	7700	7064	8209	-0.22	0.00	0.00
Napsa	3382	3113	3597	-0.21	0.00	0.05
Hnrnpk	20730	19426	21773	-0.16	0.00	0.03
Tapbp	5746	6276	5322	0.24	0.00	0.03
Rnf167	2231	2457	2051	0.26	0.00	0.03
Afap1l1	2976	3315	2704	0.29	0.00	0.03
Eif3f	2225	2483	2018	0.30	0.00	0.03
Mycbp2	1329	1486	1203	0.30	0.00	0.02
Vim	5468	6131	4938	0.31	0.00	0.00
Igfbp4	9599	10774	8658	0.32	0.00	0.00
Bnip2	1877	2109	1692	0.32	0.00	0.04
Hoxa9	2111	2401	1880	0.35	0.00	0.04
Pde4b	3636	4138	3234	0.36	0.00	0.01
Retreg2	2301	2648	2023	0.39	0.00	0.03
Snapc2	883	1017	776	0.39	0.00	0.05

Clk1	2753	3170	2418	0.39	0.00	0.00
Lrwd1	1353	1558	1188	0.39	0.00	0.02
Cpne3	1396	1613	1223	0.40	0.00	0.05
Clk4	1418	1639	1241	0.40	0.00	0.02
Dock8	2715	3154	2364	0.42	0.00	0.00
Pck2	2541	2957	2209	0.42	0.00	0.00
Gpr171	10226	11908	8881	0.42	0.00	0.00
Reep4	984	1146	854	0.42	0.00	0.00
Pecam1	1668	1942	1448	0.42	0.00	0.00
Ggta1	896	1044	778	0.42	0.00	0.05
Fem1c	1053	1227	913	0.42	0.00	0.02
H3f3b	27111	31603	23518	0.43	0.00	0.00
Ogt	3243	3787	2809	0.43	0.00	0.01
Gramd1a	3693	4318	3193	0.44	0.00	0.00
Gna15	1472	1724	1271	0.44	0.00	0.00
Usf1	1236	1449	1065	0.44	0.00	0.04
Pim3	903	1061	776	0.45	0.00	0.00
Madd	1374	1616	1180	0.45	0.00	0.00
Gls	568	668	487	0.46	0.00	0.04
Hjurp	5432	6398	4660	0.46	0.00	0.00
Myct1	1365	1608	1171	0.46	0.00	0.00
Myb	5630	6635	4827	0.46	0.00	0.00
Atf4	2090	2464	1791	0.46	0.00	0.01
Aff4	989	1166	846	0.46	0.00	0.02
Hspa8	18892	22288	16174	0.46	0.00	0.00
Tuba1a	786	929	672	0.47	0.00	0.00
Fzr1	3212	3796	2745	0.47	0.00	0.01
Tspyl1	2761	3276	2348	0.48	0.00	0.02
Topors	2508	2978	2131	0.48	0.00	0.00
Noa1	1243	1477	1056	0.48	0.00	0.00
Map3k4	860	1023	730	0.49	0.00	0.01
Tpra1	1062	1263	901	0.49	0.00	0.03
Decr2	681	813	575	0.50	0.00	0.04
Depdc1b	947	1132	798	0.50	0.00	0.00
Hpcal1	548	656	461	0.51	0.00	0.01
Pnrc1	5599	6726	4698	0.52	0.00	0.01
Arhgap17	1190	1429	998	0.52	0.00	0.04
Sirpa	1013	1219	848	0.52	0.00	0.04
Prex1	1728	2088	1439	0.54	0.00	0.05
Pkig	691	836	575	0.54	0.00	0.02
Cep350	606	734	504	0.54	0.00	0.01
Csrnp1	934	1131	776	0.54	0.00	0.01
Cxxc1	1609	1950	1336	0.54	0.00	0.02
Pik3r4	757	917	628	0.54	0.00	0.00
Scarf1	906	1099	752	0.55	0.00	0.00
Pak4	492	597	408	0.55	0.00	0.04

Ctla2a	4836	5882	4000	0.56	0.00	0.00
4930453N24Rik	762	929	628	0.56	0.00	0.02
Endod1	640	782	526	0.57	0.00	0.03
Il10ra	714	875	584	0.58	0.00	0.04
Mir6236	1595	1957	1305	0.58	0.00	0.00
Mdm4	740	909	605	0.59	0.00	0.00
Gch1	1045	1284	853	0.59	0.00	0.00
Apoe	2264	2784	1849	0.59	0.00	0.00
Hmmr	1588	1952	1296	0.59	0.00	0.01
Parg	1324	1630	1079	0.59	0.00	0.02
Ppm1m	475	585	387	0.60	0.00	0.02
Ints8	857	1058	696	0.60	0.00	0.04
Nkx2-3	999	1234	811	0.60	0.00	0.05
Pi4kb	558	690	452	0.61	0.00	0.04
Stom	770	956	621	0.62	0.00	0.02
Tjap1	512	638	411	0.63	0.00	0.03
Tgfbr2	1275	1593	1021	0.64	0.00	0.00
Adcy7	1928	2412	1540	0.65	0.00	0.00
Cbl	611	765	487	0.65	0.00	0.03
Gm23935	1863	2338	1483	0.66	0.00	0.00
Tsc22d1	12542	15794	9940	0.67	0.00	0.00
Kdm8	271	342	215	0.67	0.00	0.05
Banp	653	822	517	0.67	0.00	0.01
Nagpa	904	1139	716	0.67	0.00	0.03
Ccl9	2609	3292	2063	0.67	0.00	0.00
Gm25994	169	216	132	0.71	0.00	0.03
2700049A03Rik	923	1179	718	0.71	0.00	0.00
Ubc	8436	10775	6566	0.71	0.00	0.00
Neat1	998	1276	776	0.72	0.00	0.00
Fam43a	915	1171	710	0.72	0.00	0.02
Dock1	353	452	273	0.72	0.00	0.03
Foxm1	867	1117	667	0.74	0.00	0.04
Cds2	547	707	419	0.76	0.00	0.01
Tnfaip3	449	583	342	0.77	0.00	0.02
Gm26917	38344	49778	29196	0.77	0.00	0.05
Dusp6	3604	4686	2738	0.78	0.00	0.00
Tcn2	1411	1838	1070	0.78	0.00	0.00
Selenop	5440	7086	4124	0.78	0.00	0.00
Sgk1	546	712	413	0.78	0.00	0.01
Gm37352	1252	1634	946	0.79	0.00	0.00
Flnb	629	821	474	0.79	0.00	0.01
Arrdc3	1609	2104	1213	0.79	0.00	0.00
Gem	1477	1932	1113	0.80	0.00	0.00
Ptger4	662	870	496	0.81	0.00	0.00
Lgmn	353	467	262	0.83	0.00	0.00
Dyrk3	515	687	377	0.86	0.00	0.03

Scai	249	333	182	0.87	0.00	0.03
C030037D09Rik	480	643	351	0.87	0.00	0.00
Rgcc	323	434	234	0.89	0.00	0.00
Rad54b	507	683	365	0.90	0.00	0.00
Nipal3	150	203	108	0.91	0.00	0.04
Plod1	312	423	224	0.91	0.00	0.05
Slc26a11	590	799	423	0.92	0.00	0.00
Tsc22d3	4213	5713	3013	0.92	0.00	0.00
Bambi	431	585	307	0.93	0.00	0.00
Plxdc2	315	429	224	0.93	0.00	0.04
Btg1	1665	2268	1183	0.94	0.00	0.00
Spp1	329	452	231	0.97	0.00	0.02
Mpo	24516	33756	17124	0.98	0.00	0.05
Sntb2	200	279	136	1.03	0.00	0.04
Zfp36l1	215	301	146	1.04	0.00	0.00
Dnajb1	3759	5276	2545	1.05	0.00	0.00
Sertad1	657	923	443	1.06	0.00	0.00
Il6st	1089	1534	732	1.07	0.00	0.00
Hist1h1c	2755	3883	1853	1.07	0.00	0.00
Junb	12883	18192	8637	1.07	0.00	0.00
Hvcn1	120	170	79	1.09	0.00	0.00
Ctsl	1175	1669	781	1.10	0.00	0.00
Trib1	310	441	204	1.11	0.00	0.00
Ier2	21641	30914	14222	1.12	0.00	0.00
Rgs1	8570	12249	5627	1.12	0.00	0.00
Lrrk2	221	318	144	1.13	0.00	0.03
Rgs2	5118	7337	3342	1.13	0.00	0.00
Tfpi	1307	1881	847	1.15	0.00	0.00
Ier5	1310	1890	846	1.16	0.00	0.00
Pde4dip	348	505	223	1.18	0.00	0.00
Rhob	2498	3649	1577	1.21	0.00	0.00
Disc1	76	113	47	1.23	0.00	0.04
Sik1	349	516	217	1.25	0.00	0.00
Hist1h2bc	757	1119	468	1.26	0.00	0.00
Ppp1r15a	6186	9140	3823	1.26	0.00	0.00
Zfp36	16356	24193	10087	1.26	0.00	0.00
Ccl3	2443	3614	1506	1.26	0.00	0.00
Ccl4	5945	8822	3644	1.28	0.00	0.00
Jun	52812	78982	31876	1.31	0.00	0.00
Dhx40	396	596	236	1.33	0.00	0.00
Fzd9	177	267	105	1.34	0.00	0.02
Fcgrt	755	1142	445	1.36	0.00	0.00
1700055D18Rik	83	126	49	1.36	0.00	0.04
Nr4a2	98	149	57	1.37	0.00	0.02
Dusp1	29073	44372	16834	1.40	0.00	0.00
Spry1	453	696	259	1.42	0.00	0.00

A130071D04Rik	93	144	53	1.44	0.00	0.03
AA465934	296	459	165	1.47	0.00	0.00
Serinc3	22397	34823	12456	1.48	0.00	0.00
Nfkbid	633	992	346	1.52	0.00	0.00
Gadd45g	89	139	48	1.52	0.00	0.00
Dusp5	1731	2753	913	1.59	0.00	0.00
Pmaip1	177	281	93	1.59	0.00	0.00
Serpine2	102	164	52	1.62	0.00	0.02
Egr1	23962	38401	12412	1.63	0.00	0.00
Klf4	238	383	122	1.65	0.00	0.00
Fos	69010	112003	34615	1.69	0.00	0.00
Nos3	31	51	15	1.73	0.00	0.02
Gm24119	28	47	13	1.76	0.00	0.01
Nfkbiz	878	1458	414	1.81	0.00	0.00
Btg2	9557	16002	4401	1.86	0.00	0.00
Thbd	305	514	138	1.89	0.00	0.00
Cd38	131	223	58	1.93	0.00	0.00
Fosb	773	1312	342	1.94	0.00	0.00
Gm28731	19	33	8	1.96	0.00	0.04
Mical2	39	67	16	2.00	0.00	0.04
Cd36	114	197	48	2.03	0.00	0.00
Plpp3	246	424	103	2.03	0.00	0.00
Plpp1	84	146	35	2.05	0.00	0.00
Fam196b	48	83	19	2.05	0.00	0.04
Tcf7l1	53	92	21	2.09	0.00	0.04
Timp3	220	384	89	2.09	0.00	0.00
Aldob	47	83	19	2.09	0.00	0.04
Tspan7	135	239	52	2.18	0.00	0.00
S100a16	30	55	11	2.19	0.00	0.02
Nr4a1	2210	3917	846	2.21	0.00	0.00
Nid1	98	175	37	2.22	0.00	0.05
Klf6	8750	15643	3236	2.27	0.00	0.00
8430408G22Rik	444	795	164	2.27	0.00	0.00
Dnase1l3	95	172	34	2.30	0.00	0.00
Id3	150	270	54	2.31	0.00	0.00
Clec14a	122	221	43	2.35	0.00	0.00
Cd69	3590	6495	1267	2.36	0.00	0.00
Clca3a1	75	137	25	2.41	0.00	0.00
Igf1	32	60	10	2.41	0.00	0.03
Egr2	190	347	64	2.43	0.00	0.00
Klf2	5168	9491	1709	2.47	0.00	0.00
Cyp4b1	258	476	84	2.49	0.00	0.00
Epas1	40	75	12	2.51	0.00	0.04
Ackr1	214	402	64	2.64	0.00	0.00
Mafb	337	633	100	2.65	0.00	0.00
Nrp2	36	68	10	2.65	0.00	0.03

Fabp4	485	912	143	2.67	0.00	0.00
Sox18	134	253	38	2.69	0.00	0.00
Ubd	150	283	43	2.69	0.00	0.00
Kcnj8	111	210	31	2.70	0.00	0.00
Cldn5	157	298	45	2.71	0.00	0.00
Ptprb	65	125	18	2.74	0.00	0.01
Rasip1	83	159	23	2.74	0.00	0.00
Tm4sf1	66	127	18	2.76	0.00	0.01
Lrg1	754	1437	208	2.78	0.00	0.00
Stab2	263	501	72	2.79	0.00	0.00
Rhoj	106	204	28	2.83	0.00	0.00
Flt4	151	290	40	2.84	0.00	0.00
Mmrn2	165	319	43	2.87	0.00	0.00
Igfbp7	266	516	66	2.94	0.00	0.00
Plvap	741	1439	182	2.98	0.00	0.00
Id1	96	188	23	2.98	0.00	0.00
Cdh5	36	70	8	3.02	0.00	0.02
Nr2f2	17	34	3	3.04	0.00	0.03
Slco2a1	38	74	8	3.08	0.00	0.03
Atf3	239	471	53	3.11	0.00	0.00
Plk2	856	1694	186	3.18	0.00	0.00
Sparc	607	1202	130	3.20	0.00	0.00
Pparg	146	291	31	3.21	0.00	0.04
Thrsp	21	42	4	3.23	0.00	0.03
Adamts5	91	184	17	3.36	0.00	0.00
Enpp6	53	108	9	3.39	0.00	0.02
Tspan15	66	134	11	3.46	0.00	0.01
1810011O10Rik	22	46	3	3.47	0.00	0.00
Kdr	260	528	46	3.51	0.00	0.00
Gpr182	80	163	13	3.51	0.00	0.00
Ldb2	48	98	7	3.54	0.00	0.01
Gpihbp1	52	106	8	3.55	0.00	0.02
Hspb1	18	38	2	3.59	0.00	0.00
Gm6213	5	11	0	3.64	0.00	0.02
AC113508.1	34	71	5	3.69	0.00	0.02
Flrt2	6	12	0	3.74	0.00	0.02
Map1b	35	74	4	3.82	0.00	0.00
F8	116	240	16	3.83	0.00	0.00
Fam167b	48	100	6	3.84	0.00	0.00
Eda	26	56	3	3.89	0.00	0.03
Flrt3	28	58	3	3.94	0.00	0.02
Amotl1	8	17	0	3.96	0.00	0.04
Spock2	7	15	0	4.02	0.00	0.05
Prickle2	7	16	0	4.06	0.00	0.03
Adcy4	22	46	2	4.11	0.00	0.02
Dclk1	11	23	0	4.14	0.00	0.03

Aldh1a2	7	17	0	4.15	0.00	0.04
Sema3a	128	270	14	4.18	0.00	0.04
Il13ra2	21	44	1	4.21	0.00	0.01
Fermt2	19	40	1	4.28	0.00	0.00
Kcnq1	8	19	0	4.30	0.00	0.03
Dpysl3	17	37	1	4.37	0.00	0.00
Tfpi2	9	20	0	4.37	0.00	0.02
Ces2e	9	20	0	4.42	0.00	0.02
Gzma	18	40	1	4.43	0.00	0.00
Lipg	26	57	2	4.44	0.00	0.00
Nrcam	11	25	0	4.48	0.00	0.00
C5ar1	23	50	1	4.50	0.00	0.00
Stab1	88	190	7	4.60	0.00	0.00
Amotl2	22	49	1	4.85	0.00	0.00
Oit3	13	29	0	4.91	0.00	0.00
Fmo1	35	77	2	4.95	0.00	0.00
Igfbp2	13	30	0	4.96	0.00	0.00
Ibsp	16	37	0	4.98	0.00	0.00
Heph	14	31	0	4.99	0.00	0.00
Efcab5	14	32	0	5.03	0.00	0.00
Gpr174	15	34	0	5.13	0.00	0.00
Adamts4	22	49	0	5.16	0.00	0.00
Dll1	17	38	0	5.30	0.00	0.00
Afap1l2	62	137	2	5.38	0.00	0.03
Hspa1a	267	586	13	5.43	0.00	0.00
Hspa1b	650	1423	31	5.49	0.00	0.00
Col6a3	59	132	1	5.99	0.00	0.00
Pxdn	28	63	0	5.99	0.00	0.00
Cyr61	35	79	0	6.07	0.00	0.00

Table 16 Commonly regulated DEGs between Tgm2-KO LT-HSCs and MPPs versus their corresponding Tgm2-WT counterparts

Up-regulated						Down-regulated	
Myb	Hoxa9	Nfkbid	Zfp36	Hist1h2bc	Egr2	Gbp11	9030619P08Rik
Vim	H3f3b	Rgs1	Sertad1	Plvap	Dusp5	Tgm2	Cirbp
Apoe	Pkig	Hist1h1c	Zfp36l1	Nr4a2	Id1	Thbs1	Pcp4l1
Tsc22d3	Ctla2a	Ubc	Dusp1	AA465934	Fosb	Slc13a2	Nhp2
Gpr171	Ccl4	Tuba1a	Sik1	Serinc3	Klf4	Creb5	Mat2a
Tsc22d1	Csrnp1	Ier5	Rgs2	Igfbp7	Klf2	Micu1	Fam212a
Hspa8	Dusp6	Dyrk3	Arrdc3	Nfkbiz	Atf3	Myl10	Ncl
Topors	Atf4	Btg1	Plk2	Sparc	Hspa1a	Klf10	
Ptger4	Jun	Rhob	Fos	Lrg1	Adamts5		
Clk1	C030037D09Rik	Egr1	Spry1	Cd69	Hspa1b		
Gm37352	Junb	Ppp1r15a	Dnajb1	Nr4a1			
Gem	Ier2	Sgk1	Btg2	Klf6			